Alma Mater Studiorum · Università di Bologna

Scuola di Scienze
Dipartimento di Fisica e Astronomia
Corso di Laurea Magistrale in Fisica

Quantum quenches in $\mathbb{Z}_n$ symmetric spin chains: an iTEBD study

Relatore:
Prof. Francesco Ravanini

Correlatore:
Prof. Gábor Takács

Presentata da:
Octavio Pomponio

Anno Accademico 2016/2017

Sommario

Lo studio della dinamica dei sistemi quantistici fuori dall'equilibrio ha introdotto delle problematiche ancora irrisolte in fisica. Negli ultimi anni si è assistito a un enorme progesso teorico in questo campo, mosso da incredibili progressi tecnologici sia nell'ambito di gas atomici e molecolari a basse temperature, che hanno reso possibile la manipolazione di sistemi quantistici con molti gradi di libertà, che in quello di algoritmi in grado di simulare l'evoluzione temporale.

In questa lavoro rivolgiamo la nostra attenzione su di un semplice paradigma: lo studio della dinamica fuori dall'equilibrio di sistemi quantistici isolati unidimensionali a seguito della variazione di uno o più parametri del sistema (quench quantistico). In particolare viene studiata la dinamica di catene di spin con simmetria $\mathbb{Z}_n$ e come questa venga modificata dalla rottura esplicita di tale simmetria.

La parte originale del lavoro è nello studio della propagazione dell'entanglement nel modello di Potts con campo longitudinale nella sua fase paramagnetica, dove si è osservato, come recentemente nel modello di Ising con campo longitudinale, un repentino aumento nel tasso di produzione di entanglement. Questo si associa alla comparsa di una nuova particella nello spettro dell'Hamiltoniana dopo il quench. Il fenomeno viene spiegato come la versione fuori dall'equilibrio del noto paradosso di Gibbs.

Tutti i risultati numerici della tesi sono stati ottenuti con l'algoritmo iTEBD sviluppato dall'autore.

Contents

Introduction

At the dawn of quantum theory, classical statistical mechanics was an already well-established field of research. As the mathematical background of the new quantum mechanics was settled, John Von Neumann spent significant efforts in order to generalize the fundamental concept of ergodicity and to prove the tendency of a quantum state to evolve towards the state of maximum entropy [1]. Numerous questions raised back then are still without answer. In particular it is a fundamental assumption of classical statistical mechanics that a closed system with many degrees of freedom samples ergodically all the points in phase space that share the same amount of energy. To understand the limits of this assumption, it is important to find and study systems that are not ergodic and thus do not reach thermal equilibrium.

Within this framework, one dimensional closed quantum systems play an essential role, in particular integrable ones. The latter enjoy an extensive number of conservation laws that affect their dynamics preventing thermalization.

Lot of theoretical results were achieved in the last decade. This renewed interest for the topic was certainly motivated by a series of advances in experimental techniques which made possible to manipulate quantum systems with many degrees of freedom. A whole new range of methods in the field of ultracold atomic and molecular gases, including optical lattices and ion trapping [2, 3, 4], allow to engineer strongly-interacting quantum systems with the possibility of tuning with high accuracy their parameters.

This led to a massive interest in questions concerning out of equilibrium dynamics of such systems. In this context the so called *quantum quench* [5] is the most studied protocol to drive a system out of equilibrium: an isolated quantum system composed of many particles and ruled by a Hamiltonian H is prepared in a state that is not an eigenstate of the latter, and it is let evolve.

Even in this simple set up it is not trivial at all to describe the system dynamics with exact results. This is way significant efforts are also spent for the development of

numerical methods that allow the study of the properties of many-body quantum systems. In recent years increasing attention has been paid to algorithms that express the state of the system as a tensor network. Among them the *matrix product state* (MPS) [6], the *density matrix renormalization group* (DMRG) [7] algorithm to compute ground states and the *time evolving block decimation* (TEBD) [8] algorithm to simulate evolution.

The present manuscript is set within this context. Its aim is to study dynamics of spin chains with $\mathbb{Z}_n$ symmetry after a quantum quench both with analitic methods and numerical simulations. In particular the TEBD algorithm for infinite chains, developed by the author, was used both to simulate unitary time evolution and to compute groundstates of one dimensional models. The code is tested with the paradigmatic Ising model with transverse field, with $\mathbb{Z}_2$ symmetry, since exact solutions for its dynamics are known [9, 10], and used to study the 3−state quantum Potts model, a $\mathbb{Z}_3$ symmetric model that is the simplest generalization of the transverse field Ising model. It is interesting to study their similarities and their differences in the dynamics since while the Ising model is integrable, the Potts model it is not. This might give valuable informations about the relation between integrability and *relaxation*. It is then studied how the dynamics of these models is affected by the addition of a longitudinal field, which results in the breaking of integrability for the Ising model. The Ising and Potts models are also paradigmatic for their simple description of the phenomenon know as spontaneous symmetry breaking: they can describe situations where the equations of motion obey certain symmetries ($\mathbb{Z}_n$ in this case), but the lowest energy vacuum solutions do not exhibit that same symmetry. Particular attention is then paid in this work to the study of symmetries after a quantum quench. The work is structured as follows.

In chapter 1 some aspects of one dimensiona quantum system are presented. We introduce the main experimental motivations to study such systems. The concept of quantum integraiblity is introduced and compared with the well established classical counterpart. The introduction of entanglement entropy follows, with a discussion on its importance for the deduction of many quantum features. A digression about quantum phase transitions concludes the chapter.

In chapter 2 we recollect some useful notions about out of equilibrium dynamics in one dimensional systems. The relation between (non) integrability and equilibration is introduced as well as the concept of quantum quench. Afterwards, a very helpful picture is presented: the spreading of correlations throughout the system as propagation of quasi-particle excitations after a quantum quench and how it helps in the description

of the evolution of observables [5]. The evolution of entanglement entropy is eventually outlined [11].

The content of chapter 3 is aimed at describing the algorithm used to simulate the evolution of quantum systems after a quench. After introducing a useful representation for quantum states, the *matrix product state* (MPS) *representation*, the infinite Time Evolving Block Decimation algorithm is presented and it is explained how this can be adapted for the computation of ground states. The chapter ends with details on the simulations.

In chapter 4 the models under study are introduced. Their dynamics is described along with the the results of the simulations. As far as the Ising model is concerned, the latter are compared to exact predictions and some of them are reobtained thoughout the chapter.

In the last chapter the reults of the dynamics of the very same models with the addition of a longitudinal field, and the consequent explicit symmetry breaking, is reported. In particular we focus on the ferromagnetic phase of the Ising model, reproducing the results obtained in [12], and the paramagnetic phase of the Potts model, demonstrating that the phenomenon of sudden increase in the entanglement production rate observed in the Ising model in a recent work [13] is present also in its direct generalization.

Chapter 1

Quantum one dimensional systems

Many years later, as he faced the firing squad, Colonel Aureliano Buendía was to remember that distant afternoon when his father took him to discover ice.

- Gabriel García Márquez, *One Hundred Years of Solitude*

In this chapter some key aspects of one dimensional quantum systems are introduced. We start with experimental results and technological advances that motivates their theoretical study and proceed with the definition of quantum integrability. Afterwards, entanglement entropy is introduce, a meaningful physical quantity crucial in the whole discussion of the present manuscript. We conclude the chapter with a digression about quantum phase transitions.

1.1 Experimental motivations

In recent years the study of nonequilibrium dynamics of quantum many-body systems has been increasingly motivated by a series of advances in the field of ultracold atomic and molecular gases. These systems are nowadays crucial for the study of nonequilibrium quantum phenomena.

First of all, quantum gases exhibit a high degree of isolation from environmental sources of decoherence and can therefore be regarded as closed quantum systems. Furthermore their dilute nature and the low temperatures result in relative long observation times, that allow the study of late time relaxation.

Secondly, it is possible to dynamically tune the parameters of the Hamiltonian ruling the quantum system by means of Fashenbach resonances [2, 3], that allow to change interparticle separation by changing the external magnetic field, and optical potentials [4].

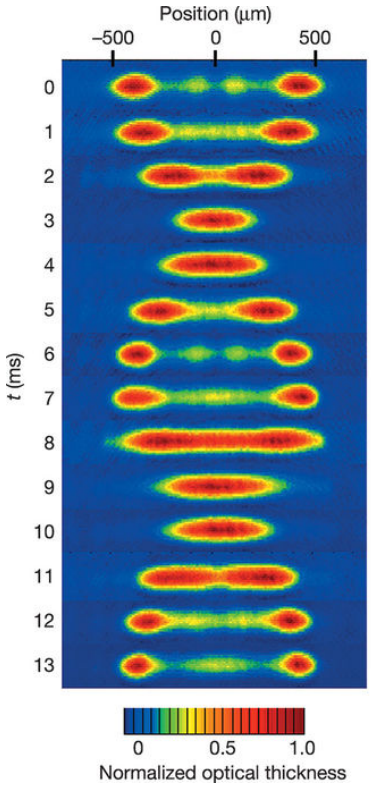

Figure 1.1: Absorption images in the first osillation cycle of the Quantum Newton's Cradle experiment. Figure taken from [14].

One of the most famous experiments that motivated the recent theoretical work is the quantum Newton's cradle [14], which renewed the interest for issues such as the relation between thermalization and quantum integrability.

It is indeed a fundamental assumption of statistical mechanics that a closed system with many degrees of freedom ergodically samples all equal energy points in phase space. To understand the limits of this assumption, it is important to study systems that are not ergodic and thus do not reach thermal equilibrium.

In this experiment, Kinoshita, Wenger and Weiss loaded a Bose-Einstein condensate composed by $2 \cdot 10^5$ atoms of ^{87}Rb into the combination of a two-dimensional optical lattice and a crossed dipole trap. The combination of light traps builds a 2D array of distinct

parallel Bose gases. The dynamics within each tube, containing from 40 to 250 atoms, is strictly one-dimensional since the potential is chosen so that the lowest transverse excitation exceeds all other energies in the problem and there is negligible tunnelling among the tubes.

After putting the atoms in a superposition of states with opposite momenta, they are allowed to evolve for a variable time t in the crossed dipole trap and absorption images are taken to study the atoms positions at different times (Fig. 1.1). Then the momentum distribution is measured at subsequent times. It turns out that the system reaches a stationary configuration but does not thermalize on the time scales available for the experiment; more precisely, the momentum distribution eventually reached is non Gaussian.

The system described above is in close relation with the Lieb-Liniger model, which is integrable, plus harmonic potential. Hence the results of the experiment suggested that the non gaussianities were caused by the integrability of the system. Note that the crossed dipole trap breaks the integrability of the system: this also suggests a certain stability of non-thermalization when an integrable hamiltonian is perturbed via a non-integrable term.

1.2 One dimensional quantum systems

The object of study are isolated many-body quantum system, that are characterized by the absence of any coupling to its environment. Consider a one dimensional lattice of such kind with a time-independent, translationally invariant Hamiltonian H and with N sites (Fig. 1.2). On each site we define degrees of freedom which introduce a local Hilbert space of finite dimension.

For definiteness, let's introduce as example the XY model with N sites, whose Hamiltonian has the form:

$$H = \sum_{j=1}^{N} h_j, \qquad h_j = -\frac{1}{2}\left\{ \left(\frac{1+\gamma}{2}\right)\sigma_j^x\sigma_{j+1}^x + \left(\frac{1-\gamma}{2}\right)\sigma_j^y\sigma_{j+1}^y + h\sigma_j^z \right\} \tag{1.1}$$

where $\vec{\sigma}_j$ is the vector of Pauli matrices $\sigma_j^x, \sigma_j^y, \sigma_j^z$ and the index j indicates that the operator acts non trivially only on site j:

$$\vec{\sigma}_j = \mathbb{1} \otimes \cdots \otimes \mathbb{1} \otimes \vec{\sigma} \otimes \ \mathbb{1} \otimes \cdots \otimes \mathbb{1}. \tag{1.2}$$

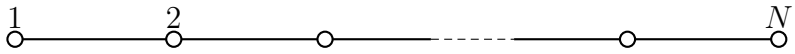

Figure 1.2: Graphical representation of one-dimensional lattice. On each site resides a local Hilbert space isomorphic to $\mathbb{C}^d$ for some finite d model dependent.

On each site there is a local Hilbert space isomorphic to $\mathbb{C}^2$ spanned by the eigenstates of the σ^z operator:

$$\sigma^z |\uparrow\rangle = |\uparrow\rangle \qquad \sigma^z |\downarrow\rangle = -|\downarrow\rangle . \tag{1.3}$$

The Hilbert space of the whole system is then $\mathcal{H} = (\mathbb{C}^2)^{\otimes N}$.

With this simple model in mind, key aspects of one dimensional quantum systems will be introduced and discussed in the following paragraphs.

1.3 Integrable systems

First of all, what does *integrability* mean for quantum systems? And how integrability of a certain model implies its *solvability*? A physical system is commonly identified as a topological space of states $\mathcal{M}$ (usually a manifold, albeit often infinite dimensional) with a bijective evolution map

$$U_t : \mathcal{M} \to \mathcal{M} \tag{1.4}$$

parametrised by a real parameter t identified as time. Every state in $\mathcal{M}$ encodes physical observable predictions, while the evolution map depicts how these predictions change in time.

1.3.1 Classical integrability

For classical one dimensional systems, $\mathcal{M}$ is a $2n$ simplectic manifold described by the coordinates $(q_i, p_i) \in \mathbb{R}^2$, $i \in \{1, \dots, n\}$, with canonical Poisson brackets

$$\{q_i, p_j\} = \delta_{ij}. \tag{1.5}$$

A physical observable is then a real (smooth) function F of these coordinates. Denoting by $\mathcal{F}$ the real linear space of observables, we have for any $F, G \in \mathcal{F}$

$$\{F, G\} = \sum_k \frac{\partial F}{\partial q_k}\frac{\partial G}{\partial p_k} - \frac{\partial F}{\partial p_k}\frac{\partial G}{\partial q_k}. \tag{1.6}$$

The bijective map U_t is related to a particular function on phase space, the Hamiltonian $H = H(q, p)$, that gives the equations of motion of the system

$$\frac{dF}{dt} = \{F, H\}. \tag{1.7}$$

The operator

$$D_H F(\mathbf{q}, \mathbf{p}) = \{F, H\}\Big|_{(\mathbf{q},\mathbf{p})} \tag{1.8}$$

acts as infinitesimal generator of the evolution map and U_t can be expressed as Lie series

$$U_t = \sum_{n=0}^{\infty} \frac{t^n}{n!} D_H^n \equiv \exp\{tD_H\}. \tag{1.9}$$

The evolution equation is such, in most physical cases, that time evolution of a given state is continuous. However the map U_t can be very complicated. In particular, although it may be almost everywhere continuous, this continuity is almost nowhere uniform in time. In many cases, two nearby states map to states that are very far apart, and that become exponentially further apart as t is increased (*chaos*). Integrability is essentially the opposite of chaos: the map U_t is as nice as it can be. It possesses infinitely many invariant submanifolds that foliate $\mathcal{M}$, parametrised by as many continuous parameters as there are "degrees of freedom", and on these submanifolds, states that start nearby stay nearby uniformly in time. To clarify these concepts we introduce the definition of *Liouville integrability* [15].

Definition 1 (First integral)**.** *A function $F \in \mathcal{F}$ is a* first integral *of a system with hamiltonian function H if its Poisson bracket with H itself is identically equal to zero.*

$$\{F, H\} = 0 \tag{1.10}$$

Definition 2 (Involution)**.** *Two functions $F_1, F_2 \in \mathcal{F}$ are* in involution *if their Poisson bracket is equal to zero.*

$$\{F_1, F_2\} = 0 \tag{1.11}$$

Definition 3 (Liouville integrability)**.** *A dynamical system (of $2n-$dimensional phase space) is* Liouville integrable *if there exists n independent first integrals I_k, with $k \in \{1, \ldots, n\}$, in involution.*

The independence of the latter means that at generic points on the symplectic manifold, the tangent space of the surface defined by $I_k = const.$ exists $\forall k$ and is $n-$dimensional.

It is now possible to state the Liouville theorem on integrable systems.

Theorem 1 (Liouville theorem)**.** *Consider a Liouville integrable system with a set of first integrals* $\{F_k\}$*. Consider the set*

$$M_{\mathbf{f}} = \{(\mathbf{q}, \mathbf{p}) : F_i(\mathbf{q}, \mathbf{p}) = f_i = const., \ \ i \in \{1, \ldots, n\}\}. \tag{1.12}$$

Then

1. $M_{\mathbf{f}}$ *is a smooth manifold, invariant under the phase flow with hamiltonian function* $H = F_1$

2. *If the manifold* $M_{\mathbf{f}}$ *is compact and connected, then it is diffeomorphic to the* $n-$*dimensional torus*

$$T^n = \{(\phi_1, \ldots, \phi_n), \phi_i \in [0, 2\pi[\}$$

3. *The evolution map with hamiltonian function* H *determines a conditionally periodic motion on* $M_{\mathbf{f}}$*, i.e., in angle variables*$\{\phi_j\}$ *and their canonical conjugate action variables* $\{I_j\}$*,* $j = 1, \ldots, n$*,*

$$\{\phi_j, I_k\} = \delta_{j,k}$$

we have that action variables are purely functions of the first integrals, hence are invariant under time evolution. This implies that angles evolve linearly with time:

$$\{\phi_j, H\} = \frac{\partial H}{\partial I_j} \qquad \Rightarrow \qquad \phi_j(t) = \frac{\partial H}{\partial I_j} t + \phi_j(0)$$

4. *The canonical equations with hamiltonian function* H *can be integrated by quadratures.*

1.3.2 Quantum integrability

When it comes to quantum theory, the definition of integrability it is not straightforward. One may wish to emulate the classical case following canonical quantization [16], supplanting Poisson brackets by commutators

$$\{F, G\} \to -i[F, G] \tag{1.13}$$

and ask for many integrals of motions (in involution) as there are degrees of freedom. Having the XY model in mind, the problem is that for any finite N, the Hamiltonian (1.1) is a finite-dimensional Hermitian matrix $2^N \times 2^N$ and can be diagonalized. In the diagonal basis, any other matrix that is diagonal will communte with the Hamiltonian. There are 2^N of such matrices, all independent from each other. Hence, we have automatically a greater number of conserved quantities then the number of degrees of freedom. Obviously this doesn't mean that every quantum chain is integrable: since these conserved quantities exist for every system, they can't have any profound meaning or impact. There is no universally accepted definition of integrability for quantum spin chains (see for example [17, 18]). One of the main concepts that is commonly accepted as being fundamental, however, is that of *locality*. We now introduce some concepts related to this feature [19].

Definition 4 (local quantum spin chain)**.** *A quantum spin chain model is* local *if the Hamiltonian H, as the thermodynamicl limit is taken, is always on the form*

$$H = \sum_k h_k \tag{1.14}$$

and there exists a $r > 0$ (N independent) such that $\forall k$ the operator h_k is supported on sites lying within the interval $[k - r, k + r]$.

Definition 5 (local operator)**.** *An operator $\mathcal{O}_n$ is* local *around the site n*

$$\exists r > 0 : [\mathcal{O}_n, h_m] = 0 \quad \forall m : |n - m| > r. \tag{1.15}$$

Two operators $\mathcal{O}_n, \mathcal{O}'_m$ are said to be local with respect to each other *if they commute for $|n - m|$ large enough.*

Definition 6 (local conserved quantity)**.** *A* local conserved quantity *(or charge) is an operator Q supported on the whole chain, such that it commutes with the hamiltonian function*

$$[Q, H] = 0 \tag{1.16}$$

and such that Q is a sum over n of uniformly *local operators around n:*

$$Q = \sum_n q_n, \qquad \exists r > 0 : [q_n, h_m] = 0 \qquad \forall |n - m| > r \tag{1.17}$$

Using these concepts we can define integrability as follows:

Definition 7. *(quantum integrability) A local quantum spin chain model is integrable if, in the thermodynamical limit, there exist infinitely many local conserved quantities $Q^{(k)}$ that are in involution,*

$$[Q^{(k)}, Q^{(l)}] = 0 \qquad \forall k, l \tag{1.18}$$

and whose densities are local with respect to each other.

In integrable models the Hamiltonian H can be written as [17]

$$H = \sum_k \epsilon(k)\eta_k^\dagger \eta_k + E_0 \tag{1.19}$$

where the creation and annihilation operators $\eta_k^\dagger, \eta_k$ act on the ground state of the system and produce quasi particle excitations with dispersion relation $\epsilon(k)$ and E_0 is the ground state energy. The Hamiltonian of the system can be namely decomposed into a set of harmonic oscillators (the analogue of action-angle variables for classical dynamical systems). In this picture the conserved charges are simply the occupation number of each single-particle eigenmode $n_k = \eta_k^\dagger \eta_k$. It is important to remark that the existence of a quasi-particle description is not a sufficient condition to write the hamiltonian function as (1.19). It is indeed necessary that the quasi-particles mantain their identity upon scattering between each other. This is ensured by the complete factorization of many-body scattering amplitudes into $2-$body scattering processes [20].

1.4 Entanglement entropy

Many quantum features can be deduce by studying quantities that are non local observables. Entropy is one of these quantities and builds the basis for a statistical description of nature. As already introduced in previous sections, an isolated quantum system evolves unitarily and if the system is prepared in a pure state it will remain in a pure state with zero entropy.

However we can characterize the entropy of a subsystem, that is generally in a mixed state, computing the Von Neumann entropy of its reduced density matrix, also called *entanglement entropy*.

The entanglement of a subsystem with the rest of the system measures how the configuration of the former depends on the configuration of the latter and how far it

is from being a pure state. To put this into formulae, we first introduce the Schmidt decomposition.

1.4.1 Schmidt decomposition

Let us consider a bipartition of the Hilbert space of a spin chain $\mathcal{H} = \mathcal{H}_L \bigotimes \mathcal{H}_R$ of a $1D$ system, where $\mathcal{H}_L(\mathcal{H}_R)$ describes all the states defined on the left (right) of a given bond.

Any pure state $|\psi\rangle$ defined on the whole system can be written as

$$|\psi\rangle = \sum_{ij} \Psi_{ij} |i\rangle_L \otimes |j\rangle_R , \tag{1.20}$$

where $\{|i\rangle_L\}$ and $\{|j\rangle_R\}$ are orthonormal bases of $\mathcal{H}_L$ and $\mathcal{H}_R$ with dimensions N_L and N_R respectively. From this representation we can introduce the reduced density operator of a part of the system tracing out the degrees of freedom of the other part

$$\rho_{L/R} = \mathrm{Tr}_{R/L} |\psi\rangle \langle\psi| , \tag{1.21}$$

which expressed with respect to the orthonormal bases take the form

$$\rho_L = \Psi\Psi^\dagger \qquad \rho_R = \Psi^\dagger\Psi \tag{1.22}$$

We can now perform a *singular value decomposition* (SVD) of the matrix Ψ. The SVD guarantees for an arbitrary matrix M of dimension $(n \times m)$ the existence of a decomposition

$$M = USV^\dagger, \tag{1.23}$$

where:

- U is of dimension $(n \times \min(n, m))$ and has orthonormal columns, i.e. $U^\dagger U = \mathbb{1}$; if $n \leq m$, U is then unitary;
- S is of dimension $(\min(n, m) \times \min(n, m))$ and diagonal with non negative entries $S_{aa} \equiv \Lambda_a$. These are the so-called *singular values*. The number r of non-zero singular values is the (*Schmidt*) rank, or bond dimension, of M. Furthermore we choose to put the singular values in descending order;
- V is of dimension $(\min(n, m) \times m)$ and has orthonormal rows, i.e. $VV^\dagger = \mathbb{1}$; if $n \geq m$, V is then unitary;

For practical importance in the following, it is useful to define a topology induced by the inner product $\langle M, N\rangle = \mathrm{Tr}\, M^\dagger N$. The latter defines the Frobenius norm

$$\|M\|_F^2 = \langle M, M\rangle = \mathrm{Tr}\, M^\dagger M = \mathrm{Tr} \sum_k (M^\dagger)_{ji} M_{ik} = \sum_{ij} |M_{ij}|^2. \tag{1.24}$$

In this topology the optimal approximation of the matrix M by a matrix M' of rank $r' < r$ is given by [21]

$$M' = US'V^\dagger \qquad S' = diag(s_1, s_2, \dots, s_{r'}, 0, \dots), \tag{1.25}$$

i.e. one sets all but the first r′ singular values to be zero.

The SVD is at the basis of a very compact representation of quantum states living in a bipartite universe L/R called the *Schmidt decomposition*.

The pure state $|\psi\rangle$ can be expressed as

$$\begin{aligned} |\psi\rangle &= \sum_{ij} \Psi_{ij} |i\rangle_L \otimes |j\rangle_R = \sum_{ij} \sum_{\alpha=1}^{\min(N_L,N_R)} U_{i\alpha} S_{\alpha\alpha} V^*_{j\alpha} |i\rangle_L \otimes |j\rangle_R \\ &= \sum_{\alpha=1}^{\min(N_L,N_R)} \Lambda_\alpha \Big(\sum_i U_{i\alpha} |i\rangle_L \Big) \otimes \Big(\sum_j V^*_{j\alpha} |j\rangle_R \Big) \\ &= \sum_{\alpha=1}^{\min(N_L,N_R)} \Lambda_\alpha |\alpha\rangle_L \otimes |\alpha\rangle_R \end{aligned} . \tag{1.26}$$

Due to the orthonormality properties of U and $V^\dagger$, the sets $\{|\alpha\rangle_L\}$ and $\{|\alpha\rangle_R\}$ are also orthonormal bases of $\mathcal{H}_L$ and $\mathcal{H}_R$, i.e.,

$$\langle \alpha | \alpha' \rangle_L = \sum_{ii'} {}_L\langle i | U^*_{i\alpha} U_{i'\alpha'} |i'\rangle_L = \sum_{ii'} (U^\dagger)_{\alpha i} U_{i'\alpha'} \delta_{ii'} = \sum_i (U^\dagger)_{\alpha i} U_{i\alpha'} = \delta_{\alpha\alpha'} \tag{1.27}$$

Restricting the sum over the r positive nonzero values of $\{\Lambda_a\}$, we obtain the *Schmidt decomposition*:

$$|\psi\rangle = \sum_{\alpha=1}^{r} \Lambda_\alpha |\alpha\rangle_L \otimes |\alpha\rangle_R \tag{1.28}$$

Furthermore, if the pure state $|\psi\rangle$ is normalized:

$$\sum_{\alpha=1}^{r} \Lambda_\alpha^2 = 1 \tag{1.29}$$

1.4.2 Entanglement Entropy and area law

An important aspect of the Schmidt decomposition is that it gives meaningful information about the *entanglement* between the degrees of freedom in $\mathcal{H}_L$ and $\mathcal{H}_R$ because the values Λ_α give a measure of the overlap between the states of the two subsystems. To better understand their meaning, we analyse two extreme cases. The firs one is given by

$$\Lambda_\alpha = \delta_{\alpha,\alpha_0} \qquad |\psi\rangle = |\alpha_0\rangle_L \otimes |\alpha_0\rangle_R \,. \tag{1.30}$$

This state os separable and there is no entanglement. A measure on the L subsystem will not affect a measure on the R subsystem.

Every other state is entangled and the opposite situation to the previous one is when

$$\Lambda_\alpha = \frac{1}{\sqrt{\mathcal{N}}} \qquad |\psi\rangle = \frac{1}{\sqrt{\mathcal{N}}} \sum_\alpha^{\mathcal{N}} |\alpha\rangle_L \otimes |\alpha\rangle_R \,, \tag{1.31}$$

where $\mathcal{N} = \min(N_L, N_R)$. This is the maximally entangled state.

It is important to remark that the Schmidt basis coincides with the eigenbasis of the reduced density matrix of the two subsystems, that share the same spectrum:

$$\begin{aligned} \rho_L &= \sum_\alpha \Lambda_\alpha^2 \, |\alpha\rangle_L \, \langle\alpha|_L \\ \rho_R &= \sum_\alpha \Lambda_\alpha^2 \, |\alpha\rangle_R \, \langle\alpha|_R \end{aligned} \tag{1.32}$$

But what provides a good measure of entanglement? It was proved in [22] that an entanglement measure S is fixed uniquely after imposing the following conditions:

1. S is invariant under local unitary transformations (that implies that S is a function of the Λ_α^2 only);
2. S is continuos;
3. S is additive when several copies of the system are present:

$$S(|\psi\rangle \otimes |\phi\rangle) = S(|\psi\rangle) + S(|\phi\rangle). \tag{1.33}$$

This conditions are satisfied by the von Neumann entropy of the reduced density matrix

$$S(\rho_L) = -\operatorname{Tr}[\rho_L \log \rho_L] = -\sum_\alpha \Lambda_\alpha^2 \log \Lambda_\alpha^2 = S(\rho_R) \equiv S, \tag{1.34}$$

which corresponds to the Shannon entropy with $p_\alpha = \Lambda_\alpha^2$.

Note that as we wanted an unentangled product state, where the pure state is describe by only one Schmidt value, has $S = 0$. Conversely, S is maximum for a maximally entangled state.

The definition of entanglement entropy is formally the same of thermal entroyp. This similarity though is only apparent since they exhibit different behaviours when the system size is changed. Thermal entropy S_T scales indeed withe the number of microstates. These can be approximated withe the volume of the phase space accessible to the system. Since the latter is a direct product of the configuration space with its tangent bundle, it is natural that S_T scales with the volume accessible to the system. In d spatial dimensions

$$S_T \backsimeq l^d, \tag{1.35}$$

where l is a typical length of the system.

The situation is different for entanglement entropy. To see this difference let's consider ground states of local, short range Hamiltonians of a bipartite system in d dimensions. In general we expect that for non degenerate ground states of gapped Hamiltonians, the entangled degrees of freedom are the ones placed near the surface that separates the two subsystems. This is because of the finiteness of the correlation length, suggesting that the entanglement entropy scales with the area of the surface that divides the two subsystems [23, 24]:

$$S \backsimeq \left(\frac{l}{\epsilon}\right)^{(d-1)}, \tag{1.36}$$

where ϵ is a non-universal short-distance cut-off.

For one dimensional systems the previous expression leads to bounded entanglement entropy and the following theorem was indeed proved in [25]:

Theorem 2. *Consider a short range Hamiltonian H with a unique ground state with a gap ΔE to the first excited state. Then, for any bond chosen for the bipartition L/R,*

$$S_L \leq S_{max}, \tag{1.37}$$

where

$$S_{max} = c_0 \xi' \log(\xi') \log(d) 2^{\xi' \log d} \tag{1.38}$$

with c_0 constant and $\xi' = 6\xi = 6 \max(2v/\Delta E, \xi_C)$.

When the Hamiltonian is gapless there is a violation to this law since ξ diverges and for one dimensional critical systems it has been shown [26] that

$$S = \frac{c}{3} \log\left(\frac{l}{\epsilon}\right), \tag{1.39}$$

where c is the *central charge* of the correspondent conformal field theory describing the model [27]. In this sense entanglement entropy signals the emergence of quantum phase transitions, main topic of the next section.

On the other hand, excited states are usually characterized by maximal entanglement and actually follow a volume law. Indeed they resemble classical states, where entanglement entropy reduces to thermodynamic entropy.

In conclusion, in the full Hilbert space of the system, among *typical states*, which follow a volume law, there are untypical rare states (usually represented by ground states) that are slightly entangled and can be described by only a relatively small number of Schmidt values.

This provides an extremely useful approach to compress quantum states by truncating the Schmidt decomposition. It is natural to approximate a state $|\psi\rangle$ by some $|\psi'\rangle$ spanned over state spaces of L and R that have dimension r' only. This problem can be related to the SVD, because the 2-norm of $|\psi\rangle$ is identical to the Frobenius norm of the matrix Ψ. The optimal approximation is therefore given in the 2-norm by the optimal approximation of Ψ by Ψ' in the Frobenius norm, where Ψ' is a matrix of rank r' (1.25).

When $|\psi\rangle$ follows an *area law*, we can therefore always truncate the Schmidt decomposition at some finite χ. That is $\forall\epsilon > 0$, $\exists\chi$ finite such that

$$\left\| |\psi\rangle - \sum_{\alpha=1}^{\chi} \Lambda_\alpha |\alpha\rangle_L \otimes |\alpha\rangle_R \right\| < \epsilon, \tag{1.40}$$

being χ non extensive.

This particular property of area law states is intimately related to the MPS representation of one dimensional quantum states.

1.5 Quantum phase transitions

Classical phase transitions manifest in thermodynamic quantities as non analicities. Very often the transition is between an ordered and a disordered phase. In this situation an

order parameter m can be constructed which is zero in the disordered phase and nonzero in the ordered phase.

In the modern classification scheme, phase transitions are divided into two broad categories: *first order* and *second order* phase transitions. First order phase transitions are those that involve a latent heat. At the transition point, a system either absorbs or releases a fixed amount of energy, while its temperature stays constant. First order phase transitions are characterized by a finite value of the correlation length. In turn, this implies the presence of a mixed-phase regime, in which some parts of the system have completed the transition and others have not.

The second class of phase transitions consists of the continuous phase transitions, also called second order phase transitions. These have no associated latent heat and they are also characterized by the divergence of the correlation length at the critical point. In second order phase transitions the order parameter vanishes continuosly at the critical point T_c

$$m \sim (T_c - T)^{\beta} \qquad T \to T_c^- \tag{1.41}$$

and many other thermodynamic quantities show non analytic behavior, chracterized by some other *critical exponents* like β . In particular the correlation lenght ξ diverges

$$\xi \sim (T_c - T)^{-\nu} \qquad T \to T_c^{\pm}, \tag{1.42}$$

meaning that the microscopic details of the models become irrelevant and *universal behaviours are observed*: different models that enjoy the same dimensionality and simmetries behave alike at critical points and are described by the same set of critical exponents [28].

In classical models, phase transitions are driven by thermal fluctuations. On the other hand, quantum phase transitions deal with systems at zero temperature, i.e. with the ground state physics of the system. As a consequence, thermal fluctuations are absent but the system can have fluctuations due to the Heisenberg principle [29].

Consider a Hamiltonian whose degrees of freedom reside on the sites of a lattice, and which varies as a function of a dimensionless coupling g. Let us follow the evolution of the ground state energy of $H(g)$ as a function of g. For the case of a finite lattice, this ground state energy will generically be a smooth, analytic function of g. The main possibility of an exception comes from the case when g couples only to a conserved quantity (i.e., $H(g) = H_0 + gH_1$ where H_0 and H_1 commute). This means that H_0 and H_1 can be simultaneously diagonalized and so the eigenfunctions are independent of g even though the eigenvalues vary with g: then there can be a level crossing where an

excited level becomes the ground state at $g = g_c$ creating a point of non-analyticity of the ground state energy as a function of g. If instead we consider an infinite lattice, an avoided level crossing between the ground state and an excited state in a finite lattice can then become progressively sharper as the system size increases. This means that, increasing the system's size, the energy difference between the levels becomes smaller and smaller so that eventually in the limit of an infinite system, the energy exhibits some non analytic behaviour. We will call these quantum phase transitions, and in particular we will encounter phase transitions of the second order. These are the transitions at which the characteristic scale of the fluctuations of energy above the ground state vanishes as g approaches g_c. Let Δ represent an energy scale, given by the gap between the ground state and the first excitation above the ground state. Generally, in the neighbourhood of the critical point g_c, vanishes with a power law behaviour

$$\Delta \simeq J|g - g_c|^{zv}, \tag{1.43}$$

where J is the energy scale of a characteristic microscopic coupling.

The ratio of the exponents in (1.42) and (1.43) is z, the *dynamic critical exponent*: the characteristic energy scale vanishes as the z^{th} power of the charactertistic inverse length scale

$$\Delta \simeq \xi^{-z}. \tag{1.44}$$

The XY model, already introduced in section 1.2, despite its apparent simplicity, has a rich two dimensional phase diagram characterized by two quantum phase transitions. We recall its Hamiltonian:

$$H = \sum_{j=1}^{N} -\frac{1}{2}\left\{\left(\frac{1+\gamma}{2}\right)\sigma_j^x\sigma_{j+1}^x + \left(\frac{1-\gamma}{2}\right)\sigma_j^y\sigma_{j+1}^y + h\sigma_j^z\right\} \tag{1.45}$$

The model has symmetris for $\gamma \to -\gamma$ and $h \to -h$. The Hamilonian (1.45) can be diagonalized (see [30]) and the dispersion relation of the quasi-particle excitation is given by

$$\epsilon(k) = \sqrt{(h - \cos k)^2 + \gamma^2 \sin^2 k}, \tag{1.46}$$

so that the spectrum is gapped for most values of parameters but we have gapless excitations for $\gamma = 0, h < 1$ and for $h = 1$. The latter signals a transition from a doubly degenerated ground state (for $h < 1$) to a single ground state system (for $h > 1$). This is in analogy, with the classical two-dimensional Ising model, where it is well known that the

critical temperature separates a region of vanishing order parameter at high temperatures from a region of spontaneously broken $\mathbb{Z}_2$ symmetry at low temperatures where the order parameter can assume two opposite finite values.

It is important to remark that spontaneous symmetry breaking at a quantum level can happen only in the thermodynamic limit. This follows from the existence of the tunnel effect. Let us consider a double-well potential with two ground states $|+\rangle$ and $|-\rangle$. The tunnel effect removes degeneracy since allows the transition between these two states and the Hamiltonian acquires a non zero matrix element between the states $|+\rangle$ and $|-\rangle$. Denoting by H the matrix of the Hamiltonian between these two states, we get

$$H = \begin{bmatrix} \epsilon_0 & \epsilon_1 \\ \epsilon_1 & \epsilon_0 \end{bmatrix} \tag{1.47}$$

The energy eigenstates are now given by the symmetric and antysymmetric combinations of the two ground states

$$\begin{aligned} |S\rangle &= \frac{1}{\sqrt{2}}(|+\rangle + |-\rangle) \\ |A\rangle &= \frac{1}{\sqrt{2}}(|+\rangle - |-\rangle), \end{aligned} \tag{1.48}$$

with eigenvalues respectively

$$\begin{aligned} E_S &= \epsilon_0 + \epsilon_1 \\ E_A &= \epsilon_0 - \epsilon_1. \end{aligned} \tag{1.49}$$

It can be shown that $\epsilon_1 < 0$ so that the ground state is the symmetric one.

If we prepare the system in the state $|+\rangle$ and consider its time evolution

$$|+, t\rangle = \frac{1}{\sqrt{2}} e^{-iE_S t}(|S\rangle + e^{-i\Delta E t}\,|A\rangle), \tag{1.50}$$

with $\Delta E = E_A - E_S$, so that the state oscillates between $|+\rangle$ and $|-\rangle$ with a period given by $T = 2\pi/\Delta E$.

The splitting of the fundamental states decreases with the height of the potential between the two minima, that conversely increases linearly with the system's size for translational invariant sytems. Therefore for infinite systems we may have spontaneous symmetry breaking.

Chapter 2

Introduction to quantum quenches

Freedom is the freedom to say that two plus two makes four.
If that is granted, all else follows.

- George Orwell, *1984*

In this chapter the problem of quantum many body systems out of equilibrium is introduced together with the role played by integrability (for reviews see [31, 32, 33]). It will be specified in what sense a one dimensional quantum system may relax and if it can be described by some statistical ensemble in the long time limit. Among different ways to drive a system out of equilibrium the concept of quantum quench is presented and compared to the more familiar adiabatic evolution. Furthermore it is depicted how correlations spread after a quantum quench and how this can be interpreted as due to propagation of quasi-particles excitations. With the same picture, the evolution of entanglement entropy after a quantum quench is described.

2.1 Out of equilibrium dynamics

2.1.1 Relaxation in isolated quantum systems

In statistical mechanics of classical systems, a generic isolated system in the thermodynamic limit prepared in a generic initial state evolves towards, in the long time limit, a well defined stationary state. The latter is the one that maximizes the entropy [34, 35] and the whole system is described by a microcanonical ensemble with total energy equal to the initial one.

Since we are considering an isolated quantum system, it is necessary to specify in what sense it may relax to a stationary state al late times after we have driven it out of equilibrium. If we prepare the system in a pure state $|\psi_0\rangle$ that is not an eigenstate of the Hamiltonian of the system H, it will remain in a pure state, since evolution is unitary

$$|\psi(t)\rangle = e^{-iHt} |\psi_0\rangle \tag{2.1}$$

instead of a statiscal ensemble, which is by definition a mixed state. Consider, for instance, the following class of hermitian operators

$$\mathcal{O}_{kl} = |k\rangle \langle l| + |l\rangle \langle k| . \tag{2.2}$$

Expanding the pure state in the energy eigenstates

$$H |n\rangle = |n\rangle E_n \tag{2.3}$$

$$|\psi(t)\rangle = \sum_n \langle n|\psi_0\rangle e^{-iE_n t} |n\rangle , \tag{2.4}$$

the expectation values in the state $|\psi(t)\rangle$ of these operators can be expressed as

$$\begin{aligned} \langle\psi(t)| \mathcal{O}_{kl} |\psi(t)\rangle &= \langle\psi(t)|k\rangle \langle l|\psi(t)\rangle + c.c. \\ &= e^{i(E_k - E_l)t} \langle\psi_0|k\rangle \langle l|\psi_0\rangle + c.c.. \end{aligned} \tag{2.5}$$

We see that generically it exhibits periodic oscillatory behaviour in time. Hence the observables $\mathcal{O}_{kl}$ do not relax at late imes. In general the whole evolution is periodic or quasi-periodic, that is, the system will return to its initial state or arbitrary close to it: the whole isolated system cannot relax to a steady state.

Figure 2.1: Finite subsystem A and rest of the system.

Locality plays again a crucial role (note that operators like $\mathcal{O}_{kl}$ are generally nonlocal in the sense explained above). Even if the whole system cannot relax, subsystems of a much larger system are not isolated and they may therefore thermalize due to the thermal bath with the rest of the system. Isolated quantum many-body systems can namely relax *locally* in space. Using the density matrix formalism, this is equivalent to saying that the density matrix of the whole system is pure while the density matrix of the subsystem is

mixed and the latter can be therefore described by a statistical ensemble [36, 37, 38, 39]. To clarify these concepts, let's consider a quantum spin chain of N sites initially in a pure state $|\psi_0\rangle$, whose time evolution is ruled by an Hamiltonian H. We partition the system into an arbitrary but finite subsystem A and its complement $\bar{A}$ (Fig. 2.1). The density matrix of the entire system at a certain time t is given by

$$\rho_{A\cup\bar{A}}(t) = |\psi(t)\rangle\langle\psi(t)| = e^{-iHt}|\psi_0\rangle\langle\psi_0|e^{iHt} \tag{2.6}$$

which is a pure state. The reduced density matrix of the subsystem A is obtain by tracing out the degrees of freedom of the rest of the system:

$$\rho_A(t) = \mathrm{Tr}_{\bar{A}}\left[\rho_{A\cup\bar{A}}(t)\right] \tag{2.7}$$

The question is if it exists a "virtual" mixed state $\rho^{\mathrm{SS}}_{A\cup\bar{A}}$ capable of describing the stationary state of $\rho_A(t)$, i.e.

$$\lim_{t\to\infty}\lim_{N\to\infty}\rho_A(t) = \lim_{N\to\infty}\mathrm{Tr}_{\bar{A}}\left[\rho^{\mathrm{SS}}_{A\cup\bar{A}}\right]. \tag{2.8}$$

If such virtual mixed state exists for any finite subsystem A, then the system is said to relax *locally* and $\rho^{\mathrm{SS}}_{A\cup\bar{A}}$ describes the stationary state of the system.

Any expectation value of a local observable $\mathcal{O}_A$ having its support on A can be now computed in the long time limit with a statistical ensamble as

$$\lim_{t\to\infty}\mathrm{Tr}\left[\rho(t)\mathcal{O}_A\right] = \mathrm{Tr}\left[\rho^{\mathrm{SS}}_{A\cup\bar{A}}\mathcal{O}_A\right]. \tag{2.9}$$

It is important to remark that the thermodynamic limit is taken keeping the subsystem A finite, and that it has to be done before the long time limit, otherwise quantum recurrences are impossible to avoid.

2.1.2 Non-integrability and thermalization

An important question about the dynamics of a closed many-body quantum system is if interactions within the system are sufficient to make the system behave *ergodically*,which is at the basis of statistical mechanics.

Let us consider a classical system with N degrees of freedom in d spatial dimensions, represented by a point in the $2dN$ dimensional phase space; given an initial condition

$\mathbf{X_0} = (\mathbf{q_0}, \mathbf{p_0})$, the Hamiltonian $H(\mathbf{q}, \mathbf{p})$ is ergodic if the trajectory of the system in the phase space covers uniformly the constant energy hypersurface selected by the initial condition, for almost every initial state. This condition allows the replacement of time averages with phase space averages weighted with the microcanonical ensemble; hence for any operator $\mathcal{O}$:

$$\begin{aligned} \langle O \rangle_{\text{time}} &\equiv \lim_{T\to\infty} \frac{1}{T} \int_0^T dt \mathcal{O}(\mathbf{q}(t), \mathbf{p}(t)) \\ &= \int d^{dN}q d^{dN}p \mathcal{O}(\mathbf{q}, \mathbf{p}) \delta[H(\mathbf{q}, \mathbf{p}) - H(\mathbf{q_0}, \mathbf{p_0})] \equiv \langle O \rangle_{mc} \end{aligned} \tag{2.10}$$

Equations of motions for classical non integrable systems are not exactly solvable and non linear equations. KAM's theory [15] states that if the non linear amplitudes overcome a certain threshold, chaos emerges and the ergodic hypothesis is satisfied for these systems.

The most straightforward generalization of ergodicity to quantum system was performed by von Neumann [1]. We can define a microcanonical ensemble for quantum systems with the following procedure: given an Hamiltonian H with eigenstates $|n\rangle$ of energy E_n, we can coarse grain the spectrum on energy shells of width δE, in such a way that it remains smallon macroscopic scales but it contains many states. Denoting with $\mathcal{S}(E)$ the set of eigenstates of H with energy between E and $E + \delta E$, we can define the microcanonical distribution as

$$\rho_{mc}(E) = \sum_{n \in \mathcal{S}(E)} \frac{1}{N(E)} |n\rangle \langle n| , \tag{2.11}$$

where $N(E)$ is the number of states in the shell. But given now a generic initial condition in a microcanonical shell

$$|\psi_0\rangle = \sum_{n \in \mathcal{S}(E)} c_n |n\rangle , \tag{2.12}$$

the long time average of the density matrix of the system is not given, in general, by the microcanonical ensemble (2.11). Assuming the eigenstates of the system not to be degenerate, we indeed obtain

$$\begin{aligned} \lim_{T\to\infty} \frac{1}{T} \int_0^T dt |\psi(t)\rangle \langle\psi(t)| &= \sum_{m,n} c_m \bar{c}_n |m\rangle \langle n| \lim_{T\to\infty} \frac{1}{T} \int_0^T dt e^{-i(E_m - En)t} \\ &= \sum_n |c_n|^2 |n\rangle \langle n| \equiv \rho_{\text{diag}}, \end{aligned} \tag{2.13}$$

where the last step follows from a stationary phase approximation. This is the so called *diagonal ensemble* [40, 41, 42]. Note that this ensemble depends on the choice of the initial states through the overlaps $c_n = \langle n|\psi_0\rangle$ and the requirement $\rho_{mc} = \rho_{\text{diag}}$ implies that $|c_n|^2 = 1/N(E)$ for every n, which is obviously not satisfied for any initial state. Quantum ergodicity in the sense above is therefore almost never realizable. The reason is in the linearity of Schrödinger's equation, hence we cannot expect an emergence of quantum chaos.

However there are many evidences of both experimental [43, 44] and numerical nature [40, 45] that shows that thermalization can occur. The commonly accepted explanation for this behaviour is the ETH (Eigenstate Thermalization Hypothesis) [46, 47, 48]: instead of explaining the ergodicity of a thermodynamic system through the mechanism of dynamical chaos, one should instead examine the properties of matrix elements of observable quantities $\mathcal{O}_k$ in individual energy eigenstates of the system. The requirement

$$\text{Tr}\left[\rho_{mc}\mathcal{O}_k\right] = \text{Tr}\left[\rho_{\text{diag}}\mathcal{O}_k\right] \tag{2.14}$$

implies that matrix elements of these observables are constant on the energy shell and equal to the microcanonical average:

$$\text{Tr}\left[\rho_{\text{diag}}\mathcal{O}_k\right] = \sum_n |c_n|^2 \langle n|\mathcal{O}_k|n\rangle = \text{Tr}\left[\rho_{mc}\mathcal{O}_k\right] \sum_n |c_n|^2 = \text{Tr}\left[\rho_{mc}\mathcal{O}_k\right]. \tag{2.15}$$

In this picture even the initial state is a thermal but the coherence between the eigenstates initially hides it (Fig. 2.2) and time dynamics reveals it through dephasing [41].

It is important to remark, though, it has been proof that ETH is not a necessary condition to quantum thermalization [49] and that it does not apply to all cases, for example to many body localized states [50, 51]

2.1.3 Integrability and equilibration

Considering now integrable quantum systems as defined in paragraph 1.3.2, expectation values of the conserved quantities $Q^{(k)}$ are time independent

$$\text{Tr}\big(\rho(t)Q^{(k)}\big) = \text{Tr}\big(e^{-iHt}\rho(0)e^{iHt}Q^{(k)}\big) = \text{Tr}\big(\rho(t)Q^{(k)}\big) \equiv E^{(k)}, \tag{2.16}$$

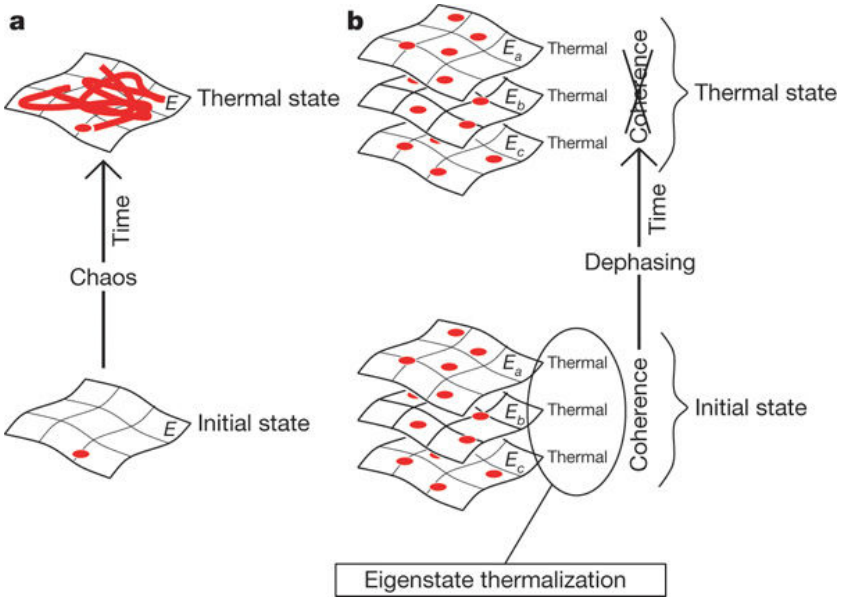

Figure 2.2: In classical mechanics (left), time evolution constructs the thermal state from an initial state that generally bears no resemblance to the former. In quantum mechanics (right), according to the ETH, every eigenstate of the hamiltonian always implicitly contains a thermal state. The coherence between the eigenstates initially hides it, but time dynamics reveals it through dephasing. Figure taken from [41].

where the invariance of the trace under cyclic permutations and the fact that $[Q^{(k)}, H] = 0$ were used.

An immediate consequence is that such systems cannot thermalize because the system retains memory of the initial expecation values of all conserved quantities at all times. The works of Jaynes [34, 35] on the maximum entropy ensemble then suggest that the stationary state density matrix is given by a *generalized Gibbs ensemble* (GGE) [40]

$$\rho^{\mathrm{SS}} \equiv \rho^{\mathrm{GGE}} = \frac{e^{\sum_n \lambda_n Q^{(n)}}}{\mathrm{Tr}\left(e^{\sum_n \lambda_n Q^{(n)}}\right)}. \tag{2.17}$$

The Lagrange multipliers λ_k are fixed by the initial conditions (2.16), requiring

$$\lim_{N\to\infty} \frac{E^{(k)}}{N} = \lim_{N\to\infty} \frac{1}{N} \mathrm{Tr}\left(\rho^{\mathrm{GGE}} Q^{(k)}\right) \tag{2.18}$$

To distinguish this process from thermalization it has been given the name of *equilibration*. This conjecture motivates the need of a clear characterization of quantum integrable systems and it also recovers part of the analogy with the classical case: even if the thermalization mechanism may be different, integrability is still a sufficient condition for non-thermalization.

Nevertheless, this definition of GGE suffers from the same ambiguities of the definition of integrability. Instead of using local conserved quantities, GGE are often formulated using conserved mode occupation numbers [40]. The crucial point is that conservation laws are usually linearly related to the mode occupation number. This implies that the GGE describing the stationary state can be constructed either from the local conservation laws or from the mode occupation number. There are though cases in which this is not valid. In this cases the stationary state is not always locally equivalent to a GGE [52, 53, 54].

2.2 Definition of a quantum quench

In the previous sections we did not specify how the system is put out of equilibrium or which are the initial conditions of the system. Indeed there can be many possible ways to perturb a system and the outcome is expected to depend on the particular choice made. We now introduce the concept of *quantum quench* [5].

First suppose we have a quantum system prepared in an eigenstate $|\psi_{n,0}\rangle$ of the hamiltonian function H at time $t = 0$. For $t > 0$ we make H time dependent and we ask how the initial state evolves. Since the hermiticity of the Hamiltonian is preserved, at each t we have an instantaneous orthonormal basis of eigenvector

$$H_t \left|\psi_{n,t}\right\rangle = \left|\psi_{n,t}\right\rangle E_{n,t} \qquad \left\langle\psi_{n,t}|\psi_{m,t}\right\rangle = \delta_{n,m} \qquad \sum_n \left|\psi_{n,t}\right\rangle \left\langle\psi_{n,t}\right| = \mathbb{1} \ \ \forall t \tag{2.19}$$

Integrating the time dependent Schrödinger equation

$$i\frac{\partial}{\partial t}\left|\psi_{n,t}\right\rangle = H_t \left|\psi_{n,t}\right\rangle = E_{n,t}\left|\psi_{n,t}\right\rangle, \tag{2.20}$$

one finds

$$\left|\psi_{n,t}(t)\right\rangle = e^{i\theta_n(t)}\left|\psi_{n,t}\right\rangle, \tag{2.21}$$

where $\theta_n(t)$ is the so called *dynamical phase factor*:

$$\theta_n(t) = \int_0^t dt' E_{n,t'}. \tag{2.22}$$

Thanks to the completness relation the initial state can be expressed in terms of the instantaneous eigenstates and evolved

$$\left|\psi_{n,0}(t)\right\rangle = \sum_m c_{m,t} e^{i\theta_m(t)}\left|\psi_{m,t}\right\rangle \qquad c_{m,0} = \delta_{n,m}. \tag{2.23}$$

The coefficients $c_{n,t}$ can be found substituting the latter expression in the time dependent Schrödinger equation:

$$i\sum_m e^{i\theta_m(t)}\{\dot{c}_{m,t}\left|\psi_{m,t}\right\rangle+i\dot{\theta}_m(t)c_{m,t}\left|\psi_{m,t}\right\rangle+c_{m,t}|\dot{\psi_{m,t}}\rangle\}=\sum_m e^{i\theta_m(t)}c_{m,t}E_{m,t}\left|\psi_{m,t}\right\rangle, \quad (2.24)$$

which implies

$$\dot{c}_{l,t}=-\sum_m e^{-i\int_0^t dt'(E_{m,t'}-E_{l,t'})}c_{m,t}\left\langle\psi_{l,t}\middle|\dot{\psi_{m,t}}\right\rangle. \quad (2.25)$$

An expression for $\left\langle\psi_{l,t}\middle|\dot{\psi_{m,t}}\right\rangle$ is found by differentiating the eigenvalues equation in (2.19) and projecting on $|\psi_{l,t}\rangle$:

$$\langle\psi_{l,t}|\dot{H}_t\left|\psi_{m,t}\right\rangle+E_{l,t}\left\langle\psi_{l,t}\middle|\dot{\psi_{m,t}}\right\rangle=\dot{E_{m,t}}\delta_{l.m}+E_{m,t}\left\langle\psi_{l,t}\middle|\dot{\psi_{m,t}}\right\rangle. \quad (2.26)$$

Equation (2.25) then becomes

$$\dot{c}_{m,t}=-c_{m,t}\left\langle\psi_{m,t}\middle|\dot{\psi}_{m,t}\right\rangle-\sum_{l\neq m}e^{-i\int_0^t dt'(E_{m,t'}-E_{l,t'})}c_{l,t}\frac{\langle\psi_{m,t}|\dot{H}_t\left|\psi_{l,t}\right\rangle}{E_{l,t}-E_{m,t}}. \quad (2.27)$$

From here it follows that if

$$|\langle\psi_{m,t}|\dot{H}_t\left|\psi_{l,t}\right\rangle|\ll|E_{l,t}-E_{m,t}|\qquad\forall l,m \quad (2.28)$$

then

$$c_{m,t}=e^{i\alpha_m(t)}c_{m,0}, \quad (2.29)$$

where $\alpha_m(t)$ is called *geometric phase*:

$$i\alpha_m(t)=-\int_0^t dt'\left\langle\psi_{m,t'}\middle|\dot{\psi_{m,t'}}\right\rangle. \quad (2.30)$$

Note that $\alpha_m(t)$ is real since

$$0=\frac{d}{dt}\langle\psi_{m,t'}|\psi_{m,t'}\rangle=\left\langle\psi_{m,t'}\middle|\dot{\psi_{m,t'}}\right\rangle+\overline{\left\langle\psi_{m,t'}\middle|\dot{\psi_{m,t'}}\right\rangle}. \quad (2.31)$$

The evolution of the initial state is eventually given by

$$|\psi_{n,0}(t)\rangle=e^{i\alpha_n(t)}e^{i\theta_n(t)}\left|\psi_{n,0}\right\rangle. \quad (2.32)$$

This is essentially the *adiabatic theorem* by Max Born and Vladimir Fock [55]: if (2.28) holds (the Hamiltonian varies slowly with respect to the gap between the $E_{n,t}$ and the

rest of the energy spectrum), the initial state evolves without changing quantum numbers and picking up phase factors. The phase factor $\alpha_n(t)$ can also be cancelled out by an appropriate choice of gauge (if the adiabatic evolution is not cyclic, otherwise it becomes a gauge invariant physical quantity known as Berry phase [56]).

A quantum quench occurs when the adiabatic aproximation (2.28) is not valid. This can happen either when the Hamiltonian variation rate is not small enough, or when there is no gap between the energy eigenvalue of the initial state and the rest of the spectrum. In both cases there isn't a precise theoretical approach to the problem and perturbation theory cannot be applied since the change in the Hamiltonian isn't small in general. Seminal works on quantum quenches ([57, 11, 58, 5, 59, 60]) investigated different ways of taking the system out of equilibrium. In this thesis we concentrate on a standard procedure which is called *sudden quench*.

In a sudden quench the many-body system is prepared in a pure state which is an eigenstate of the initial Hamiltonian, the latter depending on a set of parameters $\{g_i^0\}$:

$$H(\{g_i^0\})\,|\psi_0\rangle = |\psi_0\rangle\,E \tag{2.33}$$

At $t = 0$ we suddenly quench the set of parameters to new values $\{g_i\}$ and, since the system remains isolated, consider the unitary time evolution with the new Hamiltonian $H(\{g_i\})$. At times $t > 0$ the state of the system is found solving the time-dependent Schrödinger equation

$$|\psi(t)\rangle = e^{iH(\{g_i\})t}\,|\psi_0\rangle\,. \tag{2.34}$$

Furthermore, the quench is said to be *global* if the change of the coupling constants $\{g_i^0\}$ is the same in the whole chain.

Throughout this work, we consider as initial pure state $|\psi_0\rangle$ the ground state of the system, mainly for two reasons:

- they exhibit low entanglement entropy;

- they allow us to deal with quantum phase transitions.

These two features were introduced in the previous chapter.

A crucial property of a global quantum quench is that energy in conserved at all $t > 0$ and the post-quench energy density is larger than the ground state energy per site. This means that through the quantum quench we explore a region of Hilbert space that is macroscopically different from the sector containing the ground state and low-lying excitations [33].

2.3 Spreading of correlations after a quantum quench

How does the system behave after a quantum quench? And hat is the theoretical picture that allow us to compute expectation values of local operators? Let's consider an integrable quantum system. Suppose that the latter is mappable into a free fermion model, hence both the pre-quench and the post-quench Hamiltonians can be put in the diagonal form (1.19).

$$\begin{aligned} &\text{Pre-quench:} && H(\{g_i^0\}) = \sum_k \epsilon_{\{g_i^0\}}(k)\tilde{\eta}_k^\dagger \tilde{\eta}_k + E_0(\{g_i^0\}) \\ &\text{Post-quench:} && H(\{g_i\}) = \sum_k \epsilon_{\{g_i\}}(k)\eta_k^\dagger \eta_k + E_0(\{g_i\}), \end{aligned} \tag{2.35}$$

with the corresponding vacua, satisfying

$$\begin{aligned} \tilde{\eta}_k \left|0;\{g_i^0\}\right\rangle &= 0 \qquad \forall k \\ \eta_k \left|0;\{g_i\}\right\rangle &= 0 \qquad \forall k \end{aligned} \tag{2.36}$$

with fermionic commutation relations

$$\{\eta_k, \eta_p^\dagger\} = \delta_k, p. \tag{2.37}$$

It is possible to put in relation the two sets of creation and annihilation operators through a Bogoliubov transformation [61]:

$$\begin{aligned} \tilde{\eta}_p &= \sum_k (\Theta_{pk}\eta_k + \Omega_{pk}\eta_k^\dagger) \\ \tilde{\eta}_p^\dagger &= \sum_k (\Theta_{kp}^*\eta_k^\dagger + \Omega_{kp}^*\eta_k). \end{aligned} \tag{2.38}$$

The physical interpretation of Ω is the following: suppose one desires to compute the number of quasi-particles excitations of the pre-quench Hamiltonian on the vacuum of the quenched system $\langle 0;\{g_i\}|\,\tilde{\eta}_p^\dagger\tilde{\eta}_p\,|0;\{g_i\}\rangle$. Taking (2.36) and (2.38) into account:

$$\tilde{\eta}_p \left|0;\{g_i\}\right\rangle = \sum_k (\Theta_{pk}\eta_k + \Omega_{pk}\eta_k^\dagger)\left|0;\{g_i\}\right\rangle = \sum_k \Omega_{pk}\left|1_k;\{g_i\}\right\rangle, \tag{2.39}$$

so that

$$\langle 0;\{g_i\}|\,\tilde{\eta}_p^\dagger\tilde{\eta}_p\,|0;\{g_i\}\rangle = \sum_k |\Omega_{pk}|^2. \tag{2.40}$$

Hence the new vacuum is filled with quasi-particle of the pre-quench Hamiltonian (and viceversa). Indeed, since both sets of quasi-particles can be used to generate the Fock

space, we can express the ground state of the pre-quench Hamiltonian as excited states of the quenched system. We can define this relation by taking (2.36) into account:

$$\tilde{\eta}_p \left|0; \{g_i^0\}\right\rangle = 0 = \sum_k (\Theta_{pk}\eta_k + \Omega_{pk}\eta_k^\dagger) \left|0; \{g_i^0\}\right\rangle . \tag{2.41}$$

Multiplying this expression by $\sum_p \Theta_{ip}^{-1}$ we find the equation

$$\eta_i \left|0; \{g_i^0\}\right\rangle = \sum_k \aleph_{ik}\eta_k^\dagger \left|0; \{g_i^0\}\right\rangle , \tag{2.42}$$

where

$$\aleph_{ik} = -\sum_p \Theta_{ip}^{-1}\Omega_{pk}. \tag{2.43}$$

The solution of (2.43) is given by [62]

$$\left|0; \{g_i^0\}\right\rangle = \exp\left\{\frac{1}{2}\sum_{ik} \aleph_{ij}\eta_i^\dagger\eta_k^\dagger\right\} |0; \{g_i\}\rangle . \tag{2.44}$$

In our models, that are translational invariant, we'll see that

$$\aleph_{ik} = \delta_{i,-k}\aleph_{i,-i} \equiv \delta_{i,-k}\aleph_i, \tag{2.45}$$

that give us an expression of the pre-quench ground state as *boundary state* [63] (more on the matter in Appendix A):

$$\left|0; \{g_i^0\}\right\rangle = \exp\left\{\sum_{k>0} \aleph_k\eta_k^\dagger\eta_{-k}^\dagger\right\} |0; \{g_i\}\rangle , \tag{2.46}$$

where the function $\aleph$ is referred as *kernel* of the state.

This gives a precise physical interpretation for what happens after a quantum quench in this case: when changing the set of parameters in the Hamiltonian, the state of the system is a superposition of excited states given by pairs of quasi-particles with opposite momenta (in such a way the total momentum is conerved). These excitations propagate with a dispertion relation given by the post-quench Hamiltonian $\epsilon_{\{g_i\}}(k)$ and have therefore a maximum velocity of propagation given by

$$v_{\max} = \max_k \left|\frac{d\epsilon_{\{g_i\}}(k)}{dk}\right|. \tag{2.47}$$

This means that even if the models are non-relativistic there exists a maximum velocity of propagation of the information. This feature has a profound impact on time depenence of the expectation values of local operators after a quench.

Suppose we want to calculate the connected correlation function of a local operator $\mathcal{O}$, whose support is a single site of the chain:

$$G_2^c(l;t) = \langle\psi(t)|\,\mathcal{O}_k\mathcal{O}_{k+l}\,|\psi(t)\rangle - \langle\psi(t)|\,\mathcal{O}_k\,|\psi(t)\rangle\,\langle\psi(t)|\,\mathcal{O}_{k+l}\,|\psi(t)\rangle\,. \tag{2.48}$$

At $t = 0$, the state is characterized by a finite correlation length ξ and the correlation function is extremely small at large spatial separations:

$$G_2^c(l;t) \propto e^{-l/\xi}. \tag{2.49}$$

At times $t > 0$ quasi-particles start propagating throughout the system. A measurement at site k will be influenced by quasi-particles within *the backwards light cone* $[k - v_{\max}t, k + v_{\max}t]$. At time

$$t = \frac{l}{2v_{\max}} \tag{2.50}$$

the backwards light cones emanating from site k and site $k + l$ touch and the the average measurements of the two sites become correlated.

This physical interpratation was given by Calabrese and Cardy [11, 58] and light cone effects after quantum quenches have been analyzed and observed various of models. In Fig. 2.3 the time dependent part of the connected density-density correlator of a one dimensional fermionic pairing model is displayed.

2.3.1 Relation to Lieb-Robinson bounds

As shown by Lieb and Robinson [64, 65], the velocity of information transfer in quantum spin chains in effectively bounded and there exists a causal structure in commutators of local operators at different times. Given two local operators $\mathcal{O}_X$ and $\mathcal{O}_Y$ having their supports on X and Y respectively that are spatially separated by distance L,

$$||[\mathcal{O}_X(t), \mathcal{O}_Y(0)]|| \leq c\min\{\mu(X), \mu(Y)\}\|\mathcal{O}_X\|\|\mathcal{O}_Y\|e^{-\frac{L-vt}{\xi'}}, \tag{2.51}$$

where $\mu(X)$ indicates the numbers of sites in X, $\|.\|$ denotes the operator norm and c, v and ξ' are constants.

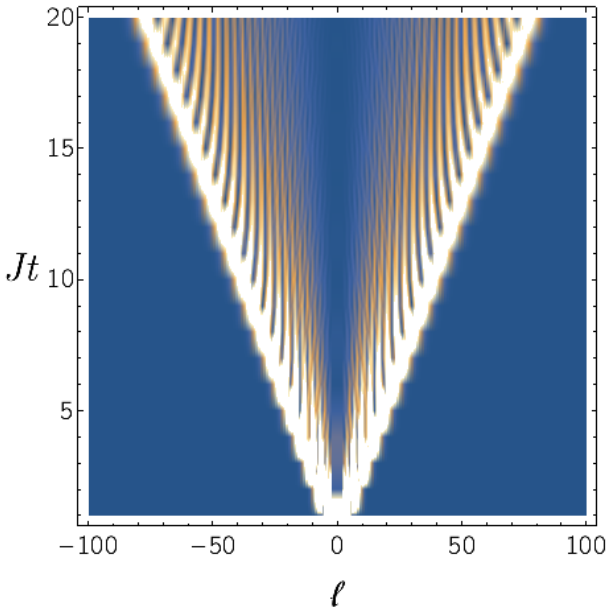

Figure 2.3: Time dependent part of the connected density-density correlator after a quantum quench. A light cone effect is clearly visible [33].

The Lieb-Robinson bound has important consequences for quantum quenches starting in initial states with finite correlation lengths and evolving under short-ranged Hamiltonians. It was shown in [66] that (2.51) implies a bound on the connected two point functions

$$\langle\psi(t)|\,\mathcal{O}_X\mathcal{O}_Y\,|\psi(t)\rangle - \langle\psi(t)|\,\mathcal{O}_X\,|\psi(t)\rangle\,\langle\psi(t)|\,\mathcal{O}_Y\,|\psi(t)\rangle \leq c'(\mu(X)+\mu(Y))e^{-\frac{L-2vt}{\chi}}, \quad (2.52)$$

with c' and χ constants.

2.4 Entanglement entropy after a quantum quench

How does entanglement entropy evolve after a sudden quench? We showed with the quasi-particle description that after a quench from the ground state, whose entanglement entropy follows an area law, the new state for $t > 0$ is given by a boundary state, obtained as superposition of excited states. Hence one should expect that in the long time limit entanglement entropy follows a volume law.

It was actually proved in [11] that the entropy in one dimensional models between the degrees of freedom in an interval A of length l and its complement $\bar{A}$, starting

from a pure state which is not an eigenstate of the Hamiltonian that determines time evolution, increases linearly with time t up to $t^* = l/2v$, after which it saturates at a value proportional to l.

This result was obtained using path integral methods of quantum field theory as well as with explicit computations for the transverse Ising spin chain, but it is believed to hold in a wider class of systems, since it can be derived by causality arguments with the quasi-particle description already introduced.

The initial state $|\psi_0\rangle$ has an extensively high energy relative to the ground state of the post-quenched Hamiltonian and therefore acts as a source of quasiparticle excitations, emitted in pairs from any point of the initial state. Those quasi-particles originating from different points (further apart than the correlation length ξ typical of the initial state) are incoherent, but pairs of particles originating from the same point or from points within ξ are highly entangled. Suppose that the cross section for producing such a pair of particles of momenta p' and p'' from a certain point in space is $\sigma(p', p'')$ and that since they separate they move classically, with no interaction between them.

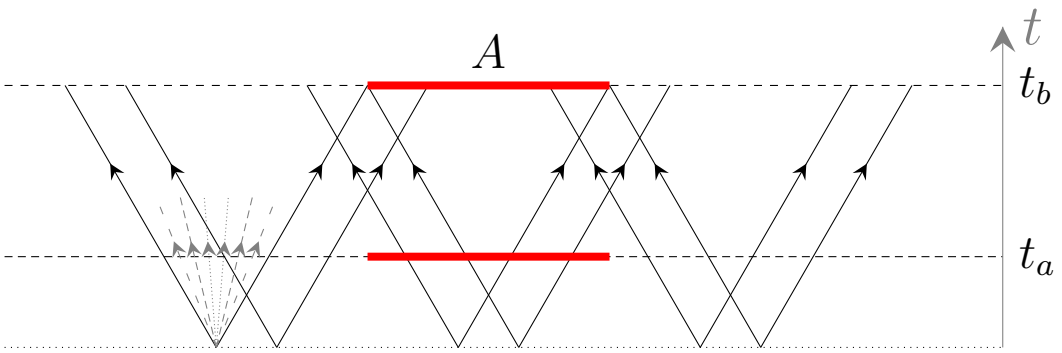

Figure 2.4: Space-time picture illustrating how oppositely moving correlated quasi-particles increase entanglement between an interval A and the rest of the system.

The classical velocity is given by $v(p) = d\epsilon/dp$, where $\epsilon(p)$ is the dispersion relation and we fix the maximum allowed speed to 1, that is $|v(p)| \leq 1$. A quasi-particle generated at $(x, t = 0)$ is therefore at $x + v(p)t$ at time t. Consider these quasi-particles as they reach either A or $\bar{A}$ at time t. The entanglement between the two sets increases if a pair of entangled particles emitted from a point x arrives simultaneously at $x' \in A$ and $x'' \in \bar{A}$ (Fig. 2.4). The entanglement entropy between x' and x'' is proportional to the length of the interval in x for which this can be satisfied. Thus the total entanglement entropy is

$$S_A(t) \simeq \int_{x' \in A} dx' \int_{x'' \in \bar{A}} dx'' \int_{-\infty}^{\infty} dx \int dp' dp'' \sigma(p', p'') \delta(x' - x - v(p')t) \delta(x'' - x - v(p'')t) \qquad (2.53)$$

Considering now that A is an interval of length l then the total entanglement is twice that between A and the real axis to the right of A, which corresponds to taking $p' < 0$, $p'' > 0$ in the above. The integration over the coordinates then gives $\max((v(p') + v(p''))t, l)$ (see Fig. 2.5), so that

$$\begin{aligned} S_A(t) \simeq 2t \int_{-\infty}^{0} dp' \int_{0}^{\infty} dp'' \sigma(p', p'') \{v(-p') + v(p'')\} \theta(l - [v(-p') + v(p'')]t) \\ + 2l \int_{-\infty}^{0} dp' \int_{0}^{\infty} dp'' \sigma(p', p'') \theta([v(-p') + v(p'')]t - l), \end{aligned} \tag{2.54}$$

where $\theta(x)$ is the Heaviside step function. Since $|v(p)| \leq 1$, the second term cannot contribute if $t < t* = l/2$ so that $S_A(t)$ is strictly proportional to t. On the other hand, as $t \to \infty$, the first term is negligible and S_A is asymptotically proportional to l.

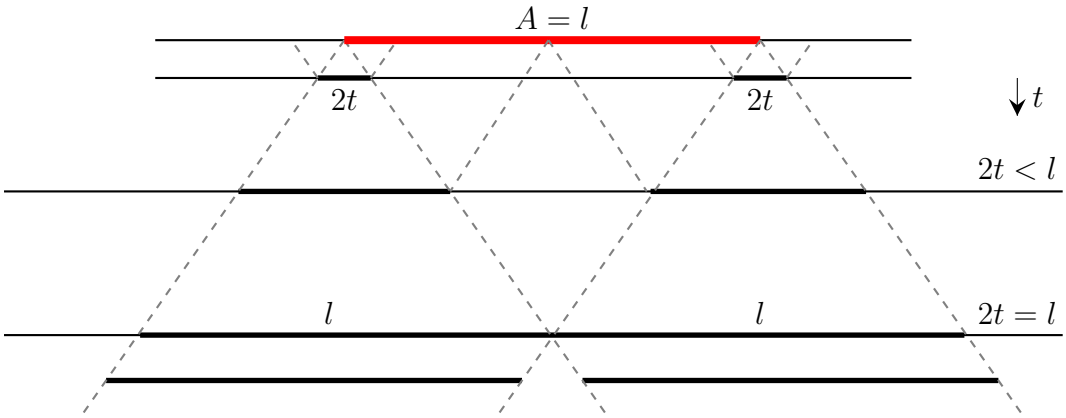

Figure 2.5: Space-time picture of the entanglement entropy dynamics. For times such that $2t < l$ the entanglement entropy increases linearly with time; for later times it saturates to a value proportional to the lenght l of the subsystem considered.

However, unless $|v| = 1$ everywhere (as in the conformal field theory case), S_A is not strictly proportional to l for $t > t^*$ and there is a slow increase towards the asymptotic value. This can be understood since, on the lattice, there are quasi-particles excitations which travel with a group velocity that is less than the maximum allowed value.

Chapter 3

The infinite Time Evolving Block Decimation algorithm

This belief is handed down in Beersheba: that, suspended in the heavens, there exists another Beersheba, where the city's most elevated virtues and sentiments are poised, and that if the terrestrial Beersheba will take the celestial one as its model the two cities will become one.

- Italo Calvino, *Invisible Cities*

The content of this chapter is aimed at describing the algorithm used in the code written to simulate the evolution of quantum systems after a quench. After introducing a useful representation for quantum states, the *matrix product state* (MPS) *representation*, the infinite Time Evolving Block Decimation algorithm is presented and it is explained how this can be adapted for the computation of ground states. The chapter ends with the parameters of the simulations run.

3.1 Matrix Product States

Suppose our quantum system is composed by a lattice of L sites with d-dimensional Hilbert spaces $\mathcal{H}_k \simeq \mathbb{C}^d$, $i = 1, \ldots, L$, spanned by the local bases $|\sigma_k\rangle$. We can express the most general quantum state on the lattice as

$$|\psi\rangle = \sum_{\sigma_1,\ldots,\sigma_L} C_{\sigma_1\ldots\sigma_L} |\sigma_1 \ldots \sigma_L\rangle \,. \tag{3.1}$$

We now introduce a representation of the state, and therefore of the coefficient $C_{\sigma_1\dots\sigma_L}$, called *Matrix Product State* (MPS) representation, that gives a more local notion of the state.

By means of the SVD, we can reach this representation in different ways [21]:

Left-canonical MPS

First of all the state vector with d^L components can be reshaped into a matrix of dimension $(d \times d^{L-1})$, their coefficients being related as

$$\Psi_{\sigma_1,(\sigma_1\dots\sigma_L)} = C_{\sigma_1\dots\sigma_L}. \tag{3.2}$$

Performing now the SVD (1.23) on the matrix Ψ, we obtain

$$C_{\sigma_1\dots\sigma_L} = \Psi_{\sigma_1,(\sigma_1\dots\sigma_L)} = \sum_{\alpha_1}^{r_1} U_{\sigma_1,\alpha_1} S_{\alpha_1,\alpha_1} (V^\dagger)_{\alpha_1,\sigma_1\dots\sigma_L} \equiv \sum_{\alpha_1}^{r_1} U_{\sigma_1,\alpha_1} C_{\alpha_1\sigma_2\dots\sigma_L} \tag{3.3}$$

Note that the index α_1 takes at most d values. The matrix U_{σ_1,α_1} can be combined in a collection of d row vectors A^{σ_1} with entries $A^{\sigma_1}_{\alpha_1} = U_{\sigma_1,\alpha_1}$; we also reshape $C_{\alpha_1\sigma_2\dots\sigma_L}$ as a matrix $\Psi_{(\alpha_1\sigma_2),(\sigma_3\dots\sigma_L)}$ of size $(r_1 d \times d^{L-2})$. The latter can be again decomposed, obtaining

$$\begin{aligned} C_{\sigma_1\dots\sigma_L} &= \sum_{\alpha_1}^{r_1}\sum_{\alpha_2}^{r_2} A^{\sigma_1}_{\alpha_1} U_{(\alpha_1\sigma_2),\alpha_2} S_{\alpha_2,\alpha_2} (V^\dagger)_{\alpha_2,(\sigma_3\dots\sigma_L)} \\ &= \sum_{\alpha_1}^{r_1}\sum_{\alpha_2}^{r_2} A^{\sigma_1}_{\alpha_1} A^{\sigma_2}_{\alpha_1,\alpha_2} \Psi_{(\alpha_2\sigma_3),(\sigma_4\dots\sigma_L)}, \end{aligned} \tag{3.4}$$

where we have again reorganized $U_{(\alpha_1\sigma_2),\alpha_2}$ into d matrices of size $(r_1 \times r_2)$, and multiplied S and $V^\dagger$, to be reshaped into a matrix Ψ of dimension $(r_2 d \times d^{L-3})$ where $r_2 \le r_1 \le d \le d^2$. Iterating the procedure we finally obtain

$$C_{\sigma_1\dots\sigma_L} = \sum_{\alpha_1,\dots,\alpha_{L-1}} A^{\sigma_1}_{\alpha_1} A^{\sigma_2}_{\alpha_1,\alpha_2} \dots A^{\sigma_{L-1}}_{\alpha_{L-2},\alpha_{L-1}} A^{\sigma_L}_{\alpha_{L-1}}. \tag{3.5}$$

The quantum state (3.1) can be then represented exactly in the form [67, 6, 68]

$$|\psi\rangle = \sum_{\sigma_1,\dots,\sigma_L} A^{\sigma_1} \dots A^{\sigma_L} |\sigma_1 \dots \sigma_L\rangle, \tag{3.6}$$

where we have express the sums over the indices α_k, called *bond indices*, as matrix multiplications. The index σ_k is instead called *physical index*.

The maximal dimensions of the matrices are reached when for each SVD involved in the computation, the number of non zero singular values is equal to the upper bound. Assuming L even, these are $(1\times d), (d\times d^2), \ldots, (d^{L/2-1}\times d^{L/2}), (d^{L/2}\times d^{L/2-1}), \ldots, (d\times 1)$. That shows that the exact representation (3.6) is of no practical use, since the bond dimension of the matrices increase exponentially towards the centre of the lattice, and approximations are necessary.

Since U matrices have orthonormal colums, we have the following A-matrices relation:

$$\begin{aligned}\delta_{\alpha_k\alpha'_k} &= \sum_{\alpha_{k-1}\sigma_k} U^{\dagger}_{\alpha_k,(\alpha_{k-1}\sigma_k)} U_{(\alpha_{k-1}\sigma_k),\alpha'_k} \\ &= \sum_{\alpha_{k-1}\sigma_k} (A^{\sigma_k\dagger})_{\alpha_k,\alpha_{k-1}} A^{\sigma_k}_{\alpha_{k-1},\alpha'_k} \\ &= \sum_{\sigma_k} (A^{\sigma_k\dagger} A^{\sigma_k})_{\alpha_k,\alpha'_k},\end{aligned} \tag{3.7}$$

or, in a more concise expression,

$$\sum_{\sigma_k} A^{\sigma_k\dagger} A^{\sigma_k} = \mathbb{1} \tag{3.8}$$

Fot later purposes it is also useful to introduce the *transfer matrix* T^L

$$T^{L,\sigma_k}_{\alpha\alpha',\beta\beta'} = \sum_{\sigma_k} A^{\sigma_k}_{\alpha\beta} (A^{\sigma_k}_{\alpha'\beta'})^*. \tag{3.9}$$

We can express the orthonormality condition in terms of the latter as

$$\delta_{\alpha,\alpha'} T^{L,\sigma_k}_{\alpha\alpha',\beta\beta'} = \eta \delta_{\beta,\beta'}, \tag{3.10}$$

with eigenvalue $\eta = 1$.

Matrices that obey this condition are referred to as *left-normalized* and matrix product states that consist only of left-normalized matrices are called *left-canonical*.

For MPS representation it is possible to introduce a pictorical way of representing states, similar to the Penrose graphical notation. If a tensor has n indices, we can representate it with some geometrical shape with n lines coming out of it. Contraction of indices are furthermore represented by joining the index lines together. With this notation the procedure to obtain a left-canonical MPS can be illustrated as in Fig. 3.1.

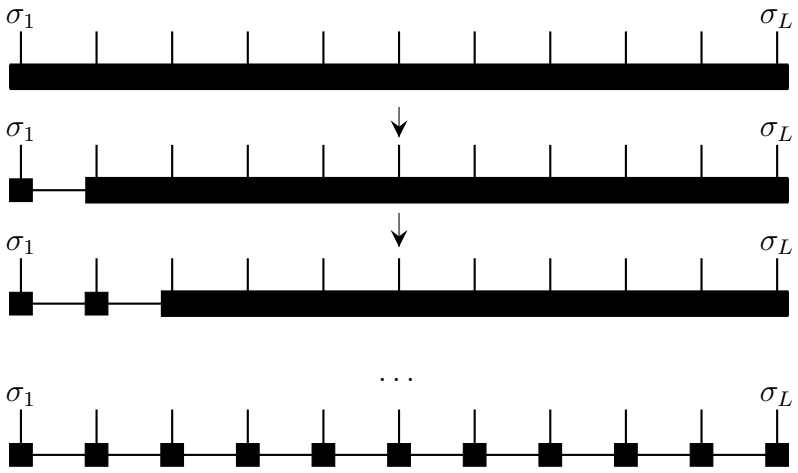

Figure 3.1: Graphical representation of the procedure to obtain a left canonical MPS.

Right-canonical MPS

This procedure is formally identical to the previous one, but starting from site L:

$$\begin{aligned} C_{\sigma_1 \ldots \sigma_L} &= \Psi_{(\sigma_1 \ldots \sigma_{L-1}),\sigma_L} \\ &= \sum_{\alpha_{L-1}}^{r_{L-1}} U_{(\sigma_1 \ldots \sigma_{L-1}),\alpha_{L-1}} S_{\alpha_{L-1},\alpha_{L-1}} (V^\dagger)_{\alpha_{L-1},\sigma_L} \\ &= \sum_{\alpha_{L-1}}^{r_{L-1}} \Psi_{(\sigma_1 \ldots \sigma_{L-2}),(\sigma_{L-1}\alpha_{L-1})} B^{\sigma_L}_{\alpha_{L-1}} \\ &= \sum_{\alpha_1,\ldots,\alpha_{L-1}} B^{\sigma_1}_{\alpha_1} B^{\sigma_2}_{\alpha_1\alpha_2} \ldots B^{\sigma_{L-1}}_{\alpha_{L-2}\alpha_{L-1}} B^{\sigma_L}_{\alpha_{L-1}}, \end{aligned} \tag{3.11}$$

where we have reshaped $(V^\dagger)_{\alpha_{L-1},\sigma_L}$ into d column vectors $B^{\sigma_L}_{\alpha_{L-1}}$, $(V^\dagger)_{(\alpha_{L-2}\sigma_L),\alpha_{L-1}}$ into d matrices $B^{\sigma_L - 1}_{\alpha_{L-2},\alpha_{L-1}}$ and so on.

We then have the MPS representation:

$$|\psi\rangle = \sum_{\sigma_1,\ldots,\sigma_L} B^{\sigma_1} \ldots B^{\sigma_L} |\sigma_1 \ldots \sigma_L\rangle , \tag{3.12}$$

B-matrices have the same maximal dimensions as the A-matrices and also

$$\sum_{\sigma_k} B^{\sigma_k} B^{\sigma_k \dagger} = \mathbb{1} \tag{3.13}$$

since every V has orthonormal rows: As in the previous case we can define a proper *transfer matrix* T^R

$$T^{R,\sigma_k}_{\alpha\alpha',\beta\beta'} = \sum_{\sigma_k} A^{\sigma_k}_{\alpha\beta}(A^{\sigma_k}_{\alpha'\beta'})^*. \tag{3.14}$$

to express the orthonormality condition as

$$T^{L,\sigma_k}_{\alpha\alpha',\beta\beta'}\delta_{\beta,\beta'} = \eta\delta_{\alpha,\alpha'}, \tag{3.15}$$

with eigenvalue $\eta = 1$.

B-matrices are referred to as *right-normalized* and MPS entirely built from such matrices are called *right-canonical*. In Fig. 3.2 the graphical representation of the procedure is illustrated.

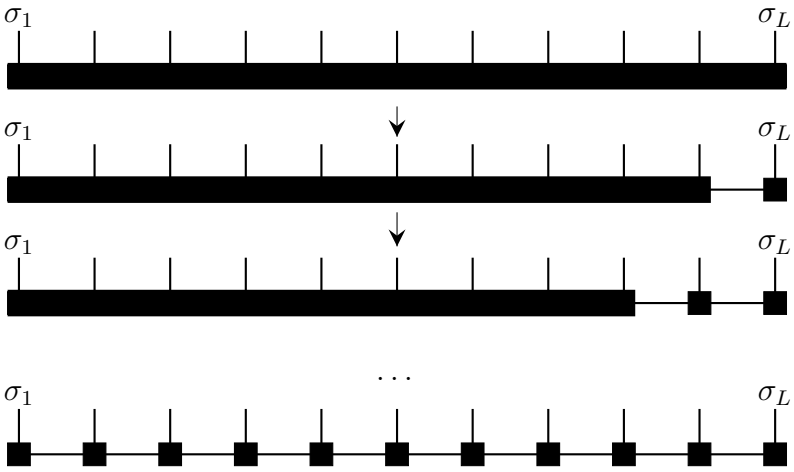

Figure 3.2: Graphical representation of the procedure to obtain a right canonical MPS.

Mixed-canonical MPS

Of course it is also possible to mix the two decompositions. Let us assume we've performed a left decomposition from site 1 to l, such that

$$C_{\sigma_1\ldots\sigma_L} = \sum_{\alpha_l}(A^{\sigma_1}\ldots A^{\sigma_l})_{\alpha_l}S_{\alpha_l,\alpha_l}(V^\dagger)_{\alpha_l,(\sigma_{l+1}\ldots\sigma_L)}. \tag{3.16}$$

Now we can carry out the successive SVDs from the right, reshaping $V^\dagger$ as in the right-canonical procedure, obtaining

$$(V^\dagger)_{\alpha_l,(\sigma_{l+1}\ldots\sigma_L)} = \sum_{\alpha_{l+1},\ldots,\alpha_{L-1}} B^{\sigma_{l+1}}_{\alpha_l,\alpha_{l+1}}\ldots B^{\sigma_L}_{\alpha_{L-1}}. \tag{3.17}$$

We end therefore with the representation

$$C_{\sigma_1 \dots \sigma_L} = A^{\sigma_1} \dots A^{\sigma_l} S B^{\sigma_{l+1}} \dots B^{\sigma_L}. \tag{3.18}$$

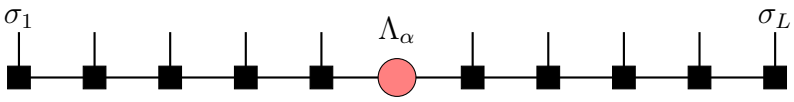

Figure 3.3: Graphical representation of the mixed-canonical MPS (3.18).

This representation is particularly useful to for obtaining the Schmidt decomposition (1.28). Identifying site $\{1, \dots, l\}$ as the L system and sites $\{l+1, \dots, L\}$ as the R system, and introducing the vectors

$$\begin{aligned} |\alpha_l\rangle_L &= \sum_{\sigma_1,\dots,\sigma_l} (A^{\sigma_1} \dots A^{\sigma_l})_{\alpha_l} |\sigma_1 \dots \sigma_l\rangle \\ |\alpha_l\rangle_R &= \sum_{\sigma_{l+1},\dots,\sigma_L} (B^{\sigma_{l+1}} \dots B^{\sigma_L})_{\alpha_l} |\sigma_{l+1} \dots \sigma_L\rangle \,, \end{aligned} \tag{3.19}$$

setting again $\Lambda_\alpha = S_{\alpha,\alpha}$ the state take the form

$$|\psi\rangle = \sum_{\alpha_l} \Lambda_{\alpha_l} |\alpha_l\rangle_L \otimes |\alpha_l\rangle_R \,, \tag{3.20}$$

which is the Schmidt decomposition provided the states on L and R are orthonormal respectively (Fig. 3.3). But this is indeed the case thanks to the left and right normalization of A adn B matrices respectively. As an example:

$$\begin{aligned} \langle\alpha|\alpha'\rangle_L &= \sum_{\sigma_1,\dots,\sigma_l} (A^{\sigma_1} \dots A^{\sigma_l})^*_{\alpha_l} (A^{\sigma_1} \dots A^{\sigma_l})_{\alpha'_l} \\ &= \sum_{\sigma_1,\dots,\sigma_l} (A^{\sigma_1} \dots A^{\sigma_l})^\dagger_{\alpha_l} (A^{\sigma_1} \dots A^{\sigma_l})_{\alpha'_l} \\ &= \sum_{\sigma_1,\dots,\sigma_l} (A^{\sigma_l \dagger} \dots A^{\sigma_1 \dagger} A^{\sigma_1} \dots A^{\sigma_l})_{\alpha_l,\alpha'_l} \\ &= \delta_{\alpha_l,\alpha'_l} \end{aligned} \tag{3.21}$$

Vidal decomposition and canonical MPS

In the previous paragraphs we have introduce different ways to represent the same state through an MPS. However the degree of non-uniqueness of the representation is much

higher: MPS are not unique in the sense that a gauge degree of freedom exists. Once that a representation

$$|\Psi\rangle = \sum_{\sigma_1,\ldots,\sigma_L} M^{\sigma_1} \ldots M^{\sigma_L} |\sigma_1 \ldots \sigma_L\rangle \tag{3.22}$$

is chosen, where M^{σ_i} is a matrix of dimension $(\chi_{i-1} \times \chi_i)$ we can perform the following transformation

$$\begin{aligned} M^{\sigma_i} &\to M^{\sigma_i} X \\ M^{\sigma_{i+1}} &\to X^{-1} M^{\sigma_{i+1}}, \end{aligned} \tag{3.23}$$

with X invertible matrix of dimension $(\chi_i \times \chi_i)$, obtaining another representation for the same state.

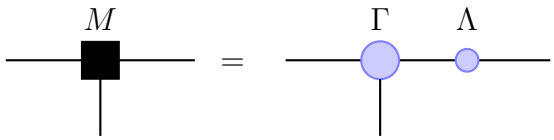

Figure 3.4: MPS representation in Vidal decomposition.

The freedom of choosing the MPS can be used to define a *canonical form* of the MPS, introduced by Vidal [69, 8, 70] and for this reason also known as *Vidal decomposition*. Without loss of generality we can write every matrix M^{σ_i} as a product of a matrix $\Gamma^{[i]\sigma_i}$ of dimension $(\chi_{i-1} \times \chi_i)$ and positive, real, square diagonal matrices $\Lambda^{[i]}$ (see Fig. 3.4),

$$|\psi\rangle = \sum_{\sigma_1,\ldots,\sigma_L} \Gamma^{[1]\sigma_1} \Lambda^{[1]} \Gamma^{[2]\sigma_2} \Lambda^{[2]} \ldots \Lambda^{[L-1]} \Gamma^{[L]\sigma_1} |\sigma_1 \ldots \sigma_L\rangle \,. \tag{3.24}$$

With this particular choice, any bond l defines a bipartition of the system into sites $L = 1, \ldots, l$ and $R = l+1, \ldots, L$ to the left and right of the bond, for which we have a *mixed-canonical MPS* (3.20).

The MPS representation $\{\Gamma^{[1]}, \Lambda^{[1]}, \ldots, \Gamma^{[N]}\}$ is said to be in *canonical form* if for every bond, the set of Schmidt states along with $\Lambda^{[l]}$ form a Schmidt decomposition of Ψ.

3.1.1 Overlaps and expectation values

MPS representation is also an efficient way of having our states for computing overlaps and observables.

Suppose one aims to compute the overlap of two pure states $|\psi\rangle$ and $|\phi\rangle$, whose MPS representation is identified by $\{M\}$ and $\{\tilde{M}\}$ respectively. Taking the adjoint of $|\phi\rangle$, the

overlap reads

$$\begin{aligned}\langle\phi|\psi\rangle &= \sum_{\{\sigma\}} \tilde{M}^{\sigma_1 *} \dots \tilde{M}^{\sigma_L *} M^{\sigma_1} \dots M^{\sigma_L} \\ &= \sum_{\{\sigma\}} (\tilde{M}^{\sigma_1 *} \dots \tilde{M}^{\sigma_L *})^T M^{\sigma_1} \dots M^{\sigma_L} \\ &= \sum_{\{\sigma\}} \tilde{M}^{\sigma_L \dagger} \dots \tilde{M}^{\sigma_1 \dagger} M^{\sigma_1} \dots M^{\sigma_L}\end{aligned} \tag{3.25}$$

Evaluating this expression (see Fig. 3.5 for the graphical representation) in detail shows the importance of finding the right (optimal) order of contractions in matrix or more generally tensor networks [21]. We have contractions over the matrix indices implicit in the matrix multiplications, and over the physical indices. If one decides to contract first the matrix indices and then the physical indices, it is necessary to sum over d^L strings of matrix multiplications, which is ex ponentially expensive. But the contractions can be reorganized as follows:

$$\langle\phi|\psi\rangle = \sum_{\sigma_L} \big(\tilde{M}^{\sigma_L \dagger} \dots \big(\sum_{\sigma_1} \tilde{M}^{\sigma_1 \dagger} M^{\sigma_1}\big) \dots M^{\sigma_L}\big) \tag{3.26}$$

In the first step the column and row vectors $\tilde{M}^{\sigma_1 \dagger}$ and M^{σ_1} are multiplied to form a matrix and sum over the (first) physical index. In the next step, a three-matrix multiplication over the second physical index is performed, and so forth. Note that from the second step the complexity does not grow anymore: computation improves from exponential to weak polynomial complexity, with total operation count $O(L\chi^3 d)$.

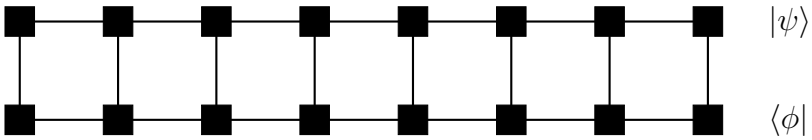

Figure 3.5: Graphical representation of the overlap (3.25).

.

What is also immediate is that for a norm calculation having a state in left or right-normalized form immediately implies that it has unitary norm.

For physical purpuses one's goal is to calculate general matrix elements $\langle\phi|\,\hat{O}^{[i]}\hat{O}^{[j]}\dots|\psi\rangle$, where $\hat{O}^{[i]}$ is some local operator acting on the local Hilbert space $\mathbb{C}^d$ of site i.

Local operators can be expressed as

$$\hat{O}^{[i]} = \sum_{\sigma_i, \sigma_i'} O^{\sigma_i, \sigma_i'} |\sigma_i\rangle \langle\sigma_i'| \tag{3.27}$$

and they can be extended to non local operators acting on the whole chain $O^{\sigma_1,\sigma_1'} \dots O^{\sigma_L,\sigma_L'}$ whose action is non trivial only on the support of the initial local operators. In the analytical expression, we again transpose and distribute the sum over local states.

As an example

$$\begin{aligned} \langle\phi|\,\hat{O}^{[i]}\hat{O}^{[j]}\,|\psi\rangle &= \langle\phi|\,\hat{O}^{[1]}\dots\hat{O}^{[L]}\,|\psi\rangle \\ &= \sum_{\sigma_L,\sigma_L'} \big(O^{\sigma_L,\sigma_L'}\tilde{M}^{\sigma_L\dagger}\dots\big(\sum_{\sigma_1} O^{\sigma_1,\sigma_1'}\tilde{M}^{\sigma_1\dagger}M^{\sigma_1}\big)\dots M^{\sigma_L}\big), \end{aligned} \tag{3.28}$$

with $\hat{O}^{[k]} = \mathbb{1}$ for $k \neq i, j$. See Fig. 3.6 for graphical representation.

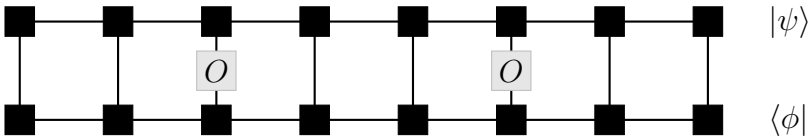

Figure 3.6: Graphical representation of (3.28).

This is the same amount of calculation as for the overlap, with the exception that formally the single sum over the physical index turns into a double sum. For typical correlators the double sum will trivially reduce to a single sum on most sites as in the example, as for most sites only the identity acts. On the few non-trivial sites, of the up to d^2 matrix elements, most will be zero for conventional operators, strongly restricting the number of terms, so essentially the operational count is $O(L\chi^3 d)$ again.

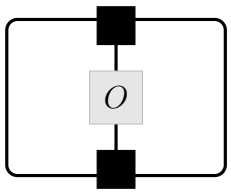

Figure 3.7: Expectation value of a local operator with single site support.

It is now straighforward to see that expectation values $\langle\psi|\hat{O}^{[l]}|\psi\rangle$ can be extremely semplified if we have a canonical MPS, or more in general a *mixed-canonical* MPS with bipartition on site l. After tensor contractions that exploit orthonormalization conditions (3.8) and (3.13), we are left with (see Fig. 3.7):

$$\langle\psi|\hat{O}^{[l]}|\psi\rangle = \sum_{\sigma_l,\sigma_l'} O^{\sigma_l,\sigma_l'}\,\mathrm{Tr}\Big(M^{\sigma_l\dagger}M^{\sigma_l'}\Big), \tag{3.29}$$

an operation of order $O(\chi^2 d^2)$, saving one order of χ in calculation time.

3.1.2 Infinite MPS and translational invariance

We now restrict our discussion to the case of *canonical* MPS, since this representation is mainly used in the sequel.

For infinite and translationally invariant systems, the set of matrices on any given site becomes the same:

$$\begin{aligned} \Gamma^{[j]\sigma_j} &\equiv \Gamma^{\sigma_j} \\ \Lambda^{[j]} &\equiv \Lambda, \end{aligned} \tag{3.30}$$

for every integer j. The infinite MPS representation in the canonical form has a number of important advantages. Firs, using the properties of the transfer matrices it is very convenient to evaluate local expectation values as well as correlation functions. Second, with the help of efficient algorithms suche as the *infinite Time Evolving Block Decimation*, time evolution, as well as ground states of a given Hamiltonian can be found in the thermodynamic limit. This is an essential property since very important features of the models considered in this work, like sponteneous symmetry breaking, can be observed only in this limit, as discussed in section 1.5.

3.2 iTEBD algorithm

Now that an efficient representation of that states was introduced, we are interested in evaluating time evolution

$$|\psi(t)\rangle = e^{-iHt} |\psi_0\rangle \equiv U(t) |\psi_0\rangle . \tag{3.31}$$

To achieve this, the infinite Time Evolving Block Decimation (iTEBD) algorithm is introduced [70]. Let H be a Hamiltonian with nearest neighbor interactions

$$H = \sum_r h^{[r,r+1]} \tag{3.32}$$

and let $|\psi_0\rangle$ and H be invariant under shifts by one lattice site.

To achive time evolution, onemakes use of the Trotter-Suzuki decomposition, which apporoximates the exponent of a sum of operators with a product of exponents of the same operators. At first order the expansion reads

$$e^{(V+W)\delta} = e^{V\delta} e^{W\delta} + O(\delta^2). \tag{3.33}$$

We can decompose the Hamiltonian as a sum

$$\begin{aligned} H &= H_{\text{odd}} + H_{\text{even}} \\ &= \sum_{r \text{ odd}} h^{[r,r+1]} + \sum_{r \text{ even}} h^{[r,r+1]}. \end{aligned} \tag{3.34}$$

In this way each term consistes of a sum of commuting operators.

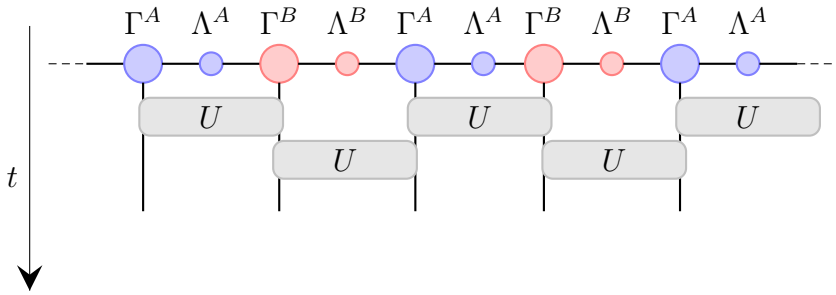

Figure 3.8: In iTEBD eash time step δt of a time evolution is approximated using a Trotter-Suzuki decomposition. The evolved state is obtained by subsequent applications of U gates.

We now divide the time into small time slices $\delta t \ll 1$ and expand the $U(t)$ operator as a sequence of small two-site gates

$$U^{[r,r+1]}(\delta t) = \exp\left(-ih^{[r,r+1]}\delta t\right), \tag{3.35}$$

which we arrange into gates U^{AB} and U^{BA},

$$U^{AB}(\delta t) = \bigotimes_{r\in\mathbb{Z}} U^{[2r,2r+1]}(\delta t), \qquad U^{BA}(\delta t) = \bigotimes_{r\in\mathbb{Z}} U^{[2r-1,2r]}(\delta t). \tag{3.36}$$

At first order $U(\delta t)$ is given by

$$U(\delta t) = U^{AB}(\delta t)U^{AB}(\delta t). \tag{3.37}$$

Because the initial state is transtaltional invariant, it could be represented with a MPS indipendent of the lattice index r as in (3.30). However we will partially break translational symmetry to simulate the action of gates (3.36) on $|\psi_0\rangle$:

$$\begin{aligned} \Gamma^{[2r]} &= \Gamma^A & \Lambda^{[2r]} &= \Lambda^A \\ \Gamma^{[2r+1]} &= \Gamma^B & \Lambda^{[2r+1]} &= \Lambda^B. \end{aligned} \tag{3.38}$$

The decomposition of the time evolution operator is shown pictorially in Fig. 3.8. The simulation of the time evolution is achieved by updating the MPS by repated application

of gates U^{AB} and U^{BA}. The update procedure for two-site transformation action on two neighboring sites n and $n+1$ is shown in Fig. 3.9. We focus on an update with a U^{AB} gate. The inequivalent BA bonds are updated similarly by exchanging A and B.

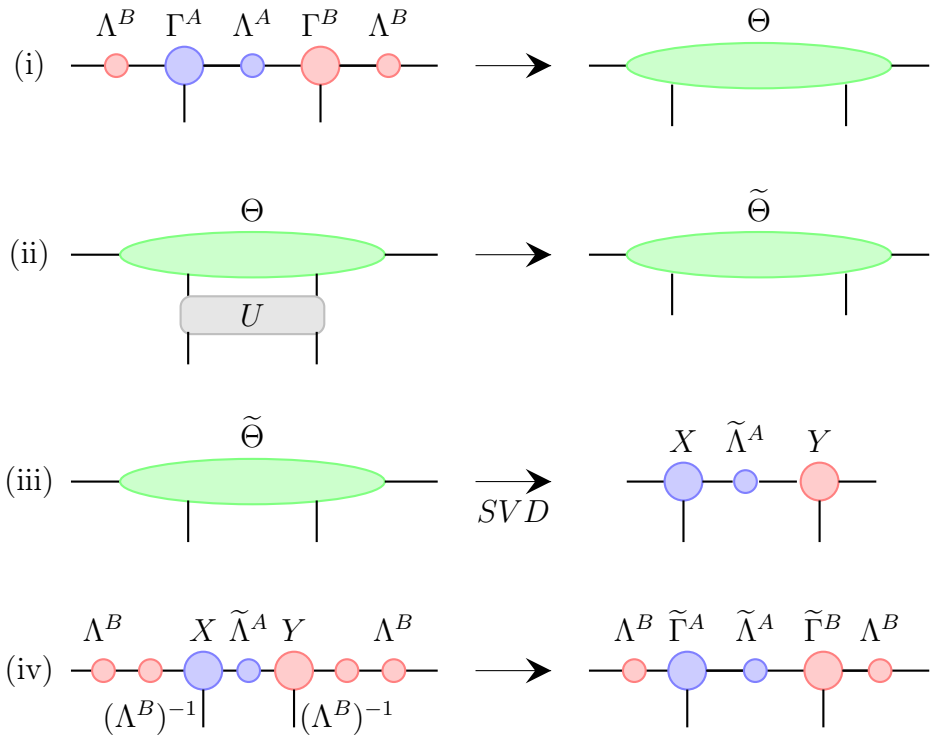

Figure 3.9: The iTEBD update scheme for unitary two-site transformation of a two-site unit cell MPS in canonical form. See section 3.2 for the description.

The wave function of a generic state $|\psi\rangle$ can be expressed in the basis spanned by the left Schmidt states on bond $n-1:n$, the local Hilbert space of sites n and $n+1$, and the right Schmidt states on bond $n+1:n+2$:

$$|\psi\rangle = \sum_{\alpha,j,k,\gamma} \Theta^{j,k}_{\alpha\gamma} |\alpha_{n-1}\rangle_L |j_n\rangle |k_{n+1}\rangle |\gamma_{n+1}\rangle_R , \tag{3.39}$$

where the wave function coefficients Θ are given by (step (i) in Fig. 3.9)

$$\Theta^{j,k}_{\alpha\gamma} = \sum_{\beta} \Lambda^B_\alpha \Gamma^{A,j}_{\alpha\beta} \Lambda^A_\beta \Gamma^{B,k}_{\beta\gamma} \Lambda^B_\gamma . \tag{3.40}$$

Recall that the physical indices j,k can take d values while bond indices α,γ have ξ

values. The local unitary update of the algorithm is given by (step (ii) in Fig. 3.9) :

$$\tilde{\Theta}^{j,k}_{\alpha\gamma} = \sum_{j'k'} U^{jk}_{j'k'} \Theta^{j',k'}_{\alpha\gamma}. \tag{3.41}$$

Next we have to extract the updated tensor $\tilde{\Gamma}^A$, $\tilde{\Gamma}^B$ and $\tilde{\Lambda}^A$ from the transformed tensor $\tilde{\Theta}$. We also want to preserve the canonical form for subsequent applications of the gate. We first reshape the tensor $\tilde{\Theta}$ by combining indices to obtain a $d\chi \times d\chi$ dimensional matrix $\tilde{\Theta}_{j\alpha;k\gamma}$. Because the basis $|\alpha_{n-1}\rangle_L |j_n\rangle$ is orthonormal, as for the right, it is natural to decompose the matrix using a SVD into

$$\tilde{\Theta}_{j\alpha;k\gamma} = \sum_{\beta} X_{j\alpha;\beta} D_{\beta}\beta Y_{\beta;k\gamma} \tag{3.42}$$

(step (iii) in Fig. 3.9).The matrix X relates to the new Schmidt states $|\beta_n\rangle_L$ to the combined bases $|\alpha_{n-1}\rangle_L |j_n\rangle$. The Schmidt states for the right site are obtained from the matrix Y in the same way. Thus the diagonal matrix D contains the Schmidt values of the updated state:

$$\tilde{\Lambda}^A = D. \tag{3.43}$$

The new tensors $\tilde{\Gamma}^A$ and $\tilde{\Gamma}^B$ can be obtained extracting the old matrices Λ^β (see step (iv) in Fig. 3.9):

$$\begin{aligned} \tilde{\Gamma}^{A,j}_{\alpha\beta} &= (\Lambda^B)^{-1}_{\alpha} X_{j\alpha;\beta} \\ \tilde{\Gamma}^{B,j}_{\beta\gamma} &= Y_{\beta;k\gamma} (\Lambda^B)^{-1}_{\gamma} \end{aligned} \tag{3.44}$$

After the update the new MPS is still in the canonical form.

The entanglement at the bond $n : n+1$ has changed in the update and the bond dimension increases to $d\chi$. Thus the amount of information in the wave function grows exponentially after successively updates. To overcome this problem it is possible to fix the maximal number of Schmidt values to χ (see (1.40)).

Note that for the update of n sites the TEBD algorithm requires $O(nd\chi^2)$ space to store an MPS and $O(nd^3\chi^3)$ time to simulate a small evolution $\exp(-iH\delta t)$, but for an infinite chain the action of the gates preserves the invariance ofthe evolved state under shift by two sites. In other words for $n = \infty$ the iTEBD requires computational space and time that scale hust as $O(d\chi^2)$ and $O(d^3\chi^3)$. Key to such dramatic cost reduction is the MPS based on the Schmidt decomposition, allowing a parallelized *local* update of tensors Γ, Λ.

3.2.1 Finding the ground state and computing observables

The iTEBD algorithm can be slightly modified to compute ground states. It is indeed sufficient to perform the Wick rotation

$$t \to -i\tau \tag{3.45}$$

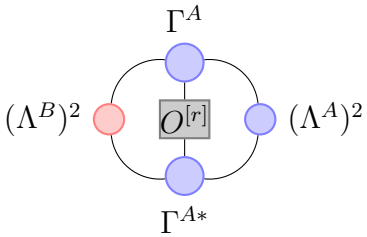

Figure 3.10: Site expectation value of the σ^z operator on a site of type A.

Then we perform the imaginary time evolution of a random state $|\psi_{rand}\rangle$ through the operator $U(-i\tau) = \exp\{-\tau H(h_0)\}$ and find the ground state as

$$|\psi_{GS}\rangle = \lim_{\tau\to\infty} \frac{\exp\{-\tau H(h_0)\}\,|\psi_{rand}\rangle}{\|\exp\{-\tau H(h_0)\}\,|\psi_{rand}\rangle\|} \equiv \lim_{\tau\to\infty} \frac{|\psi_\tau\rangle}{\||\psi_\tau\rangle\|} \tag{3.46}$$

(the state needs to be normalized as the operator $U(-i\tau)$ is not unitary).

Fort finite lattice with N sites with a Hamiltonian with gap $\Delta > 0$, simulating imaginary time evolution for large τ yields to a good approximation of the ground state since one can show that

$$|\,\langle\psi_\tau|\psi_{GS}\rangle\,| > O(\frac{e^{-2\Delta\tau}}{\delta^2}), \qquad \delta = |\,\langle\psi_{rand}|\psi_{GS}\rangle\,|. \tag{3.47}$$

Non unitary operators do not preserve the canonical form. It turns out, however, that the successive Schmidt decompositions assure a good approximation as long as the time steps are chosen small enough [71].

It is important to remark that the state of the system for a generic t is now specified by two set of tensors $\{\Gamma^A, \Lambda^A\}$ and $\{\Gamma^B, \Lambda^B\}$, while the physical state should by invariant when shifting by one site. However we can restore the original symmetry through observables. For instance, for an operator $O^{[r]}$ acting on site r, orthogonality of the Schmidt bases implies that its expactation value on a certain state $|\Psi\rangle$, identified by $\{\Gamma, \lambda\}$, is simply:

$$\langle\psi|\,O^{[r]}\,|\psi\rangle = \sum_{\alpha i\beta} (\lambda_\alpha)^2 \Gamma^i_{\alpha\beta} O^{[r]}_{ij} (\Gamma^j_{\alpha\beta})^* (\lambda_\alpha)^2 \tag{3.48}$$

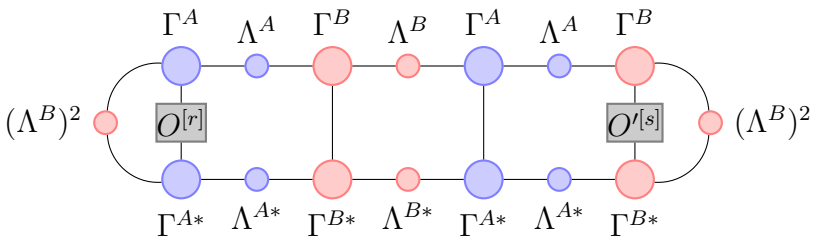

Figure 3.11: Correlation function for two sites distant 3 lattice spaces.

In our case we have a different expectation value for odd and even sites and can be computed as in Fig. 3.10. The translational invariance of the initial system is then restored taking their mean value.

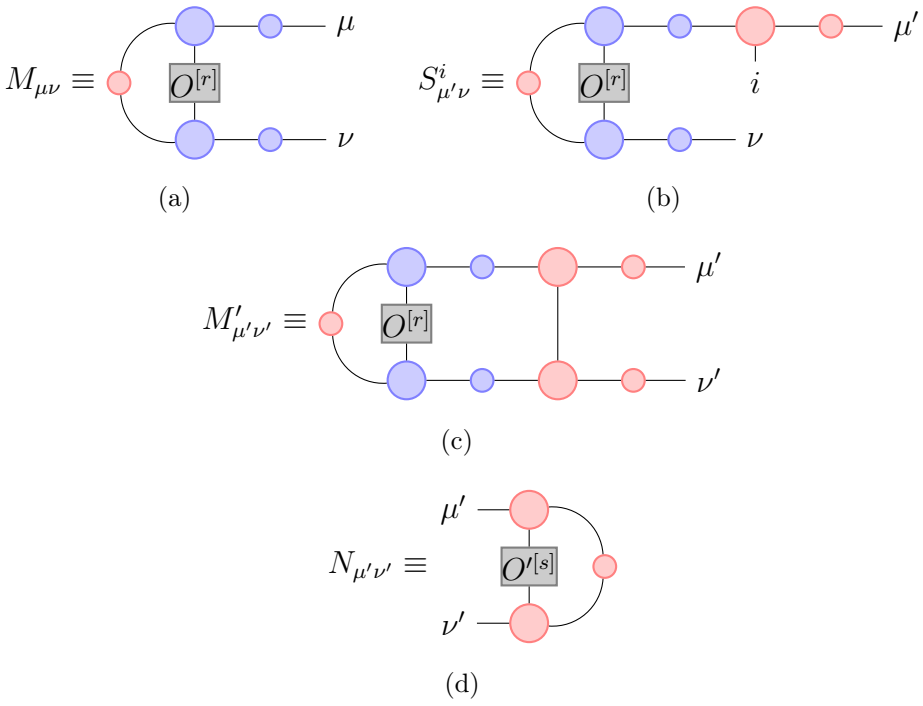

Figure 3.12: Graphical representation of the contractions needed for a two-point correlation function.

Similarly, the expression for a two-point correlator of operators $O^{[r]}$ and $O'^{[s]}$ involves only tensors of order of $(s-r)$, as illustrated in Fig. 3.11.

As [21] reports, the best way to perform this contraction is as follows (see Fig. 3.12):

(i) Create the matrix $M_{\mu\nu} = \sum_{\alpha\mu\nu} \sum_{ij} (\Lambda^B_\alpha)^2 \Gamma^{A,j}_{\alpha\nu} \Gamma^{A,i*}_{\alpha\mu} O^{[r]}_{ij} \Lambda^A_\mu \Lambda^A_\nu$;

(ii) Contract $S^{i}_{\mu'\nu} = M_{\mu\nu}\Gamma^{B,i}_{\mu\mu'}\Lambda^{B}_{\mu'}$;

(iii) Contract $M'_{\mu'\nu'} = S^{i}_{\mu'\nu}\Gamma^{B,i*}_{\nu\nu'}\Lambda^{B}_{\nu'}$;

(iv) Repeat (ii), (iii) with $M = M'$, alternating on A and B bonds for $(r-1)$ times;

(v) Contract M' with the matrix $N_{\mu\nu} = \sum_{\alpha}\sum_{ij}(\Lambda_{\alpha})^2\Gamma^{j}_{\nu'\alpha}\Gamma^{j*}_{\mu'\alpha}O'_{i}j^{[s]}$ ($\{\Gamma,\Lambda\}$ are of the A(B) kind if r is even(odd)).

3.3 Numerical details of the simulations

The iTEBD algorithm code written is composed of two different parts: the first obtains an accurate MPS description of the initial state (in our case ground states of the Ising and the three-state Potts Hamiltonian) and the second deals with the time evolution. The imaginary time evolution was implemented using a first order Suzuki-Trotter decomposition with imaginary time-step $\tau = 0.001$. We control the convergence of the imaginary time algorithm by keeping track of the energy density E_0 and waiting for it to become stationary.

Using this MPS as our initial state, we can address the real time evolution. We again use a second order Suzuki-Trotter decomposition of the evolution operator $U(\delta t)$ with time step $\delta t = 0.005$.

We adapt the number of states used to describe the reduced Hilbert space by retaining, at each time step, all Schmidt vectors corresponding to singular values larger than $\lambda_{\min} = 10^{-12}$. Once the maximum value of the bond dimension is reached, this condition is relaxed. For the Ising model the maximum bond dimension was fixed to $\chi_{\max} = [256, 512]$, while for the Potts model $\chi_{\max} = 243$. Because of the upper bound $\chi_{\max}$, the truncation procedure is the main source of error of the algorithm and puts limitations on the maximum time accessible by the simulation.

Chapter 4

Quench dynamics in $\mathbb{Z}_\eta$ symmetric models

All animals are equal, but some animals are more equal than others.

- George Orwell, *Animal Farm*

In this chapter the quantum Ising model and the 3-state quantum Potts model are introduced. Their dynamics after a quantum quench is described along with the presentation of the simulations results. As far as the Ising model is concerned, the latter are compared to the exact predictions. Some of them are reobtained throughout the chapter. The focus will be on one point functions of local observables, correlation functions and entanglement entropy.

4.1 Ising chain with transverse field

Let's start with a paradigmatic model, the quantum Ising model with transverse field, whose Hamiltonian is given by

$$H(h) = -J \sum_{j=1}^{N} [\sigma_j^z \sigma_j^z + h\sigma_j^x], \tag{4.1}$$

where σ_j^α are the Pauli matrices at site j, J is a dimensionless, positive constant and we impose periodic boundary conditions:

$$\sigma_{N+1}^\alpha = \sigma_1^\alpha. \tag{4.2}$$

The Hamiltonian of the Ising model exhibits a $\mathbb{Z}_2$ symmetry by rotations around the x-axis in spin space by 180 degrees:

$$\sigma_j^{y,z} \to -\sigma_j^{y,z}, \qquad \sigma_j^x \to \sigma_j^x \tag{4.3}$$

The Ising model is a crucial paradigm of quantum critical behaviour and quantum phase transitions. At zero temperature and in the thermodynamic limit it exhibits ferromagnetic ($h < 1$) and paramagnetic ($h > 1$) phases, separated by a quantum critical point at $h_c = 1$. For $h < 1$ and $L \to \infty$ there are two degenerate ground states related by the $\mathbb{Z}_2$ symmetry. Spontaneous symmetry breaking selects a unique ground state, in which spins align along the z-direction (*ordered phase*). On the other hand, for magnetic fields $h > 1$ the ground state is non-degenerate and as the magnetic field h is increased spins align more and more along the x-direction (*disordered phase*). The order parameter for the quantum phase transition is the ground state expectation value $\langle \sigma_j^z \rangle$.

The Ising model is integrable and its spectrum can be computed explicitly together with its eigenstates. The diagonalization of the Hamiltonian follows.

The frist step is to perform a Jordan-Wigner transformation, that maps the spin operators into a set of Majorana fermions

$$a_j = \prod_{l=1}^{j-1} \sigma_l^x \sigma_j^z \qquad b_j = i a_j \sigma_j^x, \tag{4.4}$$

with commutation relations given by

$$\{a_j, a_l\} = \{b_j, b_l\} = 2\delta_{j,l} \qquad \{a_j, b_l\} = 0. \tag{4.5}$$

The inverse transformation is given by

$$\sigma_j^x = -i a_j b_j \qquad \sigma_j^z = \prod_{l=1}^{j-1} (-i a_l b_l) a_j. \tag{4.6}$$

Note that this transformations are non local. We can combine Majorana fermions into a Dirac fermion

$$c_j = \frac{a_j + i b_j}{2}, \tag{4.7}$$

with the usual fermionic coomutation relations

$$\{c_j, c_l^\dagger\} = \delta_{j,l} \qquad \{c_j, c_l\} = \{c_j^\dagger, c_l^\dagger\} = 0. \tag{4.8}$$

The Hamiltonian (4.1) in terms of the spinless fermions reads

$$H(h) = -J\sum_{j=1}^{N-1}[c_j^\dagger - c_j][c_{j+1}^\dagger + c_{j+1}] - Jh\sum_{j=1}^{N}(c_j c_j^\dagger - c_j^\dagger c_j) - Je^{i\pi\hat{N}}(c_N - c_N^\dagger)(c_1 + c_1^\dagger), \quad (4.9)$$

where

$$\hat{N} = \sum_{j=1}^{N} c_j^\dagger c_j \quad (4.10)$$

is the fermionic number operator. Since $[H, e^{i\pi\hat{N}}] = 0$ it is possible to diagonalize the two operatros simultaneously and the Hamiltonian is block diagonal $H = H_e \oplus H_o$, where $H_{e/o}$ acts on the subspaces of the Fock space with even/odd number of fermions.

Even Fermion Number

In this sector we have $e^{i\pi N} = 1$ and

$$H_e(h) = -J\sum_{j=1}^{N}[c_j^\dagger - c_j][c_{j+1}^\dagger + c_{j+1}] - Jh\sum_{j=1}^{N}(c_j c_j^\dagger - c_j^\dagger c_j). \quad (4.11)$$

Note that the periodic boundary conditions (4.2) in spin language implies antiperiodic boundary conditions (ABC) in this sector for the fermionic operators:

$$c_{N+1} = -c_1. \quad (4.12)$$

The Hamiltonian H_e can be diagonalized by going to Fourier space

$$c(k_n) = \frac{1}{\sqrt{N}}\sum_{j=1}^{N} c_j e^{ik_n j}, \quad (4.13)$$

where the momenta k_n are quantized according to ABC:

$$k_n = \frac{2\pi(n+1/2)}{N}, \qquad -\frac{N}{2}, \ldots, \frac{N}{2} - 1. \quad (4.14)$$

The antiperiodic sector is referred to as Neveu-Schwarz (NS) sector. We can now perform a rotation in momentum space introducing the Bogoliubov fermions

$$\begin{aligned} c(k_n) &= \cos(\theta_{k_n}/2)\alpha_{k_n} + i\sin(\theta_{k_n}/2)\alpha_{-k_n}^\dagger \\ c^\dagger(-k_n) &= i\sin(\theta_{k_n}/2)\alpha_{k_n} + \cos(\theta_{k_n}/2)\alpha_{-k_n}^\dagger, \end{aligned} \quad (4.15)$$

where the Bogoliubov angle satisfies

$$e^{i\theta_{k_n}} = \frac{h - e^{ik_n}}{\sqrt{1 + h^2 - 2h\cos k_n}}. \tag{4.16}$$

In this basis H_e is diagonal:

$$H_e = \sum_{n=-N/2}^{N/2-1} \epsilon(k_n)[\alpha_{k_n}^\dagger \alpha_{k_n} - 1/2], \tag{4.17}$$

where $\epsilon(k)$ is the dispersion relation of the excitations given by

$$\epsilon(k) = 2J\sqrt{1 + h^2 - 2h\cos k}. \tag{4.18}$$

We indicate in this sector the fermion vacuum as $|0; h\rangle_{NS}$, defined by

$$\alpha_k |0; h\rangle_{NS} = 0 \qquad \forall k \in NS. \tag{4.19}$$

Odd Fermion Number

The diagonalization in this sector is performed in the same way. Here $e^{i\pi N} = 1$ and the odd Hamiltonian has the same form

$$H_o(h) = -J\sum_{j=1}^{N}[c_j^\dagger - c_j][c_{j+1}^\dagger + c_{j+1}] - Jh\sum_{j=1}^{N}(c_j c_j^\dagger - c_j^\dagger c_j), \tag{4.20}$$

but now periodic boundary conditions (PBC) have to be imposed:

$$c_{N+1} = c_1. \tag{4.21}$$

we go again into Fourier space

$$c(p_n) = \frac{1}{\sqrt{N}}\sum_{j=1}^{N} c_j e^{ip_n j}, \tag{4.22}$$

where the momenta p_n are quantized according to PBC:

$$p_n = \frac{2\pi n}{N}, \qquad -\frac{N}{2}, \ldots, \frac{N}{2} - 1. \tag{4.23}$$

The periodic sector is known as Ramond (R) sector. Defining the Bogoliubov fermions by

$$\begin{aligned} c(p_n) &= \cos(\theta_{p_n}/2)\alpha_{p_n} + i\sin(\theta_{p_n}/2)\alpha_{-p_n}^\dagger \\ c^\dagger(-p_n) &= i\sin(\theta_{p_n}/2)\alpha_{p_n} + \cos(\theta_{p_n}/2)\alpha_{-p_n}^\dagger, \end{aligned} \tag{4.24}$$

the Hamltonian H_o becomes diagonal:

$$H_o = \sum_{n=-N/2, n\neq 0}^{N/2-1} \epsilon(p_n)[\alpha^\dagger_{k_n}\alpha_{k_n} - 1/2] - 2J(1-h)[\alpha^\dagger_{k_0}\alpha_{k_0} - 1/2]. \tag{4.25}$$

We indicate in this sector the fermion vacuum as $|0;h\rangle_R$, defined by

$$\alpha_p |0;h\rangle_R = 0 \qquad \forall p \in R. \tag{4.26}$$

In the paramagnetic phase, where $h < 1$ we can write both Hamiltonians as

$$H_{e/o} = \sum_{q\in a} \epsilon(q)\alpha^\dagger_q\alpha_q + E^a_0(h), \qquad a = NS, R. \tag{4.27}$$

where $E^a_0 = -1/2\sum_{q\in a}\epsilon(q)$. This expression of the Hamiltonians holds also in the ferromagnetic phase, where $h > 1$, after a particle-hole transformation for the zero-mode (that has negative energy),

$$\alpha_0 \to \alpha^\dagger_0. \tag{4.28}$$

The ground state is $|0;h\rangle_{NS}$ in both phases. In the ferromagnetic one, for large N we have $E^{NS}_0(h) - E^R_0(h) = O(L^{-1})$ so that in the thermodynamic limit the states $|0;h\rangle_{NS}$ and $|0;h\rangle_R$ become degenerate and by spontaneous symmetry breaking one of the two combinations

$$\frac{1}{\sqrt{2}}[|0;h\rangle_{NS} \pm |0;h\rangle_R] \tag{4.29}$$

is selected as the ground state.

4.1.1 Quench protocol

We perform a *sudden global quench* of the transverse magnetic field. We assume that the system is prepared in the ground state $|\Psi_0\rangle$ of the Hamiltonian with coupling constant h_0. To reach the ground state with the iTEBD we perform imaginary time evolution as described in section 3.2.1. The infinite chain is prepared in a simple ferromagnetic state, where all the spins are aligned along the positive direction of the the z axis:

$$|\Psi_F\rangle = |\ldots\uparrow\uparrow\uparrow\ldots\rangle\,. \tag{4.30}$$

This state has a trivial MPS representation of bond dimension $\chi = 1$

$$\begin{aligned} \Gamma^{A,\uparrow} &= 1 = \Gamma^{B,\uparrow} \\ \Gamma^{A,\downarrow} &= 0 = \Gamma^{B,\downarrow} \\ \Lambda^A &= 1 = \Lambda^B. \end{aligned} \tag{4.31}$$

Then the ground state is given by

$$|\Psi_0\rangle = \lim_{\tau\to\infty} \frac{e^{-H(h_0)\tau}\,|\Psi_F\rangle}{\|e^{-H(h_0)\tau}\,|\Psi_F\rangle\|} \tag{4.32}$$

At $t = 0$ the value of the transverse magnetic field is switched to a new value h. To find the state of the system for $t > 0$ we have to consider the unitary time evolution of the ground state $|\Psi_0\rangle$ charachterized by the new Hamiltonian $H(h)$:

$$|\Psi_0(t)\rangle = e^{-iH(h)t}|\Psi_0\rangle. \tag{4.33}$$

As proved in the previous section, the Ising Hamiltonian can be diagonalized. For $H(h_0)$ we have Bogoliubov operators $\tilde{\alpha}_k$ with Bogoliubov angle θ_k^0; for $H(h)$ we have α_k and θ_k. The corresponding Bogoliubov fermions are related by a linear transformation characterized by the difference of the angles Δ_k:

$$\tilde{\alpha}_k = \cos\left(\frac{\theta_k - \theta_k^0}{2}\right)\alpha_k + i\sin\left(\frac{\theta_k - \theta_k^0}{2}\right)\alpha_{-k}^\dagger, \tag{4.34}$$

which satisfies

$$\cos\Delta_k = \frac{hh_0 - (h+h_0)\cos k + 1}{\sqrt{1+h^2-2h\cos k}\sqrt{1+h_0^2-2h_0\cos k}}. \tag{4.35}$$

Then it is possible to express the initial state of time evolution as boundary state (2.46).

$$|\Psi_0\rangle \equiv |0;h_0\rangle = \frac{1}{\mathcal{N}}\exp\left\{i\sum_k K(k)\alpha_k^\dagger\alpha_{-k}^\dagger\right\}|0;h\rangle\,, \tag{4.36}$$

with

$$K(k) = \tan\left(\frac{\Delta_k}{2}\right). \tag{4.37}$$

The quasi-particles propagate with dispersion relation $\epsilon_h(k)$ given by (4.18) and maximum velocity

$$v_{\max} = \max_k\left|\frac{d\epsilon_h(k)}{dk}\right| = 2J\min\{1,h\} \tag{4.38}$$

Since the operators α_k evolve according to

$$\alpha_k(t) = e^{it\epsilon_h(k)}\alpha_k(0), \tag{4.39}$$

the initial state evolves in a simple way:

$$|\Psi_0(t)\rangle = e^{-iH(h)t}\,|0;h_0\rangle = \frac{1}{\mathcal{N}}\exp\left\{i\sum_k K(k)e^{-i2\epsilon_h(k)}\alpha_k^\dagger\alpha_{-k}^\dagger\right\}|0;h\rangle\,. \tag{4.40}$$

We proceed studying the time evolution of the many-body system through the dynamics of the following observables and quantities:

i. **Magnetization**

$$m(t) = \langle \Psi_0(t) | \sigma_i^z | \Psi_0(t) \rangle \tag{4.41}$$

ii. **Transverse field**

$$M(t) = \langle \Psi_0(t) | \sigma_i^x | \Psi_0(t) \rangle \tag{4.42}$$

iii. **Entanglement entropy (EE)**

$$S = -\sum_{\alpha} \Lambda_\alpha^2 \ln \Lambda_\alpha^2 \tag{4.43}$$

iv. **Loschmidt Echo (LE)**

$$\mathcal{L}(t) = |\langle \Psi_0 | \Psi_0(t) \rangle|^2 \tag{4.44}$$

v. **Two-points Green function**

$$G(r;t) = \langle \Psi_0(t) | \sigma_i^z \sigma_{i+r}^z | \Psi_0(t) \rangle \tag{4.45}$$

4.1.2 Magnetization

For quenches starting in the disordered phase, i.e. $h_0 > 1$, the order parameter expectation value is zero for all times because the $\mathbb{Z}_2$ symmetry remains unbroken. For quenches that start and end in the ordered phase, i.e. $h_0, h < 1$ we can foresee two different scenarios:

i. As the final value of the coupling constant lays below the critical value, $\langle m(t) \rangle$ remains non vanishing in the limit $t \to \infty$;

ii. As the quench process has injected a certain amount of energy into the system, this will lead to disorder and symmetry restoration.

As proved in [9] the latter is what happens in the quantum Ising chain, and the order parameter decays exponentially according to:

$$m(t) \simeq (\mathcal{C}_{FF})^{\frac{1}{2}} \exp\left\{ \left[t \int_0^\pi \frac{dk}{\pi} \epsilon_h'(k) \ln |\cos \Delta_k| \right] \right\}, \tag{4.46}$$

where

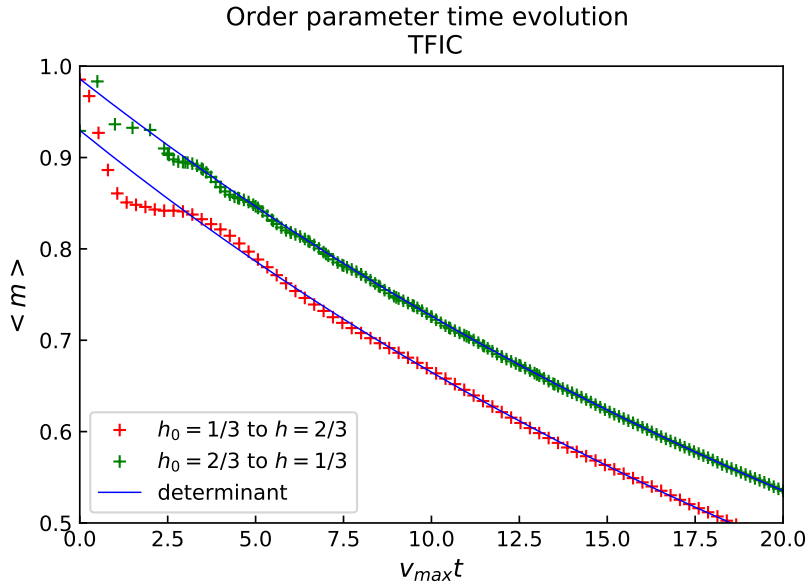

Figure 4.1: Time evolution of the magnetization.

$$\mathcal{C}_{FF} = \frac{1 - hh_0 + \sqrt{(1-h^2)(1-h_0^2)}}{2\sqrt{1-hh_0}(1-h_0^2)^{\frac{1}{4}}}. \tag{4.47}$$

This result was obtained by cluster decomposition of the order parameter two point function, which can be expressed as the determinant of a particular matrix, the former being computable in the thermodynamic limit.

Within the ferromagnetic phase two different quenches where considered (from $h_0 = 1/3$ to $h = 2/3$ and from $h_0 = 2/3$ to $h = 1/3$). The results are illustrated in Fig. 4.1 and compared to the analytic expression (4.46) valid for late times.

The results show also that the short-time behaviour after the quench is sensitive to whether the transverse field is increased or decreased. If $h_0 < h < 1$ then the magnetization decreases for short times, while it initially increases if $1 < h < h_0$.

A drawback of the algorithm is that only short times can be simulated since the bond dimension increases and always more Schmidt values that are no longer negligible are left out by the truncation. This is evident when the quench leads the system towards the critical point (where the mass gap vanishes), as seen in Fig. 4.2, where the evolution with two different maximum values of the bond dimension is considered. However the times available is sufficient to appreciate some key features of the dynamics, such as in this case the exponential decay of the magnetisation.

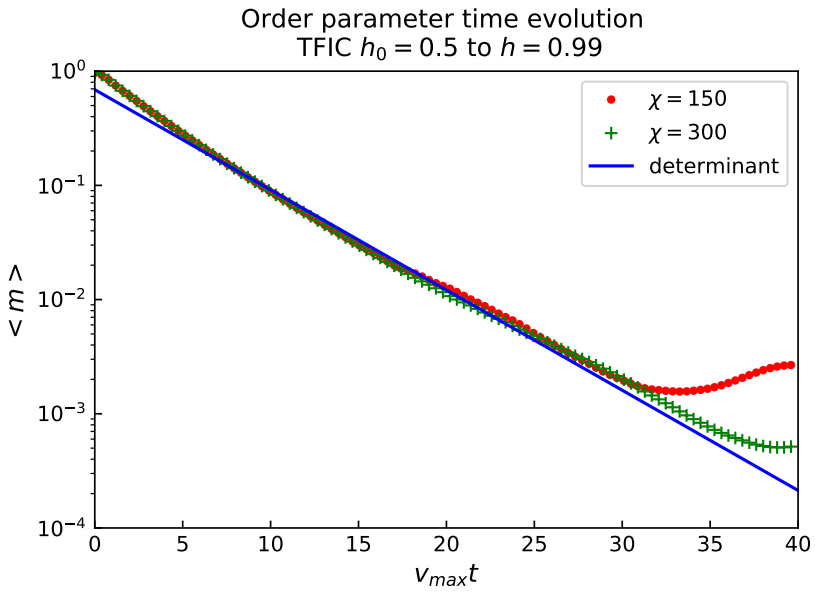

Figure 4.2: Comparison of bond dimensions near the critical value.

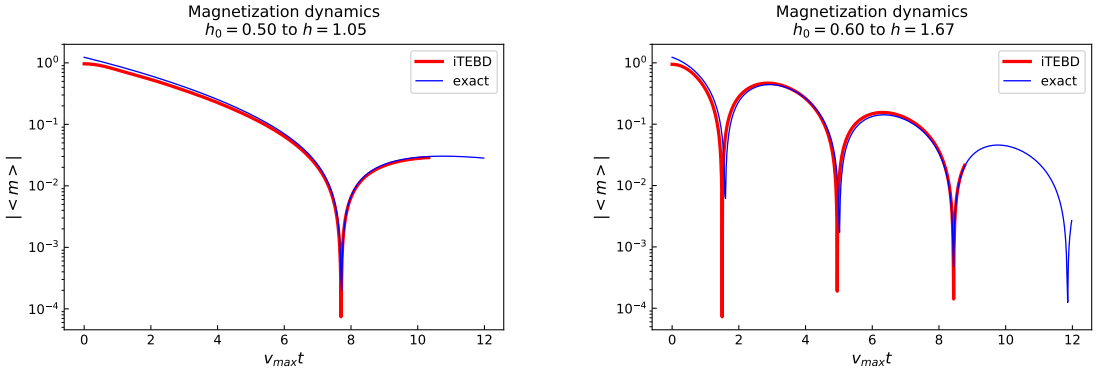

(a) (b)

Figure 4.3: Time evolution of the order parameter for quenches crossing the critical value.

For a quench from the ferromagnetic phase to the paramagnetic one, it is conjectured in [9] that the expectation value of the magnetization is given by

$$m(t) \simeq (\mathcal{C}_{FP})^{\frac{1}{2}}[1+\cos(2\epsilon_h(k_0)t+\alpha)]^{\frac{1}{2}} \exp\left\{\left[t\int_0^{\pi}\frac{dk}{\pi}\epsilon_h^{'}(k)\ln|\cos\Delta_k|\right]\right\}, \tag{4.48}$$

where k_0 is the solution of the equation $\cos\Delta_{k_0} = 0$, $\alpha(h, h_0)$ is an unknown constant,

and

$$\mathcal{C}_{FP} = \left[\frac{h\sqrt{(1-h_0^2)}}{h+h_0}\right]^{\frac{1}{2}}. \tag{4.49}$$

In the limit $h \to 1$, k_0 vanishes so that the crossover between (4.46) and (4.48) is smooth.

In Fig. 4.3 is shown the evolution of the magnetization where the final values of the external field are $h = 1.05$ and $h = 5/3$ with initial value of $h_0 = 0.5$ and $h_0 = 0.6$ respectively. The results are also compared with the analytic result (4.48).

4.1.3 Transverse field

In the Ising chain the time dependent average of the transverse field σ^x can also be evaluated exactly in the thermodynamic limit. Expressing the inverse Jordan-Wigner transformations (4.6) in terms of the Dirac fermions one has

$$\frac{1}{N}\sum_{j=1}^{N}\sigma_j^x = \frac{1}{N}\sum_{j=1}^{N}(1-2c_j^\dagger c_j). \tag{4.50}$$

Since the aim is to evaluate this expression in the evolved state (4.40), we turn to Fourier space and substitute the expression (4.15), obtaining

$$\frac{1}{N}\sum_{j=1}^{N}\sigma_j^x = \frac{1}{N}\sum_{k}[1-2\big(\cos\frac{\theta_k}{2}\alpha_k^\dagger - i\sin\frac{\theta_k}{2}\alpha_{-k}\big)\big(\cos\frac{\theta_k}{2}\alpha_k + i\sin\frac{\theta_k}{2}\alpha_{-k}^\dagger\big)] \tag{4.51}$$

Evaluating its mean value in the boundary state (4.40), we obtain

$$\begin{aligned}\frac{1}{N}\left\langle\sum_{j=1}^{N}\sigma_j^x\right\rangle = \frac{1}{N}\sum_{k}\big[\cos\theta_k - 2(\cos^2\frac{\theta_k}{2}\langle n_k\rangle) - \sin^2\frac{\theta_k}{2}\langle n_{-k}\rangle \\ + \frac{i}{2}\sin\theta_k\big\langle(\alpha_k^\dagger\alpha_{-k}^\dagger - \alpha_{-k}\alpha_k)(t)\big\rangle\big],\end{aligned} \tag{4.52}$$

using now (A.11) and (A.14) for the mean values of the number and strings of creation (or annihilation) operators,

$$\frac{1}{N}\left\langle\sum_{j=1}^{N}\sigma_j^x\right\rangle = \frac{1}{N}\sum_{k}\left[\cos\theta_k(1-\frac{2K_k^2}{1+K_k^2}) + 2\sin\theta_k\frac{\mathrm{Im}(K_k e^{-2i\epsilon_h(k)t})}{1+K_k^2}\right], \tag{4.53}$$

and taking eventually the thermodynamic limit we obtain

$$M(t) = \frac{4}{\pi}\int_0^{2\pi} dp \frac{(hh_0 + 1 - (h + h_0)\cos p)(h - \cos p) - (h - h_0)\sin^2 p \cos(2\epsilon_h(p)t)}{\epsilon_h^2(p)\epsilon_{h_0}(p)}. \tag{4.54}$$

The evolution of the transverse field for quenches both within the ferromagnetic phase and crossing the critical point are shown in Fig. 4.4 .

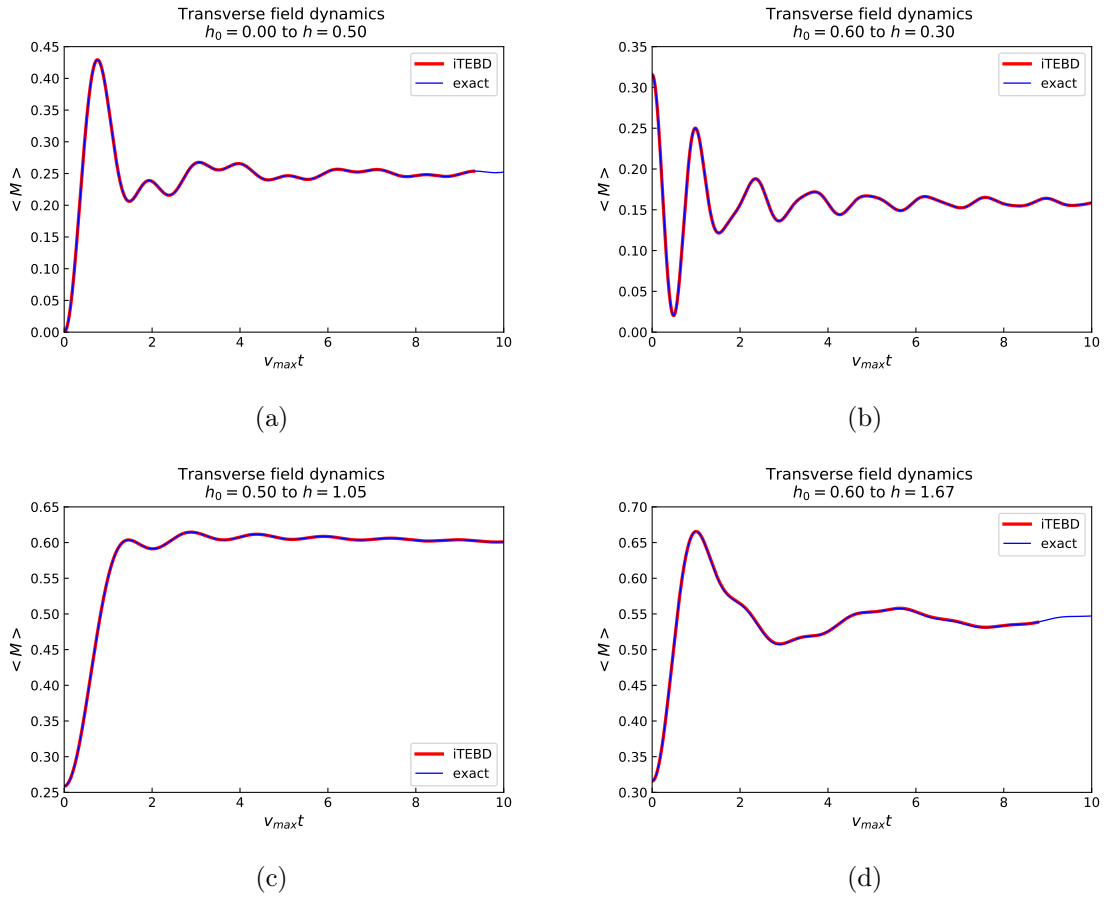

Figure 4.4: Time evolution of the transverse field for four different quenches. Relatively short times are sufficient to reach the equilibrium expectation value. Note that if the value of the transverse field is increased, the expectation value of the transverse magnetization for late times increases; conversely if $h < h_0$, $M(\infty) < M(0)$.

We can obtain the equilibrium expectation value of the transverse magnetization. Since the time dependent part cancels out in the infinite time limit due to the Riemann-Lebesgue lemma, one has

$$\lim_{t\to\infty} M(t) = \frac{1}{2\pi}\int_0^{2\pi} dp \frac{(hh_0 + 1 - (h + h_0)\cos p)(h - \cos p)}{(1 + h^2 - 2h\cos p)\sqrt{1 + h_0^2 - 2h_0\cos p}}. \tag{4.55}$$

Note that this value depends on the coupling constant of the pre-quench Hamiltonian. This means that the transverse field is a non ergodic operator since its equilibrium value after a quench strongly depends on the initial state. This result it is not surprising at all, since as discussed in section 2.1.3 the dynamics is constrained by the infinite conserved quantities due to the integrability of the model.

4.1.4 Entanglement Entropy

As discussed in section 2.4, for finite subsystems of length l the entanglement entropy with the rest of the system increases linearly with time up to $t = l/2v_{max}$, after which it saturates at a value proportional to l. If we consider the entanglement of half chain with the rest of the system in the thermodynamic limit, the entanglement entropy growth is linear for arbitrary times.

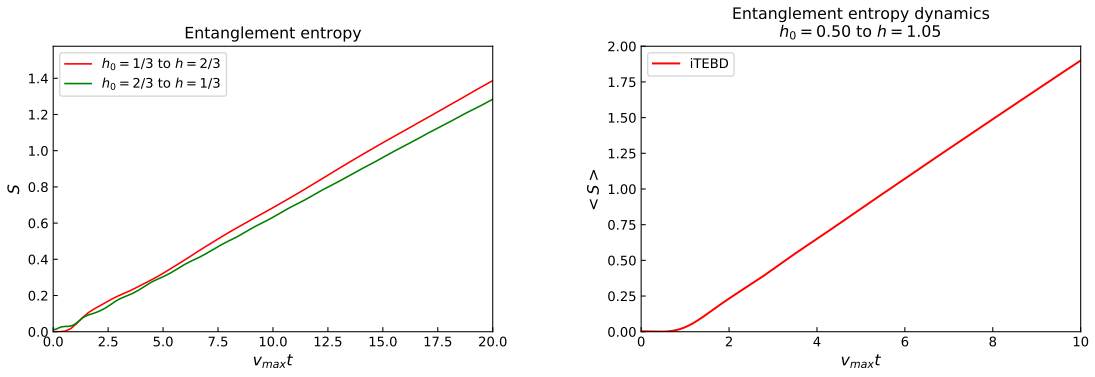

(a) (b)

Figure 4.5: Time evolution of the entanglement entropy.

This behaviour was observed in every quench considered (examples in Fig. 4.5), up to a time t_c. At $t = t_c$ the truncation error becomes considerable and the algorithm is not reliable anymore. The value of t_c can be increased increasing the bond dimension as illustrated in Fig. 4.6.

4.1.5 Loschmidt echo

Loschmidt echo gives meaningful information about the probability that the system at time t comes back to the initial state. We can express the Loschmidt echo as

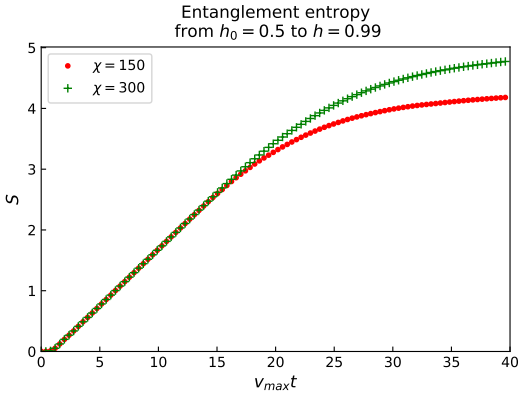

Figure 4.6: Time evolution of the entanglement entropy. Comparison between different values of the bond dimension: failure of the iTEBD algorithm.

$$\mathcal{L}(t) = e^{-LG_{h_0,h}(t)}, \tag{4.56}$$

where L is the length of the part of the chain for which we are considering the overlap. We are interested in the quantity

$$G_{h_0,h}(t) = -\frac{1}{L}\log(\mathcal{L}(t)), \tag{4.57}$$

called logarithmic Loschmidt echo (LLE). For the Ising chain, using the expressions of boundary state and its evolved (4.40) and the result (A.10)

$$\mathcal{L}(t) = \exp\left[\sum_{p>0}\log\left(\frac{1+e^{-2i\epsilon_h(p)t}K_p^2}{1+K_p^2}\right)\right]^2 \tag{4.58}$$

that in the thermodynamic limit becomes

$$\mathcal{L}(t) = \exp\left[\frac{L}{\pi}\int_0^\pi \log\left(\frac{1+e^{-2i\epsilon_h(p)t}K_p^2}{1+K_p^2}\right)^2\right], \tag{4.59}$$

which implies that the logarithmic Loshcmidt echo reads

$$G_{h_0,h}(t) = -\frac{1}{2\pi}\int_0^\pi dp \log\left(1-\sin^2\epsilon_h(p)t\frac{(h-h_0)^2\sin^2 p}{(1+h_0^2-2h_0\cos p)(1+h^2-2h\cos p)}\right) \tag{4.60}$$

The quantity for fixed L was calculated with the iTEBD algorithm as indicated in Fig. 4.7. Transfer-like matrices obtain from two subsequent sites (an odd and an even

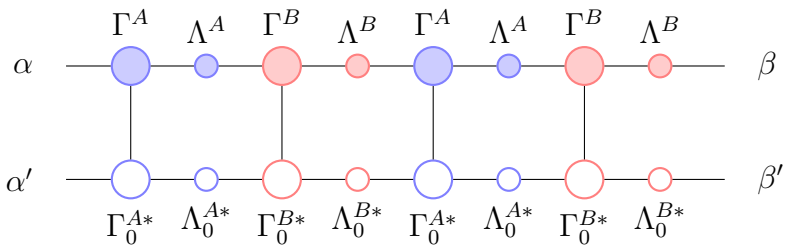

Figure 4.7: Overlap for $L = 4$ between the ground state of $H(h_0)$ and the state of the system at a certain time t after the sudden quench.

one) are contracted for $L/2$ times. The final tensor $T_{\alpha\alpha',\beta\beta'}$ can be regarded as a two indices tensor $M_{(\alpha\alpha'),(\beta\beta')}$ whose indeces spaces have dimensions equal to the product of the bond dimensions of the ground state and the state at a certain time t. The overlap is then given by the dominant eigenvalue η of such matrix, and the LLE is given by

$$G_{h_0,h}(t) = -\frac{2}{L}\log\eta(t) \tag{4.61}$$

In Fig. 4.8 is shown, for the quench $h_0 = 0.6 \to h = 0.3$, the Loschmidt echo for different lengths and the LLE. The latter is compared with the result (4.60).

The long time limit for the LLE is not as simple as the transverse magnetization one. First we expan the logarithm in the LLE

$$\begin{aligned} G_{h_0,h}(t) &= -\frac{1}{2\pi}\int_0^\pi \log\big(1-\alpha(p)\sin^2(\epsilon_h(p)t)\big) \\ &= \frac{1}{2\pi}\sum_{k=1}^{\infty}\frac{1}{k}\int_0^\pi dp(\alpha(p))^k\sin^{2k}(\epsilon_h(p)t) \coloneqq f_\alpha(t). \end{aligned} \tag{4.62}$$

The next step is to write $\sin^{2k}(\epsilon_h t)$ in its binomial expansion:

$$\sin^{2k}(\epsilon_h t) = \left(\frac{e^{i\epsilon_h(p)t}-e^{-i\epsilon_h(p)t}}{2i}\right)^{2k} = \frac{1}{4^k}\sum_{n=0}^{2k}(-1)^{k+n}\binom{2k}{n}e^{-2i(k-n)\epsilon_h(p)t}. \tag{4.63}$$

When considering the infinite time limit we use the Riemann-Lebesgue lemma on all the terms, obtaining from the binomial expansion that only the term with $k = n$ survives and

$$\lim_{t\to\infty} f_\alpha(t) = \frac{1}{2\pi}\sum_{k=1}^{\infty}\frac{1}{4^k k}\binom{2k}{k}\int_0^\pi dp(\alpha(p))^k \tag{4.64}$$

When $|\alpha(t)| < 1$ we can use the series convergence

$$\sum_{k=1}^{\infty}\frac{x^k}{4^k k}\binom{2k}{k} = \log 4 - 2\log\Big(1+\sqrt{(1-x)}\Big), \qquad |x|<1 \tag{4.65}$$

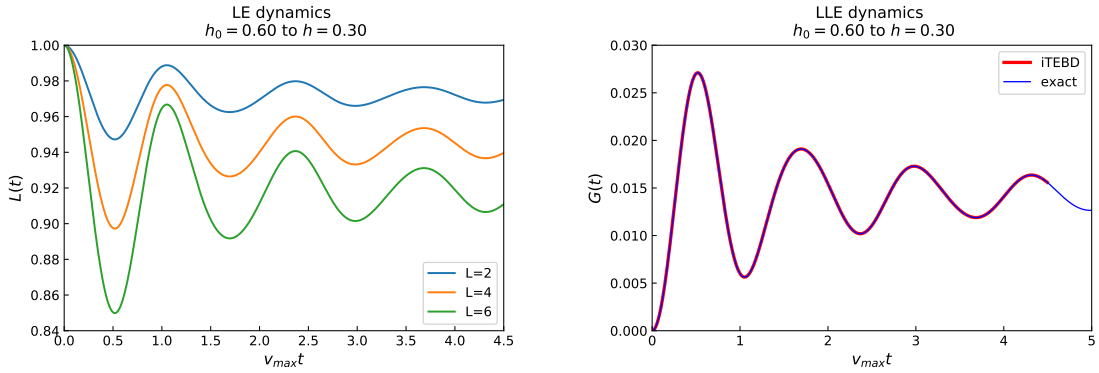

(a) (b)

Figure 4.8: Time evolution of the Loschmidt Echo (a) and of LLE (b).

That fact that the limit for $t \to \infty$ exists once the thermodynamic limit is taken is non trivial and it shows that an infinite-size system may equilibrate to a steady state after a quench.

and obtain

$$\lim_{t\to\infty} G_{h_0,h}(t) = -\frac{1}{\pi}\int_0^\pi dp \log\Big[\frac{1}{2}\Big(1 + \frac{1 + hh_0 - (h+h_0)\cos p}{\sqrt{1+h^2-2h\cos p}\sqrt{1+h_0^2-2h_0\cos p}}\Big)\Big]. \quad (4.66)$$

4.1.6 Two-point Green function

For a quench within the ordered phase the two-point function was calculated in [9] and has the following form:

$$\begin{aligned}\rho_{FF}(r,t) \simeq \mathcal{C}_{FF} \exp\Big[r\int_0^\pi \frac{dk}{\pi}\log|\cos\Delta_k|\theta_H(2\epsilon_h'(k)t - l)\Big] \\ \times \exp\Big[2t\int_0^\pi \frac{dk}{\pi}\epsilon_h'(k)\log|\cos\Delta_k|\theta_H(l - 2\epsilon_h'(k)t)\Big],\end{aligned} \quad (4.67)$$

where $\theta_H(x)$ is the Heaviside step function and $\mathcal{C}_{FF}$ is fixed by matching (4.67) to the corresponding result at infinite time [10].

The two-points correlator with the iTEBD algorithm was calculated as indicated in Fig. 3.11.

In Fig. 4.9 is shown the two-point function and the connected Green function

$$G_c(r,t) = G(r,t) - m(t)^2 \quad (4.68)$$

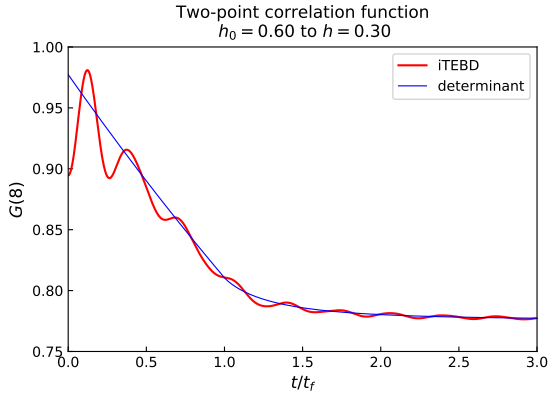

(a)

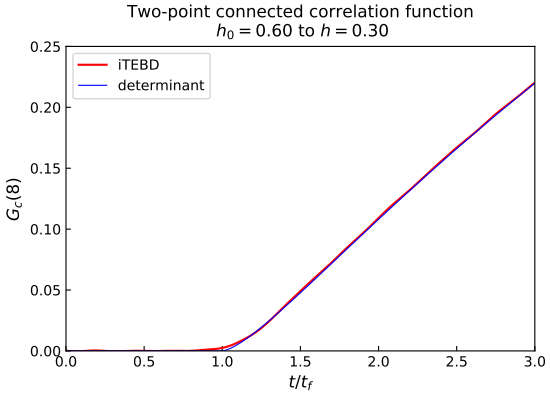

(b)

Figure 4.9: Two-point correlation function and connected correlation function for a quench within the ferromagnetic phase.

for a quench within the ferromagnetic phase. It is clear that due to the maximum speed of propagation, as a consequence of the Lieb-Robinson bound [64], all connected correlations at distance r vanish for times such that $2v_{max}t < r$ as shown clearly in Fig. 4.10.

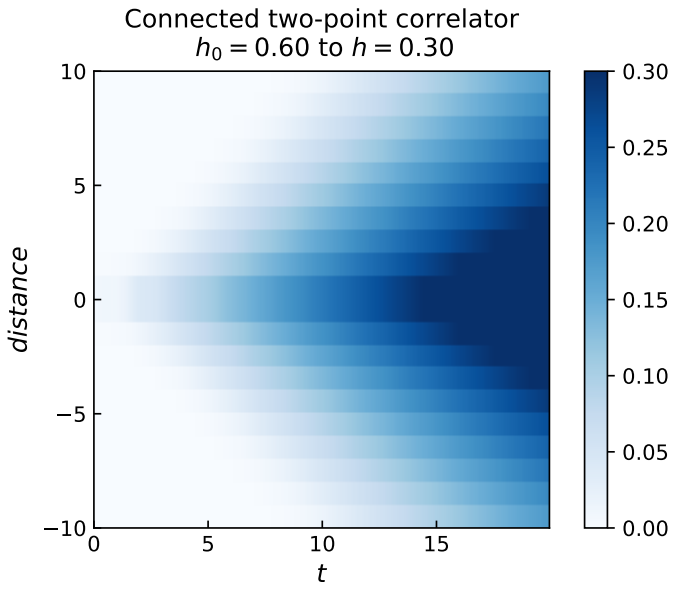

Figure 4.10: Time evolution of the connected correlation function as function of time and distance.

4.2 3-state quantum Potts model

A straightforward generalization of the quantum Ising model is the quantum q-state Potts model. It consists of a chain of generalized spins having internal quantum states $|\mu\rangle_i$, with i labeling the lattice sites and $\mu = 1, \ldots, q$ the possible internal states of the spins. The Hamiltonian of the model reads:

$$H = -J\left(\sum_i \sum_{\mu=1}^{q} P_i^\mu P_{i+1}^\mu + h \sum_i P_i\right). \tag{4.69}$$

The first term of the Hamiltonian contains the traceless projector $P_i^\mu = |\mu\rangle_i \langle\mu|_i$ which tend to align the spin at site i along the direction μ. This term promotes a ferromagnetic groundstate with a spontaneous magnetization pointing at one of the q directions. The second term, conversely, represents a *transverse field*, like in the Ising case, that perturbes the ferromagnetic regime. The traceless operator $P_i = |\lambda_0\rangle \langle\lambda_0| - 1/q$ tends to project the spin along the direction $|\lambda_0\rangle \equiv \sum_\mu \frac{|\mu\rangle}{\sqrt{q}}$. The relative strenght of these two terms is regulated by the dimensionless coupling costant h: for large values of h one finds a paramagnetic phase with a unique ground state, while for small h a ferromagnetic phase appears with q degenerate ground states, spontaneously breaking the global $\mathbb{S}_q$ symmetry (the latter can be decomposed into $\mathbb{Z}_2 \otimes \mathbb{Z}_3$). This competition leads to a quantum phase

transition for a critical value of the coupling costant h_c.

From now on, we focus on the 3−Potts model. The transition occurs at a coupling $h_c = 1$, and it is of second order: quasiparticles are gapped on both sides of the transition, but the quasiparticle gap Δ vanishes continuously at the transition as $\Delta \sim J|h-1|^{5/6}$ [72]. This second-order phase transition belongs to a different universality class from the Ising case [27].

Below the critical value the ground state is a 3−fold degenerate ferromagnet corresponding to the three different ferromagnetic alignments of the generalized spins. The elementary excitations are domain walls that move along the chain with dispersion relation

$$\epsilon_k^{\mu,\mu'} = \epsilon(k), \tag{4.70}$$

where the two indices μ and μ' denote the orientations of the ferromagnetic order parameters. These quasi-particles are gapped and their energy can be approximated for smal h as

$$\epsilon(k) \simeq J(1 - \frac{2h}{3}\cos k). \tag{4.71}$$

Conversely, for $h > h_c$ the ground state is a non degenerate paramagnet which corresponds to orienting all spins along the $|\lambda_0\rangle$ direction. Elementary excitations of this state consist of $\lambda = 1, \ldots, q-1$ possible local spin flips which propagate along the chain with dispertion relation

$$\epsilon_k^{\lambda} = \tilde{\epsilon}(k). \tag{4.72}$$

Also this excitations are gapped and for very large values of the coupling constant h one finds [72]

$$\tilde{\epsilon}(k) \simeq 3J(1 - \frac{2}{3h}\cos k). \tag{4.73}$$

4.2.1 Quench protocol

Unlike the Ising case, we now have three different magnetizations. We can name them *red*, *green* and *blue*. As initial state for the imaginary time evolution we can choose a ferromagnetic state where all the spins are aligned with one of the three directions, say *red*:

$$\begin{aligned} \Gamma^{A,r} &= 1 = \Gamma^{B,r} \\ \Gamma^{A,g} &= 0 = \Gamma^{B,g}. \\ \Gamma^{A,b} &= 0 = \Gamma^{B,b} \end{aligned} \tag{4.74}$$

Since the quantum Potts model is non integrable, we have no predictions of the time evolution of any of its observables. However, being a straightforward generalization of the Ising case, we might expect its behaviour to be qualitatively tha same.

4.2.2 Magnetizations and transverse field

We analyze the dynamics of the main local observables, that is the (red) magnetization $< P_1 >$, order parameter of the phase transition, and the transverse field $< P >$.

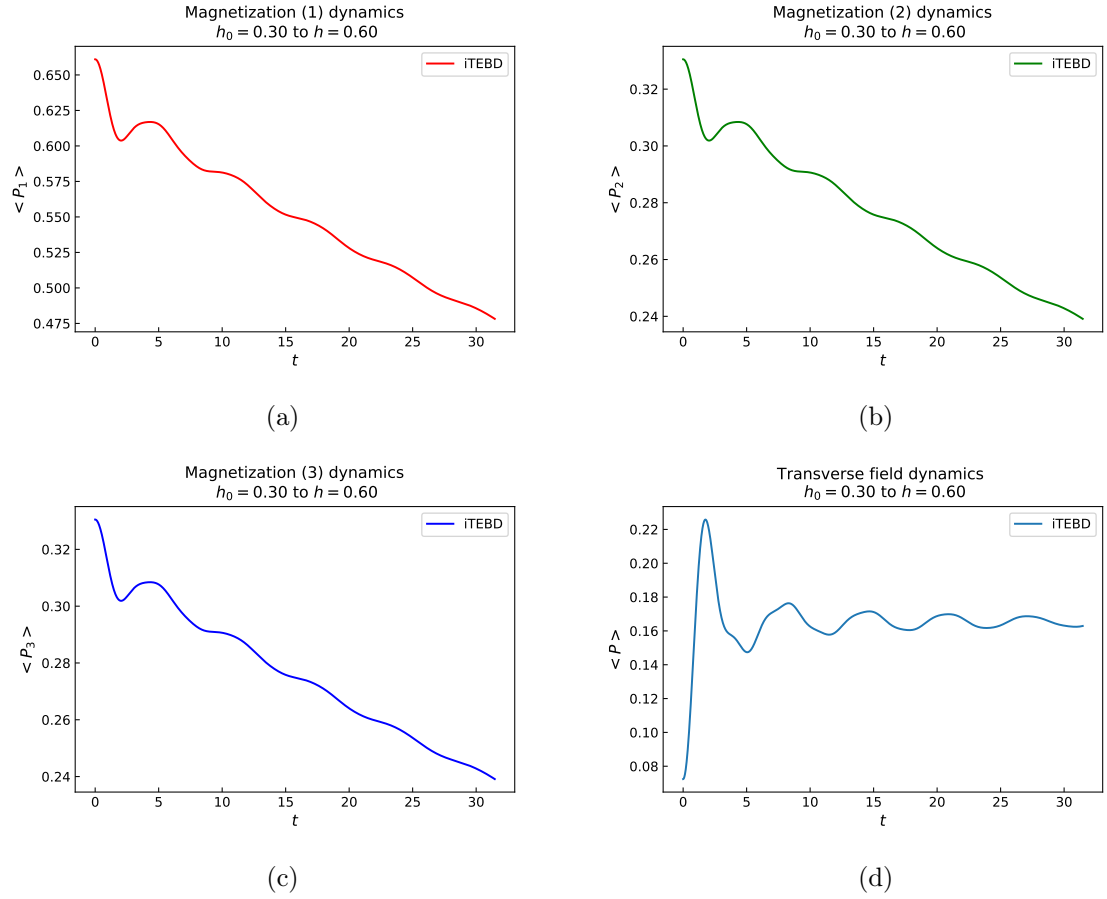

Figure 4.11: Time evolution of the three magnetizattions and of the transverse field for a quench within the ferromagnetic phase.

In Fig. 4.11 we show the time evolution of the three magnetization for a quench within the ferromagnetic phase, as well as the time evolution of the transverse field.

When both h and h_0 are below the critical value, the relaxation process is very slow.

Anyway the behaviour of $< P_1 >$ is exactly the same observed in the Ising case for very short times:

. If $h < h_0$ the equilibration process is slower. $< P_1 >$ initially increases for very short times and then starts decreasing oscillating;

. Conversely when $h < h_0$ the opposite occurs (Fig. 4.12).

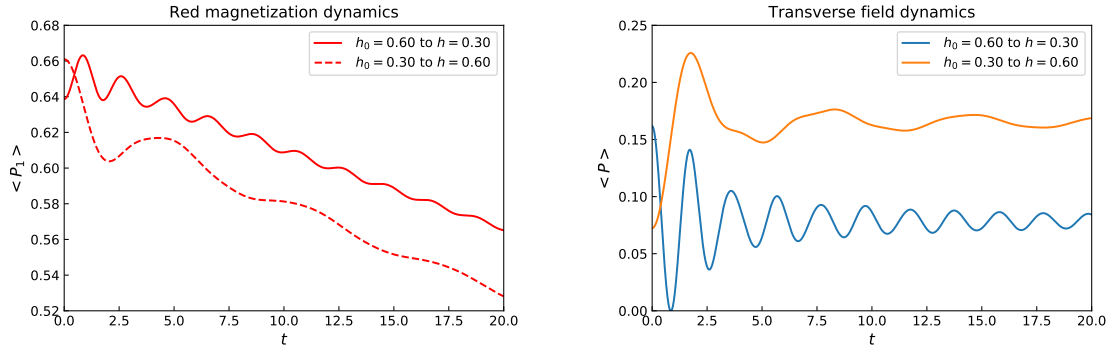

(a) (b)

Figure 4.12: Time evolution of red magnetization and transverse field for quenches within the ferromagnetic phase.

Due to the slow process of equilibration, the times available with the simulation are not sufficient to observe the value at which the magnetization relaxes but the similarities with the Ising model suggest that it may relax to zero, leading to symmetry restoration, as proved in [9].

It is observed that the equilibration value of the order parameter is zero when quanching from the ferromagnetic to the paramagnetic phase. Moreover, its amplitude is exponentially suppressed as in the Ising case. This suggest a greater stability of the magnetization while approaching equilibrium (Fig. 4.13).

As far as the transverse field is concerned, an important remark has to be made. We showed that the infinite time limit of the transverse field expectation value (4.55) depends both on h and h_0 and if $h > h_0$, we also had $M(\infty) > M(0)$. The opposite happens if the final coupling constant is smaller then the one in the pre quench Hamiltonian. As shown in Fig. 4.14 as well as in Fig. 4.12 and Fig. 4.13, the same behaviour is observed in the Potts model for the quench considered. This features is believed to hold for general quenches.

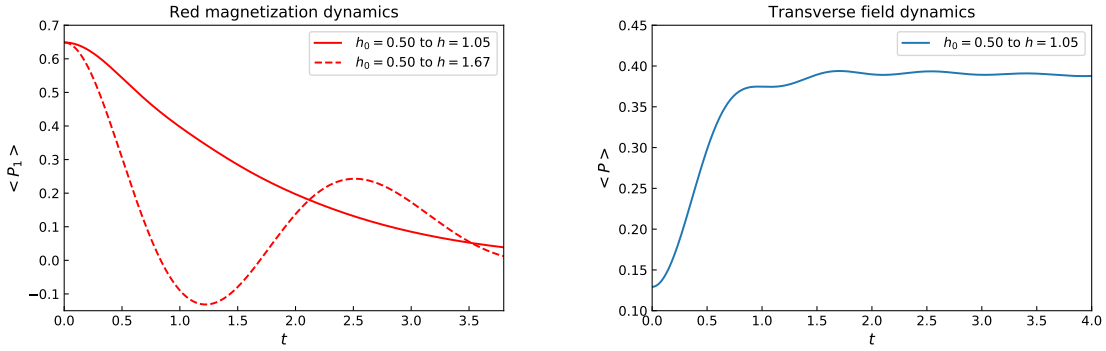

(a) (b)

Figure 4.13: Time evolution of red magnetization and transverse field for quenches to the paramagnetic phase.

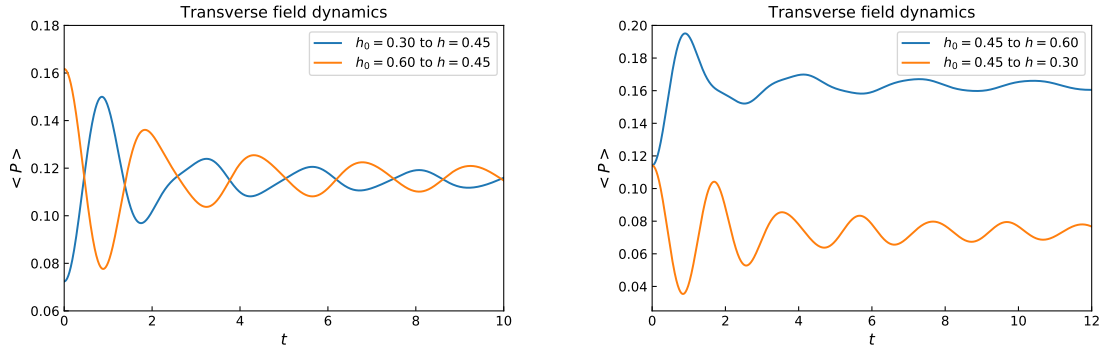

(a) (b)

Figure 4.14: Time evolution of transverse field for quenches within the ferromagnetic phase.

We remark that this similarities can be interpreted with a semiclassical picture. This approach is based on the observation that at very low temperatures only quasi-particles with energy close to the quasi-particle cap are present, $\epsilon(k) \simeq \Delta$. The energy of these quasi-particles can be approximated as [73]

$$\epsilon(k) = \Delta + \frac{k^2}{2\Delta} + o(k^4). \tag{4.75}$$

This means that as long as they don't interact, they behave like free classical particles. For low temperatures, the distribution of quasi-particles is described by Boltzmann statistics and correspondingly their density is exponentially small. This behaviour breaks when excitations get closer than the de Broglie wavelenght. In one dimensional systmes

this is bond to happen since collisions are unavoidable. However, due to the dilute nature of quasi-particles, we have only two-particle scatterings, that is what we have for integrable systems.

Chapter 5

Explicit $\mathbb{Z}_n$ symmetry breaking with longitudinal field

I may not have gone where I intended to go, but I think I have ended up where I needed to be.

- Douglas Adams, *The Long Dark Tea-Time of the Soul*

In this final chapter it is reported how the dynamics of the models is affected by the addition of a longitudinal field. For the Ising model, whose integrability gets broken, it is studied the ferromagnetic phase, reproducing the results obtained in [12]. The Potts model is analyzed in its paramagnetic phase, with focus on the entanglement entropy behaviour.

5.1 Quantum Ising model with longitudinal field: ferromagnetic phase

In the previous chapter we presented results that highlighted the validity of the quasi-particle description of quantum quenches: the initial state is a highly exited configuration in terms of the post.quench Hamiltonian, whisch acs as a source of quasi-particles excitations propagating through the system. But what happens if a confinement potential is introduced in the system? Pairs of quasi-particles move in opposite directions, but due to the confining potential the farther they go apart the stronger is the attractive force

they feel, which eventually turns the particles back leading to an oscillatory behaviour, as depicted in Fig. 5.1.

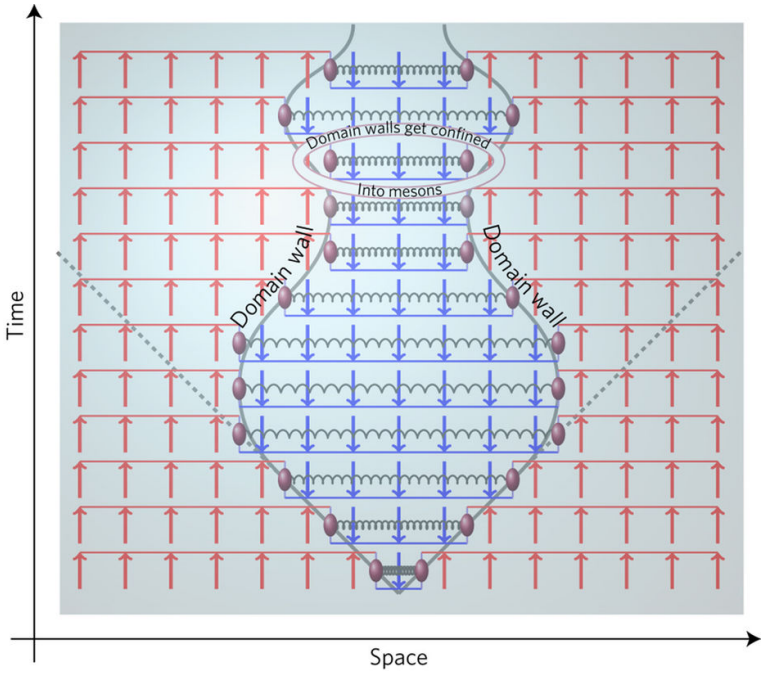

Figure 5.1: Pictorial semiclassical picture of a meson state in the Ising model: two counter-propagating domain walls bounce back and forth because of a confining interaction [12].

Confinement is known to take place in the Ising model with both transverse and longitudinal fields. This case was investigated in [12] and here some key results are reproduced. The Ising Hamiltonian with the addition of longitudinal field becomes

$$H(h) = -J \sum_{j=1}^{N} [\sigma_j^z \sigma_j^z + h_x \sigma_j^x + h_z \sigma_j^z]. \tag{5.1}$$

In the ferromagnetic phase, switching on a non-zero field h_z induces a linear attractive potential between pairs of domain walls which enclose a domain of length d and of magnetisation opposite to h_z. For small fields the potential can be approximated as $V(d) = \chi d$, with $\chi = 2Jh^z\bar{\sigma}$ [74], where $\bar{\sigma} = (1 - h_x^2)^{1/8}$. . As a result, the domain walls are confined into bound states called *mesonic states* in analogy to the phenomenon in particle physics of bound states of strong interactions. The model for $h_z \neq 0$ is no longer integrable and the spectrum can't be computed exactly.

We analyze the changes in the chain's dynamics with time evolution of the magnetization, the entanglement entropy and the two point correlation function.

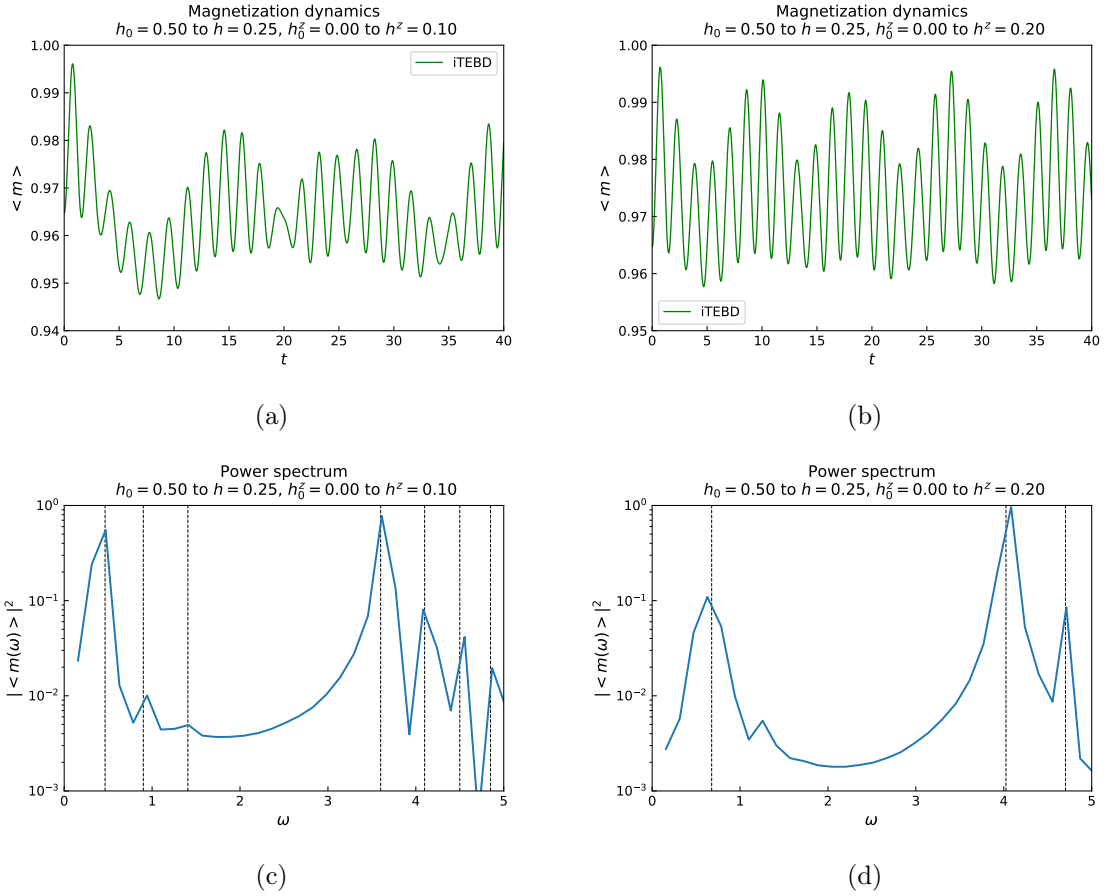

Figure 5.2: Time evolution of the longitudinal magnetization after quenching from $h^x = 0.5, h^z = 0$ to $h^x = 0.25$ and $h^z = 0.1, 0.2$. Below, their power spectrum is shown. The vertical lines are the values for the meson masses predicted by [12].

5.1.1 Magnetization

The simulation for the magnetization $m(t) = \langle \sigma^z(t) \rangle$ dynamics with longitudinal field is displayed in Fig. 5.2. It is clear that a small longitudinal field radically alters the dynamics, turning the exponential relaxation expressed by (4.46) into an oscillatory behaviour with numerous different frequencies. The qualitative change of the dynamics is the consequence of confinement [12]. This can be demonstrated by extracting the oscillation frequencies with a discrete Fourier transform of the time series, which are also reported in Fig. 5.2. The vertical lines are the values for the meson masses predicted (see [12] for details of the calculation).

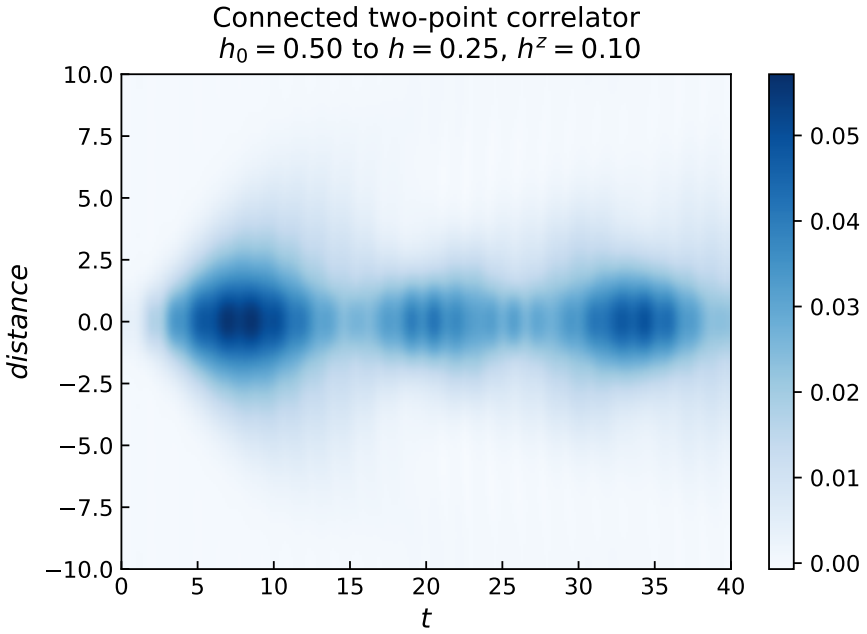

Figure 5.3: Time evolution of the connected correlation function as function of time and distance.

5.1.2 Two-point function

The two-point function is the quantity that shows the strongest effects of confinement. Indeed, when the interaction of the longitudinal field is turned on, the propagating particles are the heavy massive mesons and not the light domain walls. The former propagate with a maximal velocity which is smaller than that of the latter. By increasing h_z the region where there is light cone propagation shrinks to an almost invisible portion of the space-time. What happens is that due to the heavy masses of the mesons, the quench only provides sufficient energy to produce them at rest (see Fig. 5.3).

5.1.3 Entanglement entropy

We consider now the time evolution of the entanglement entropy of half chain. By turning on the longitudinal interaction, the linear growth of the entanglement entropy described in section 2.4 is considerably slowed down and saturates for quenches within the ferromagnetic phase with a sufficiently large longitudinal field. The latter correspond to cases in which the light-cone of the two-point function is strongly suppressed. As explained above, this is a consequence of the fact that mesons are predominantly produced at rest

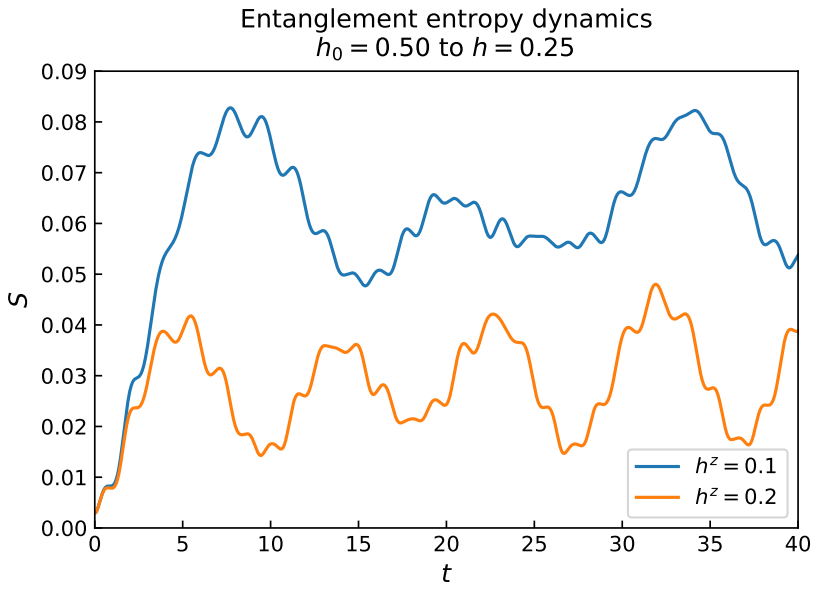

Figure 5.4: Time evolution of entanglement entropy after quenching from $h^x = 0.5, h^z = 0$ to $h^x = 0.25$ and $h^z = 0.1, 0.2$.

and then the entanglement just oscillates around a saturation value. An example of this behaviour is shown in Fig. 5.4. Actually the small fraction of mesons with non-negligible ve- locities should produce a very slow increase of the entangle- ment which however is likely too small to be observed.

5.2 3-state quantum Potts model with longitudinal field: paramagnetic phase

In the same paper where the results of the Ising model with longitudinal field were reported [12], it was also spotted a peculiar behaviour of the entanglement entropy also in the paramagnetic phase: tuning the parameters of the system, a sudden increase in the entanglement production rate was observed This gave motivation to study the paramagnetic phase also in the Potts model, which is the main topic of the section.

In a recent paper [13], prelude to this work, the phenomenon was explained for the Ising case as a dynamical manifestation of Gibbs paradox. We explain this result with the 3-state Potts model.

The Hamiltonian (4.69) is modified by the addition of a longitudinal field in the *red direction*, whose intensity is determined by the dimensionless coupling costant h_1:

$$H = -J\left(\sum_i \sum_{\mu=1}^{3} P_i^\mu P_{i+1}^\mu + h\sum_i P_i + h_1 \sum_i P_i^1\right) \tag{5.2}$$

We now analyze the entanglement entropy dynamics.

5.2.1 Entanglement entropy

When the longitudinal field is absent we expect a linear growth. This behaviour is shown in Fig. 5.5. When the difference between the value of the coupling constant pre-quench and its value post quench increases, so does the energy available to the creation and the propagation of quasi-particle excitations and the slope of the entanglement growth increases consequently. But what happens when a longitudinal field is introduced?

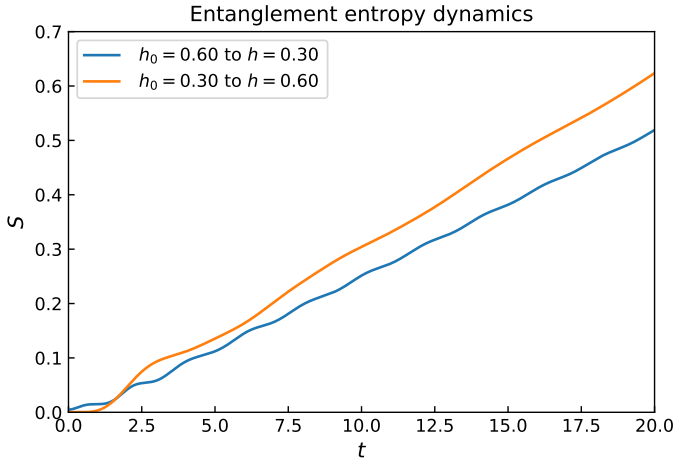

Figure 5.5: Time evolution of entanglement entropy after quenching from $h_0 = 0.3$ to $h = 0.6$ in absence of a longitudinal field.

In the following, we will consider quenches from a value $h > 1$ and a vanishing longitudinal field, to the very same value h and a non vanishing h_1, so that the longitudinal field is the only source of energy.

From Fig. 5.6 we can see that the averall linear growth remains and the average late time behaviour of the entranglement entropy can be fit with a linear behaviour apart from periodic fluctuations. It is not easy to extrapolate the frequencies of those fluctuations due to the constant shift, but we should supposedly find the same frequencies on the time evolution of both magnetizations and transverse field.

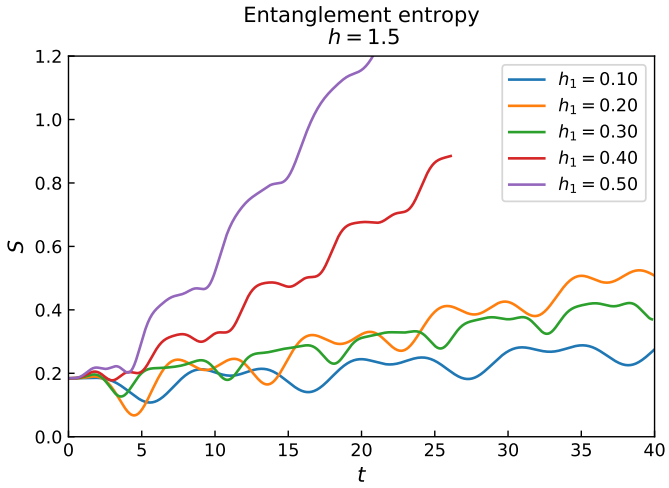

Figure 5.6: Time evolution of entanglement entropy after quenching from $h = 1.5, h_1 = 0$ to $h = 1.5, h_1 = 0.1, 0.2, 0.3, 0.4, 0.5$.

Another surprising result is that if we look at the mean entanglement production rate $\overline{\partial_t S}$ that can be obtained from the slope of the linear part of the entropy, it does not increase monotonically with h_1. It is indeed evident from Fig. 5.7 that for every value of transverse field h considered, the mean entanglement production rate reaches a maximum value, than it has a minimum and finally rapidly increases with the longitudinal field.

This behaviour can be understood by looking at the frequencies that determines time evolution. In Fig. 5.8 and Fig. 5.9 time evolution of the magnetization and transverse field for two different values of the longidutdinal field are displayed. In the first figure only one frequency appears in the spectrum, corresponding to the free fermionic excitation, while in the second figure a new particle appears. We find that for a fixed value of h there exists a cirtical value of the longitudinal field at which a new quasi-particle appears in the spectrum.

5.2.2 Relation to the Gibbs paradox

In section 1.4.2 it was highlighted the difference between entanglement entropy and thermal entropy: as far as special states like ground states is concerned, while the former exhibits an area law, the latter increases according to a volume law. However, excited states resemble classical states and entanglement entropy reduces to thermodynamic entropy. Since the post quench state is given by a superposition of excited states, at

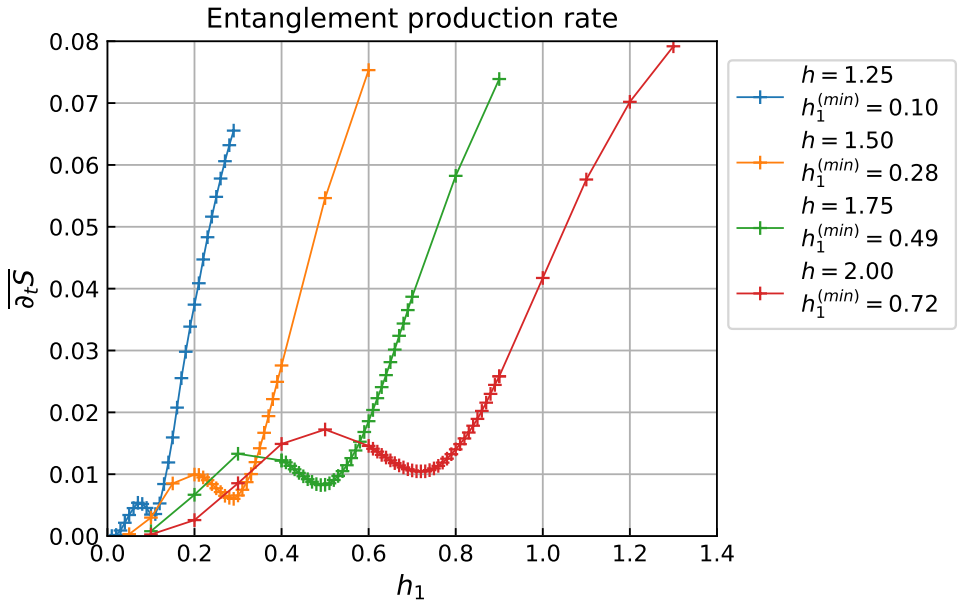

Figure 5.7: Entanglement rapidity as a function of the longitudinal field h_1 for values of the coupling costant $h = 1.25, 1.50, 1.75, 2.00$. Values of the local minima are displayed on the left.

late times the asymptotic entanglement of a large subsystem can be interpreted as the thermodynamic entropy [75].

The quasi-particle description, which is expected to be valid for sufficiently small quenches even in the non-integrable case, leads to the formula (2.54). When different quasi-particle species propagate throud the system, the formula is modified as follows:

$$\begin{aligned} S(t) \simeq 2t \sum_n \int_{-\infty}^{0} dp' \int_0^{\infty} dp'' \sigma_n(p', p'') \{v_n(-p') + v_n(p'')\} \theta(l - [v_n(-p') + v_n(p'')]t) \\ + 2l \sum_n \int_{-\infty}^{0} dp' \int_0^{\infty} dp'' \sigma_n(p', p'') \theta([v_n(-p') + v_n(p'')]t - l), \end{aligned} \tag{5.3}$$

where n enumerates the different quasi-particle species. For half the system in the thermodynamic limit, the semi-classical prediction simplifies to

$$S(t) \simeq 2t \sum_n \int dp \sigma_n(p) v_n(p), \tag{5.4}$$

considering $\sigma_n(p', p'') = \delta(p', -p'')\sigma(p')$.

This formula suggests that the entanglement production rate is a slowly varying

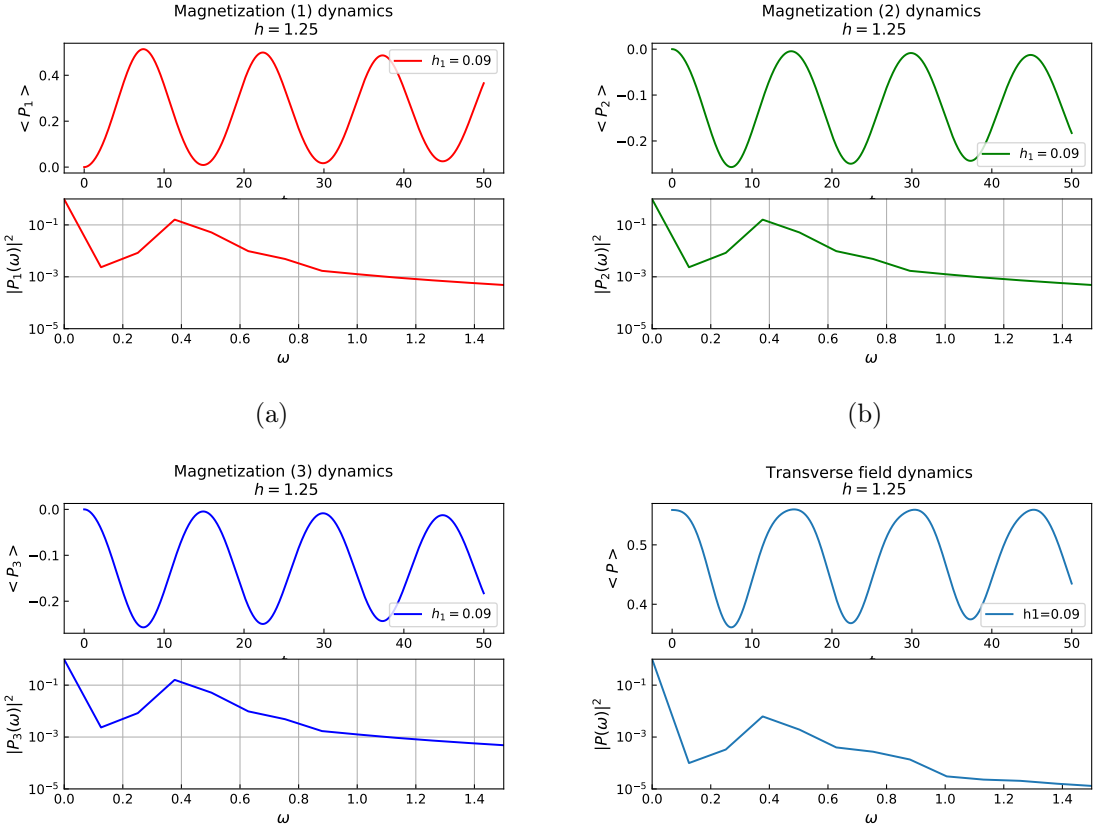

Figure 5.8: Time evolution of the three magnetizattions and of the transverse field for a quench with $g = 1.25$ and $h_1 \leq h_1^{(min)}$.

function of the quench parameter h_1, since the new quasi-particle's appearance would simply add a new species contribution, which is expected to be smaller than the term already present due to the larger mass of the bound state. However, Fig. 5.7 shows that the entanglement production rate increases by order of magnitude after passing the threshold. The flaw in the naive argument is that it neglects the contribution of species mixing, which is at the basis of the classical Gibbs paradox.

Besides the validity of the quasi-particle picture, the Fourier spectra also help explain the initial decrease of the entropy production rate (Fig. 5.8 and Fig. 5.9). The spectra show that the particle masses (excitation gaps) increase with the longitudinal field. Albeit the post-quench energy density also increases with h_1, the rising gaps prevent the particle production rate from increasing already for quite small values of h_1. As a result, the rate

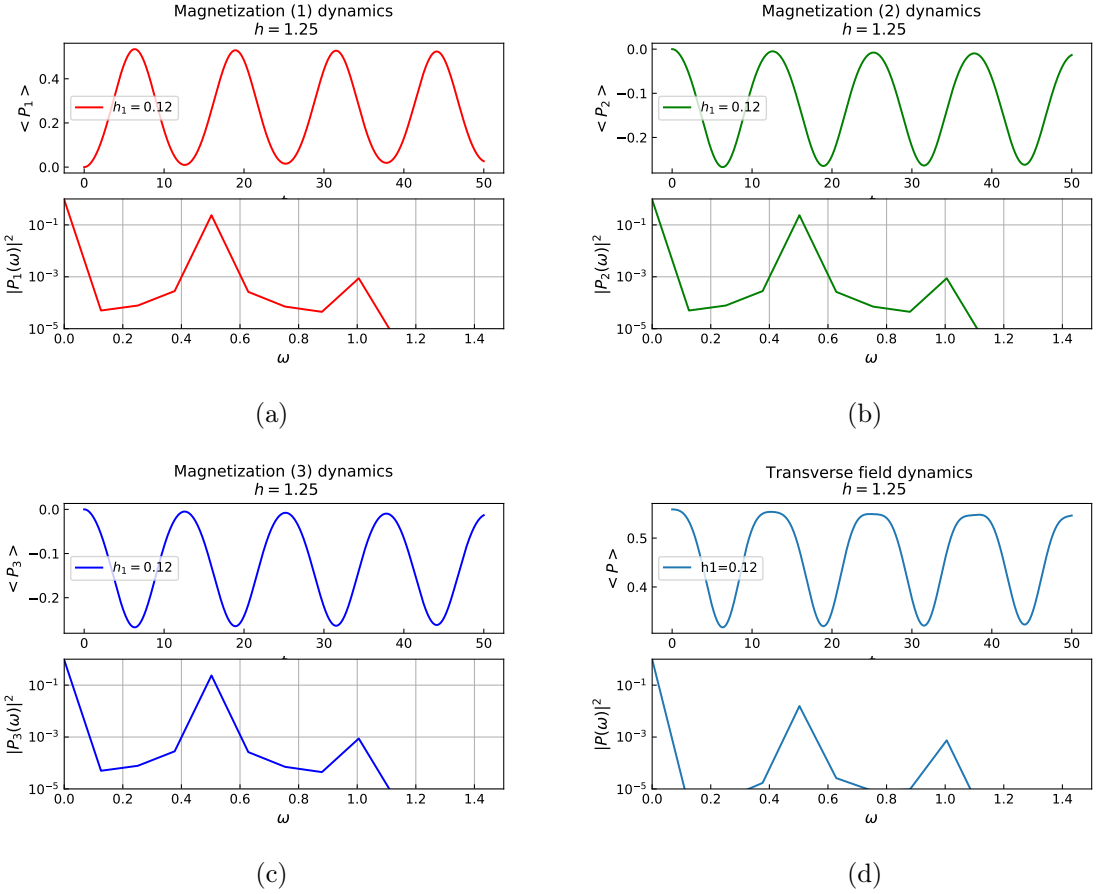

Figure 5.9: Time evolution of the three magnetizattions and of the transverse field for a quench with $g = 1.25$ and $h_1 \geq h_1^{(min)}$.

functions $\sigma_n(p)$ (which are not directly accessible) are also expected to stop growing with h_1.

For higher values of the transverse field reported in Fig. 5.8 and Fig. 5.9, it was observed that the increasing trend of the mean entanglement production rate is delayed with respect to the threshold value at which the new quasi-particle originates. This can be explained as follows. The trend change in $\overline{\partial_t S}$, although rapid, it is not a discontinuous jump, as also stated in [13], due to two effects. Firstly, the heavier second excitation is produced with a density that depends smoothly on the quench parameter h_1. Secondly, also the distinguishability of the second quasi particle peak increases gradually with h_1. As known in the case of the equilibrium Gibbs paradox, distinguishability is a key feature governing the effective number of species contributing to thermodynamic quantities. For

these reasons, instead of a discontinuous jump there is a smooth but fast transition to a substantially higher level of entropy production.

Chapter 6

Conclusive remarks and perspectives

This work was devoted to the study and understanding of several aspects of quench dynamics in one dimensional lattice spin chains. We started reviewing some fundamental problems hidden in the construction of quantum statistical mechanics itself, like the extension to the quantum world of essential concepts such as ergodicity and thermalization.

We then introduced the simplest protocol that allows to deepen the knowledge of this relations: the quantum quench. A valuable picture for the description of the dynamics after a quantum quench was introduced: the quasi-particle description. This quasi-classical picture describes the initial state as a source of entangled quasi-particles pairs which propagate to different parts of the system, resulting in the build-up of light cone spreading of correlations and entanglement growth. This picture was formalized for integrable systems with the concept of boundary states and explicitly applied for integrable quenches in the Ising spin chain. However, this semiclassical approach is expected to be valid also for sufficiently small post-quench density even in the non-integrable case, such as the 3−state Potts model. The simulations carried out throughout the manuscript validated this statement, showing Potts dynamics to be very similar in many aspects to the Ising case.

When the longitudinal field was added, the semi-classical picture of quasi-particles excitations was still the main guide in the analysis, and was capable to explained all phenomena observed. In the Ising ferromagnetic phase a mechanism that, through confinement of the elementary excitations, strongly suppresses the light-cone spreading was described; in the Potts paramagnetic phase a sudden increase in the entanglement production rate was observed and the relation with the appearance of a new quasi-particle

excitation was outlined. The phenomenon was depicted as the non-equilibrium version of the Gibbs paradox related to mixing entropy, recently observed in [13] for the Ising model with lingitudinal field.

It was explained the gradual change of the effective number of quasi-particle species characterizing the post quench state. A description of the phenomenon requires a more complete theory of entropy production with multiple quasi-particles species after a non-integrable quench, which is left open for the future.

The study of the ferromagnetic phase of the Potts models with longitudinal field it is also left for the future, where we expect a much more colourful scenario than that observed in the Ising case, due to the presence of three different magnetizations.

Appendix A

Boundary states

Consider the state with kernel $\aleph$

$$|B_\aleph\rangle = \exp\left\{\sum_{k>0} \aleph_k \eta_k^\dagger \eta_{-k}^\dagger\right\}|0\rangle = \prod_{k>0} e^{\aleph_k \eta_k^\dagger \eta_{-k}^\dagger}|0\rangle \tag{A.1}$$

where the operators η_k and $\eta_k^\dagger$ follow the usual fermionic commutation relations:

$$\{\eta_k, \eta_l^\dagger\} = \delta_{k,l} \qquad \{\eta_k, \eta_l\} = \{\eta_k^\dagger, \eta_l^\dagger\} = 0 \tag{A.2}$$

and the vacuum is defined by

$$\eta_k|0\rangle = 0 \qquad \forall k. \tag{A.3}$$

Due to (A.2) one has

$$e^{\aleph_k \eta_k^\dagger \eta_{-k}^\dagger} = 1 + \aleph_k \eta_k^\dagger \eta_{-k}^\dagger, \tag{A.4}$$

expression that allows to evaluate the inner product between boundary states:

$$\begin{aligned}\langle B_\aleph | B_{\aleph'}\rangle =& \langle 0|\prod_{k>0} e^{\bar{\aleph}_k \eta_k \eta_{-k}} \prod_{q>0} e^{\aleph'_q \eta_q^\dagger \eta_{-q}^\dagger}|0\rangle \\ =& \prod_{k>0} \langle 0|(1+\bar{\aleph}_k \eta_k \eta_{-k})(1+\aleph'_k \eta_k^\dagger \eta_{-k}^\dagger)|0\rangle = \prod_{k>0}(1+\bar{\aleph}_k \aleph'_k \langle \eta_k \eta_{-k}\rangle \eta_{-k}^\dagger \eta_k^\dagger 0) \\ =& \prod_{k>0}(1+\bar{\aleph}_k \aleph'_k) = \exp\left[\sum_{k>0} \log\left(1+\bar{\aleph}_k \aleph'_k\right)\right].\end{aligned} \tag{A.5}$$

It follows that the boundary state's norm for fermions is easly evaluated as

$$\langle B_{\aleph}|B_{\aleph}\rangle = \exp\left[\sum_{k>0}\log\left(1+|\aleph_k|^2\right)\right]. \tag{A.6}$$

To the aim of calculating the expextation values of the momenta of the number operator $n_k = \eta_k^\dagger \eta_k$, let's introduce the generating function

$$F_{\aleph}(\lambda_q) = \frac{\langle B_{\aleph}|\exp\left(\sum_{q>0}\lambda_q n_q\right)|B_{\aleph}\rangle}{\langle B_{\aleph}|B_{\aleph}\rangle} := \left\langle \exp\left(\sum_{q>0}\lambda_q n_q\right)\right\rangle_{\aleph}, \tag{A.7}$$

so thet the momenta are obtain as derivatives with respect to λ:

$$\langle n_{p_1}\dots n_{p_l}\rangle_{\aleph} = \frac{\partial^l}{\partial\lambda_{p_1}\dots\partial\lambda_{p_l}}F_{\aleph}(\lambda_q)\bigg|_{\lambda_p=0} \tag{A.8}$$

The first step to compute $F_{\aleph}(\lambda_q)$ is to understand that the exponential function $\exp\left(\sum_{q>0}\lambda_q n_q\right)$ acts on a boundary state modifying its kernel $\aleph$ to $\aleph e^{\lambda}$. Indeed, taking the boundary state definition (A.1) and the commutation relations (A.2) into account one has:

$$\begin{aligned}\exp\left(\sum_{q>0}\lambda_q n_q\right)|B_{\aleph}\rangle &= \exp\left(\sum_{q>0}\lambda_q n_q\right)\exp\left\{\sum_{k>0}\aleph_k\eta_k^\dagger\eta_{-k}^\dagger\right\}|0\rangle \\ &= \exp\left\{\sum_{k>0}\aleph_k e^{\lambda_k}\eta_k^\dagger\eta_{-k}^\dagger\right\}\exp\left(\sum_{q>0}\lambda_q n_q\right)|0\rangle \\ &= |B_{\aleph e^{\lambda}}\rangle\,.\end{aligned} \tag{A.9}$$

It follows from the inner product calculation (A.5) that

$$F_{\aleph}(\lambda_q) = \frac{\langle B_{\aleph}|B_{\aleph e^{\lambda}}\rangle}{\langle B_{\aleph}|B_{\aleph}\rangle} = \exp\left[\sum_{q>0}\log\left(\frac{1+e^{\lambda_q}|\aleph|^2}{1+|\aleph|^2}\right)\right]. \tag{A.10}$$

Taking the derivatives with respect to the λ_p and putting them to zero we finally obtain

$$\langle n_{p_1}\dots n_{p_l}\rangle_{\aleph} = \prod_{j=1}^{l}\frac{|\aleph_{p_j}|^2}{1+|\aleph_{p_j}|^2}. \tag{A.11}$$

Conversely if one aim is to calculate the mean value of a sequence of $\eta_{-k}^\dagger\eta_k^\dagger$ or their adjoint, it can be obtained in the same way with the generating funtion

$$G_{\aleph}(\lambda_q) = \frac{\langle B_{\aleph}|\exp\left(\sum_{q>0}\lambda_q\eta_{-q}^\dagger\eta_q^\dagger\right)|B_{\aleph}\rangle}{\langle B_{\aleph}|B_{\aleph}\rangle}. \tag{A.12}$$

Following the same steps it is easy to see that $\exp\left(\sum_{q>0}\lambda_q\eta^\dagger_{-q}\eta^\dagger_q\right)$ acts on a boundary state as a translation in the kernel by λ and

$$G_{\aleph}(\lambda_q)=\frac{\langle B_{\aleph}|B_{\aleph+\lambda}\rangle}{\langle B_{\aleph}|B_{\aleph}\rangle}=\exp\left[\sum_{q>0}\log\left(\frac{1+\bar{\aleph}_q(\aleph_q+\lambda_q)}{1+|\aleph_q|^2}\right)\right]. \tag{A.13}$$

We eventually obtain

$$\left\langle \eta^\dagger_{-k_1}\eta^\dagger_{k_1}\dots\eta^\dagger_{-k_l}\eta^\dagger_{k_l}\right\rangle_{\aleph}=\frac{\partial^l}{\partial\lambda_{k_1}\dots\partial\lambda_{k_l}}G_{\aleph}(\lambda_q)\bigg|_{\lambda_k=0}=\prod_{k_j=1}^{l}\frac{\bar{\aleph}_{k_j}}{1+|\aleph_{k_j}|^2} \tag{A.14}$$

Bibliography

[1] J. von Neumann, "Proof of the Ergodic Theorem and the H-Theorem in Quantum Mechanics," *ArXiv e-prints* (Mar., 2010) , arXiv:1003.2133 [physics.hist-ph].

[2] P. Courteille, R. S. Freeland, D. J. Heinzen, F. A. van Abeelen, and B. J. Verhaar, "Observation of a feshbach resonance in cold atom scattering," *Phys. Rev. Lett.* **81** (Jul, 1998) 69–72. https://link.aps.org/doi/10.1103/PhysRevLett.81.69.

[3] D. M. Stamper-Kurn, M. R. Andrews, A. P. Chikkatur, S. Inouye, H.-J. Miesner, J. Stenger, and W. Ketterle, "Optical confinement of a bose-einstein condensate," *Phys. Rev. Lett.* **80** (Mar, 1998) 2027–2030. https://link.aps.org/doi/10.1103/PhysRevLett.80.2027.

[4] R. Grimm, M. Weidemüller, and Y. B. Ovchinnikov, "Optical dipole traps for neutral atoms," vol. 42 of *Advances In Atomic, Molecular, and Optical Physics*, pp. 95 – 170. Academic Press, 2000. http://www.sciencedirect.com/science/article/pii/S1049250X0860186X.

[5] P. Calabrese and J. Cardy, "Time dependence of correlation functions following a quantum quench," *Phys. Rev. Lett.* **96** (Apr, 2006) 136801. https://link.aps.org/doi/10.1103/PhysRevLett.96.136801.

[6] S. Östlund and S. Rommer, "Thermodynamic Limit of Density Matrix Renormalization," *Physical Review Letters* **75** (Nov., 1995) 3537–3540, cond-mat/9503107.

[7] S. R. White, "Density matrix formulation for quantum renormalization groups," *Phys. Rev. Lett.* **69** (Nov, 1992) 2863–2866. https://link.aps.org/doi/10.1103/PhysRevLett.69.2863.

[8] G. Vidal, "Efficient Classical Simulation of Slightly Entangled Quantum Computations," *Physical Review Letters* **91** no. 14, (Oct., 2003) 147902, quant-ph/0301063.

[9] P. Calabrese, F. H. L. Essler, and M. Fagotti, "Quantum quench in the transverse field Ising chain: I. Time evolution of order parameter correlators," *Journal of Statistical Mechanics: Theory and Experiment* **7** (July, 2012) 07016, arXiv:1204.3911 [cond-mat.quant-gas].

[10] P. Calabrese, F. H. L. Essler, and M. Fagotti, "Quantum quenches in the transverse field Ising chain: II. Stationary state properties," *Journal of Statistical Mechanics: Theory and Experiment* **7** (July, 2012) 07022, arXiv:1205.2211 [cond-mat.stat-mech].

[11] P. Calabrese and J. Cardy, "Evolution of entanglement entropy in one-dimensional systems," *Journal of Statistical Mechanics: Theory and Experiment* **4** (Apr., 2005) 04010, cond-mat/0503393.

[12] M. Kormos, M. Collura, G. Takács, and P. Calabrese, "Real-time confinement following a quantum quench to a non-integrable model," *Nature Physics* **13** (Mar., 2017) 246–249, arXiv:1604.03571 [cond-mat.stat-mech].

[13] M. Collura, M. Kormos, and G. Takacs, "Dynamical manifestation of Gibbs paradox after a quantum quench," *ArXiv e-prints* (Jan., 2018) , arXiv:1801.05817 [cond-mat.stat-mech].

[14] T. Kinoshita, T. Wenger, and D. S. Weiss, "A quantum newton's cradle," *Nature* **440** (04, 2006) 900 EP –. http://dx.doi.org/10.1038/nature04693.

[15] V. I. Arnol'd, ed., *Mathematical methods of classical mechanics*. 1995.

[16] P. Dirac, *The principles of quantum mechanics*. 1947.

[17] B. Sutherland, *Beautiful Models: 70 Years of Exactly Solved Quantum Many-body Problems*. World Scientific, 2004. https://books.google.it/books?id=PA0xV0XxZIwC.

[18] J. Mossel and J.-S. Caux, "Exact time evolution of space- and time-dependent correlation functions after an interaction quench in the one-dimensional Bose gas,"

New Journal of Physics **14** no. 7, (July, 2012) 075006, arXiv:1201.1885 [cond-mat.stat-mech].

[19] B. Doyon and O. Castro-Alvaredo, "The Bologna Lectures on Entanglement and Non-Equilibrium Physics in Extended Quantum Systems," (Dec., 2016) .

[20] H. Bethe, "Zur theorie der metalle," *Zeitschrift für Physik* **71** no. 3, (Mar, 1931) 205–226. https://doi.org/10.1007/BF01341708.

[21] U. Schollwöck, "The density-matrix renormalization group in the age of matrix product states," *Annals of Physics* **326** (Jan., 2011) 96–192, arXiv:1008.3477 [cond-mat.str-el].

[22] G. Vidal, "On the characterization of entanglement," *J. Mod. Opt.* **47** (2000) 355, arXiv:quant-ph/9807077 [quant-ph].

[23] V. Alba, M. Fagotti, and P. Calabrese, "Entanglement entropy of excited states," *J. Stat. Mech.* **0910** (2009) P10020, arXiv:0909.1999 [cond-mat.stat-mech].

[24] J. Eisert, M. Cramer, and M. B. Plenio, "Colloquium: Area laws for the entanglement entropy," *Reviews of Modern Physics* **82** (Jan., 2010) 277–306, arXiv:0808.3773 [quant-ph].

[25] M. B. Hastings, "An area law for one-dimensional quantum systems," *Journal of Statistical Mechanics: Theory and Experiment* **8** (Aug., 2007) 08024, arXiv:0705.2024 [quant-ph].

[26] P. Calabrese and J. L. Cardy, "Entanglement entropy and quantum field theory," *J. Stat. Mech.* **0406** (2004) P06002, arXiv:hep-th/0405152 [hep-th].

[27] P. Di Francesco, P. Mathieu, and D. Sénéchal, *Conformal Field Theory*. Graduate Texts in Contemporary Physics. Springer, 1997. https://books.google.it/books?id=keUrdME5rhIC.

[28] G. Mussardo, *Statistical Field Theory: An Introduction to Exactly Solved Models in Statistical Physics*. Oxford Graduate Texts. OUP Oxford, 2009. https://books.google.it/books?id=JnLnXmBmCzsC.

[29] S. Sachdev, *Quantum Phase Transitions*. Cambridge University Press, 2011. https://books.google.it/books?id=F3IkpxwpqSgC.

[30] M. Takahashi, *Thermodynamics of One-Dimensional Solvable Models*. Cambridge University Press, 2005. https://books.google.it/books?id=ubGcM-JCT0IC.

[31] A. Polkovnikov, K. Sengupta, A. Silva, and M. Vengalattore, "Colloquium," *Rev. Mod. Phys.* **83** (Aug, 2011) 863–883. https://link.aps.org/doi/10.1103/RevModPhys.83.863.

[32] J. Eisert, M. Friesdorf, and C. Gogolin, "Quantum many-body systems out of equilibrium," *Nature Physics* **11** (Feb., 2015) 124–130, arXiv:1408.5148 [quant-ph].

[33] F. H. L. Essler and M. Fagotti, "Quench dynamics and relaxation in isolated integrable quantum spin chains," *Journal of Statistical Mechanics: Theory and Experiment* **6** (June, 2016) 064002, arXiv:1603.06452 [cond-mat.quant-gas].

[34] E. T. Jaynes, "Information theory and statistical mechanics," *Phys. Rev.* **106** (May, 1957) 620–630. https://link.aps.org/doi/10.1103/PhysRev.106.620.

[35] E. T. Jaynes, "Information theory and statistical mechanics. ii," *Phys. Rev.* **108** (Oct, 1957) 171–190. https://link.aps.org/doi/10.1103/PhysRev.108.171.

[36] S. Popescu, A. J. Short, and A. Winter, "Entanglement and the foundations of statistical mechanics," *Nature Physics* **2** (Nov., 2006) 754–758, quant-ph/0511225.

[37] M. Fagotti and F. H. L. Essler, "Reduced density matrix after a quantum quench," *Phys. Rev. B* **87** no. 24, (June, 2013) 245107, arXiv:1302.6944 [cond-mat.stat-mech].

[38] M. Cramer, C. M. Dawson, J. Eisert, and T. J. Osborne, "Exact Relaxation in a Class of Nonequilibrium Quantum Lattice Systems," *Physical Review Letters* **100** no. 3, (Jan., 2008) 030602, cond-mat/0703314.

[39] M. Cramer and J. Eisert, "A quantum central limit theorem for non-equilibrium systems: exact local relaxation of correlated states," *New Journal of Physics* **12** no. 5, (May, 2010) 055020, arXiv:0911.2475 [quant-ph].

[40] M. Rigol, V. Dunjko, V. Yurovsky, and M. Olshanii, "Relaxation in a Completely Integrable Many-Body Quantum System: An AbInitio Study of the Dynamics of the Highly Excited States of 1D Lattice Hard-Core Bosons," *Physical Review Letters* **98** no. 5, (Feb., 2007) 050405, cond-mat/0604476.

[41] M. Rigol, V. Dunjko, and M. Olshanii, "Thermalization and its mechanism for generic isolated quantum systems," *Nature* **452** (Apr., 2008) 854–858, arXiv:0708.1324 [cond-mat.stat-mech].

[42] M. Rigol, "Breakdown of Thermalization in Finite One-Dimensional Systems," *Physical Review Letters* **103** no. 10, (Sept., 2009) 100403, arXiv:0904.3746 [cond-mat.stat-mech].

[43] S. Trotzky, Y.-A. Chen, A. Flesch, I. P. McCulloch, U. Schollwöck, J. Eisert, and I. Bloch, "Probing the relaxation towards equilibrium in an isolated strongly correlated one-dimensional Bose gas," *Nature Physics* **8** (Apr., 2012) 325–330, arXiv:1101.2659 [cond-mat.quant-gas].

[44] M. Cheneau, P. Barmettler, D. Poletti, M. Endres, P. Schauß, T. Fukuhara, C. Gross, I. Bloch, C. Kollath, and S. Kuhr, "Light-cone-like spreading of correlations in a quantum many-body system," *Nature* **481** (Jan., 2012) 484–487, arXiv:1111.0776 [cond-mat.quant-gas].

[45] M. Rigol and M. Srednicki, "Alternatives to Eigenstate Thermalization," *Physical Review Letters* **108** no. 11, (Mar., 2012) 110601, arXiv:1108.0928 [cond-mat.stat-mech].

[46] J. M. Deutsch, "Quantum statistical mechanics in a closed system," *Phys. Rev. A* **43** (Feb, 1991) 2046–2049. https://link.aps.org/doi/10.1103/PhysRevA.43.2046.

[47] M. Srednicki, "Chaos and quantum thermalization," *Phys. Rev. E* **50** (Aug., 1994) 888–901, cond-mat/9403051.

[48] M. Srednicki, "The approach to thermal equilibrium in quantized chaotic systems," *Journal of Physics A Mathematical General* **32** (Feb., 1999) 1163–1175, cond-mat/9809360.

[49] J. Sirker, N. P. Konstantinidis, F. Andraschko, and N. Sedlmayr, "Locality and thermalization in closed quantum systems," **89** no. 4, (Apr., 2014) 042104, arXiv:1303.3064 [cond-mat.stat-mech].

[50] A. Pal and D. A. Huse, "The many-body localization transition," *ArXiv e-prints* (Mar., 2010) , arXiv:1003.2613 [cond-mat.dis-nn].

[51] D. Pekker, G. Refael, E. Altman, E. Demler, and V. Oganesyan, "Hilbert-glass transition: New universality of temperature-tuned many-body dynamical quantum criticality," *Phys. Rev. X* **4** (Mar, 2014) 011052. https://link.aps.org/doi/10.1103/PhysRevX.4.011052.

[52] M. Fagotti, "On conservation laws, relaxation and pre-relaxation after a quantum quench," *Journal of Statistical Mechanics: Theory and Experiment* **3** (Mar., 2014) 03016, arXiv:1401.1064 [cond-mat.stat-mech].

[53] J. Cardy, "Quantum Quenches to a Critical Point in One Dimension: some further results," *ArXiv e-prints* (July, 2015) , arXiv:1507.07266 [cond-mat.stat-mech].

[54] B. Doyon, "Thermalization and pseudolocality in extended quantum systems," *ArXiv e-prints* (Dec., 2015) , arXiv:1512.03713 [math-ph].

[55] M. Born and V. Fock, "Beweis des Adiabatensatzes," *Zeitschrift fur Physik* **51** (Mar., 1928) 165–180.

[56] B. A. Bernevig and T. L. Hughes, *Topological insulators and topological superconductors*. Princeton university press, 2013.

[57] K. Sengupta, S. Powell, and S. Sachdev, "Quench dynamics across quantum critical points," *Phys. Rev. A* **69** (May, 2004) 053616. https://link.aps.org/doi/10.1103/PhysRevA.69.053616.

[58] P. Calabrese and J. Cardy, "Quantum quenches in extended systems," *Journal of Statistical Mechanics: Theory and Experiment* **6** (June, 2007) 06008, arXiv:0704.1880 [cond-mat.stat-mech].

[59] J. Berges, S. Borsányi, and C. Wetterich, "Prethermalization," *Phys. Rev. Lett.* **93** (Sep, 2004) 142002. https://link.aps.org/doi/10.1103/PhysRevLett.93.142002.

[60] W. H. Zurek, U. Dorner, and P. Zoller, "Dynamics of a Quantum Phase Transition," *Physical Review Letters* **95** no. 10, (Sept., 2005) 105701, cond-mat/0503511.

[61] N. N. Bogolyubov, "On the theory of superfluidity," *J. Phys.(USSR)* **11** (1947) 23–32. [Izv. Akad. Nauk Ser. Fiz.11,77(1947)].

[62] N. Jose and F. Alessandro, *Modeling Black Hole Evaporation*. World Scientific Publishing Company, 2005. https://books.google.it/books?id=dOK3CgAAQBAJ.

[63] S. Ghoshal and A. B. Zamolodchikov, "Boundary S matrix and boundary state in two-dimensional integrable quantum field theory," *Int. J. Mod. Phys.* **A9** (1994) 3841–3886, arXiv:hep-th/9306002 [hep-th]. [Erratum: Int. J. Mod. Phys.A9,4353(1994)].

[64] E. H. Lieb and D. W. Robinson, "The finite group velocity of quantum spin systems," *Communications in Mathematical Physics* **28** (Sept., 1972) 251–257.

[65] B. Nachtergaele and R. Sims, "Lieb-Robinson Bounds and the Exponential Clustering Theorem," *Communications in Mathematical Physics* **265** (July, 2006) 119–130, math-ph/0506030.

[66] S. Bravyi, M. B. Hastings, and F. Verstraete, "Lieb-Robinson Bounds and the Generation of Correlations and Topological Quantum Order," *Physical Review Letters* **97** no. 5, (Aug., 2006) 050401, quant-ph/0603121.

[67] M. Fannes, B. Nachtergaele, and R. F. Werner, "Finitely correlated states on quantum spin chains," *Communications in Mathematical Physics* **144** (Mar., 1992) 443–490.

[68] S. Rommer and S. Öautstlund, "Class of ansatz wave functions for one-dimensional spin systems and their relation to the density matrix renormalization group," *Phys. Rev. B* **55** (Jan., 1997) 2164–2181, cond-mat/9606213.

[69] G. Vidal, J. I. Latorre, E. Rico, and A. Kitaev, "Entanglement in Quantum Critical Phenomena," *Physical Review Letters* **90** no. 22, (June, 2003) 227902, quant-ph/0211074.

[70] G. Vidal, "Classical Simulation of Infinite-Size Quantum Lattice Systems in One Spatial Dimension," *Physical Review Letters* **98** no. 7, (Feb., 2007) 070201, cond-mat/0605597.

[71] R. Orús and G. Vidal, "Infinite time-evolving block decimation algorithm beyond unitary evolution," *Phys. Rev. B* **78** no. 15, (Oct., 2008) 155117, arXiv:0711.3960 [cond-mat.stat-mech].

[72] Á. Rapp and G. Zaránd, "Dynamical correlations and quantum phase transition in the quantum Potts model," *Phys. Rev. B* **74** no. 1, (July, 2006) 014433, cond-mat/0507390.

[73] S. Sachdev and A. P. Young, "Low temperature relaxational dynamics of the ising chain in a transverse field," *Phys. Rev. Lett.* **78** (Mar, 1997) 2220–2223. https://link.aps.org/doi/10.1103/PhysRevLett.78.2220.

[74] B. M. McCoy and T. T. Wu, "Two-dimensional Ising field theory in a magnetic field: Breakup of the cut in the two-point function," *Phys. Rev. D* **18** (Aug., 1978) 1259–1267.

[75] S. L. Sondhi, S. M. Girvin, J. P. Carini, and D. Shahar, "Continuous quantum phase transitions," *Rev. Mod. Phys.* **69** (Jan, 1997) 315–333. https://link.aps.org/doi/10.1103/RevModPhys.69.315.